UNIVERSITY OF CALIFORNIA
RIVERSIDE

Identifying Potential Biomarkers of Posttraumatic Epilepsy

A Dissertation submitted in partial satisfaction
of the requirements for the degree of

Doctor of Philosophy

in

Neuroscience

by

Jenny Szu

December 2018

Dissertation Committee:
Dr. Devin Binder, Chairperson
Dr. Hyle Park
Dr. Byron Ford

The Dissertation of Jenny Szu is approved:

Committee Chairperson

University of California, Riverside

Acknowledgements

I would like to extend my deepest, sincerest gratitude to my advisor Dr. Devin Binder. Dr. Binder gave me a chance when others did not and has been a tremendous mentor to me over the years. He not only provides valuable insight and feedback but is constantly pushing me to think more critically as a scientist. Furthermore, Dr. Binder has allowed me to pursue my own creativity in research which has molded me into a better independent scientist. Dr. Binder is not only an incredible advisor but is also a great friend; he has always been a pillar of support during challenging times, and for this, I sincerely thank him.

A heartfelt appreciation also goes to my committee members Drs. Hyle Park, Byron Ford, Todd Fiacco, and Seema Tiwari-Woodruff. Dr. Park has been incredibly patient with me over the years in teaching me the basics of optics, OCT, and data processing and has spent countless hours coding and programming for me. Additionally, I have enjoyed all my meetings with Drs. Fiacco, Tiwari-Woodruff, and Ford as they have all provided invaluable guidance and support throughout my graduate career and have played an instrumental part in the development of my thesis project.

I would also like to acknowledge my labmates, both past and present. Dr. Jacqueline Hubbard, Dr. Jonathan Lovelace, Dr. Patricia Pirbhoy, Dr. Thomas Murphy, Carrie Jonak, Allison Peterson, and Jennifer Yonan have all made a huge impact in my graduate career. None of my success in research would have been possible without their support. A big thank you also goes to Som Chaturvedi, Dillon Patel, and Terese Garcia who are the most incredible and hardworking undergraduate students I have ever worked with. I would also like to extend my deepest gratitude to the past and present members of the NOIR lab; Dr. Carissa Rodriguez, Dr. Melissa Eberle, Dr. Yan Wang, Dr. Md. Shahid

Islam, Dr. Md. Rezuanul Haque, Dr. Koji Hirota, Dr. Md. Monirul Hasan, Dr. Michael Oliveira, Christian Oh, Minh Tong, Danielle Ornelas, and Jason Liu. Their endless support in teaching me optical imaging and analysis have contributed greatly to my thesis project.

I would also like to express heartfelt thanks to Perla Fabelo and Margarita Roman. Perla and Margarita have both helped me in tremendous ways during graduate school. They have both endured my numerous questions and emails and have been so patient and understanding with me. And finally, to the Neuroscience Graduate Program, I am forever grateful for this opportunity.

Dedication

For my mother, sister, and brother whose unconditional love and encouragement have made this all possible.

ABSTRACT OF THE DISSERTATION

Identifying Potential Biomarkers of Posttraumatic Epilepsy

by

Jenny Szu

Doctor of Philosophy, Graduate Program in Neuroscience
University of California, Riverside, December 2018
Dr. Devin K. Binder, Chairperson

Posttraumatic epilepsy (PTE) is a long-term negative consequence of traumatic brain injury (TBI) in which recurrent spontaneous seizures occur after the initial head injury. PTE develops over an undefined period where circuitry reorganization in the brain causes permanent hyperexcitability. Unfortunately, current existing antiepileptogenic drugs (AEDs) have all failed at treating PTE, and thus, there is a critical need to identify biomarkers of PTE to ultimately develop new therapeutic strategies. The pathophysiology by which trauma leads to spontaneous seizures is unknown and clinically relevant models of PTE are key to understanding the molecular and cellular mechanisms underlying the development of PTE. Current animal studies of PTE are limited and comprehensive *in vivo* electrophysiological approaches remain absent. In the present study, I aimed to identify optical and electrographic biomarkers of PTE with correlation to hippocampal histopathology at 14, 30, 60, and 90 days post injury (dpi). Here, adult male CD1 wildtype (WT) and aquaporin-4 knockout (AQP4 KO)

mice were subjected to a moderate-severe TBI in the right frontal cortex using the well-established controlled cortical impact (CCI) injury model. Additionally, mice underwent optical coherence tomography (OCT) imaging, *in vivo* video-electroencephalographic (vEEG) recordings, and immunohistochemistry and Western blot analysis for the key epileptogenic astrocytic channels AQP4 and Kir4.1. The main findings from these studies are: 1) successful implementation of CCI-based PTE in mice with chronic vEEG generated, for the first time,17% and 27% of WT and AQP4 KO mice with PTE, respectively (the highest yield of PTE reported); 2) AQP4 KO mice had a greater incidence of spontaneous seizures and PTE compared with WT mice; 3) AQP4 KO mice had longer spontaneous seizure duration compared with WT mice; 4) EEG power patterns are different between mice with and without PTE; and 5) AQP4, but not Kir4.1, is significantly upregulated in the frontal cortex and hippocampus of mice with PTE. Collectively, these findings identified specific PTE EEG phenotypes that may be modulated by AQP4 and carry significant implications for epileptogenesis after TBI which may serve as the first steps to developing surrogate biomarkers for PTE.

Table of Contents

List of Figures

List of Tables

Chapter 1: Introduction

1.1 Traumatic brain injury

Traumatic brain injury (TBI) is a worldwide health concern that affects both the civilian and military population and is the major cause of morbidity and mortality in persons under the age of 45 (Langlois, Rutland-Brown et al. 2006). In the United States, approximately 1.7 million people sustain a TBI every year, of which 275,000 are hospitalized and 52,000 results in death (Faul M., Xu L. et al. 2010). The numbers are even higher in Europe with an estimated 2.5 million people experiencing a TBI and a reported 75,000 TBI-related deaths annually (Maas, Menon et al. 2014). In addition to the serious neuropathological sequelae of TBI (such as behavioral and cognitive deficits) (Rao and Lyketsos 2000), survivors are also faced with the staggering economic burden related to TBI (Humphreys, Wood et al. 2013). For instance, a study showed that adoption of the Brain Trauma Foundation treatment guidelines to treat severe TBI will result in an estimated annual savings of $262 million in medical costs, $43 million in rehabilitation, and $3.84 billion in lifetime societal costs (Faul, Wald et al. 2007).

TBI is a disorder of heterogeneous etiology and is defined by the Centers for Disease Control and Prevention as “a disruption in the normal function of the brain that can be caused by a bump, blow, or jolt to the head, or penetrating head injury.” The leading cause of TBI is falls with the highest rates in children between the ages of 0 – 4 and adults over the age of 65 (Faul M., Xu L. et al. 2010). On the other hand, motor vehicle crashes are the leading cause of TBI-related deaths (Langlois, Rutland-Brown et al. 2004; Faul M., Xu L. et al. 2010). Head injuries resulting from sports and recreational activities are also becoming increasingly common (Langlois, Rutland-Brown et al. 2006). In particular, the development of chronic traumatic encephalopathy (CTE) (Grinberg,

Anghinah et al. 2016; Ling, Morris et al. 2017; Mez, Daneshvar et al. 2017), a considerable risk of sports-related head injuries, has recently received significant attention from both the scientific and public community. Additionally, blast TBI from explosive devices is the most common war injury (Warden 2006). For instance, during the Global War on Terror, 68% of our military personnel suffered a blast injury (Kovacs, Leonessa et al. 2014).

1.1.1 TBI classification

There are two types of injury associated with TBI; primary and secondary. The primary injury is the direct mechanical force inflicted onto the brain at the time of injury which can lead to events such as tissue deformation, breakdown of the blood-brain barrier (BBB), altered cerebral blood flow (CBF), and impaired cerebral metabolism (Pitkänen and McIntosh 2006; Werner and Engelhard 2007; Xiong, Mahmood et al. 2013). These events further lead to the delayed onset of secondary injury where cellular and molecular signaling events result in further brain damage such as axonal injury, cerebral edema, and ischemia (Pitkänen and McIntosh 2006; Xiong, Mahmood et al. 2013). Because secondary injury manifests over a variable period of time following the primary insult, it may represent a window of opportunity for treatment (Xiong, Mahmood et al. 2013).

TBI can also be classified based on the severity of injury. The widely used Glasgow Coma Scale (GCS) assesses the severity of the injury based on the level of consciousness as defined by the patient's responses to commands and cues (Teasdale and Jennett 1974; Ray, Dixon et al. 2002). The three severities of TBI include mild (GCS score 13 – 15), moderate (GCS score 9 – 12), and severe (GCS score 3 – 8) (Ray, Dixon et al. 2002). Mild TBI represents the most common severity of injury and presents with no overt damage to the brain (Salehi, Zhang et al. 2017), but patients with mild TBI can still

experience long-term negative consequences such as depression and memory deficits (Konrad, Geburek et al. 2011; Rona 2012). Moderate-severe TBI, on the other hand, results in visible structural damage within the brain and survivors are faced with lifelong disabilities (Maas, Stocchetti et al. 2008) in which everyday tasks such as walking, eating, and bathing, may present tremendous challenges (Selassie, Zaloshnja et al. 2008)

Severity of injury can be further categorized based on types of injury including focal injury, diffuse injury, and penetrating injury (Ray, Dixon et al. 2002; Pitkänen and McIntosh 2006). Types of focal injuries include epidural and subdural hematomas, contusions, and subarachnoid hemorrhage. Diffuse axonal injury (DAI) results in damage to the axons in the white matter due to rapid acceleration-deceleration of the head commonly seen during motor vehicle collisions (Meythaler, Peduzzi et al. 2001; Smith, Meaney et al. 2003; Andriessen, Jacobs et al. 2010). Penetrating head injuries result from a penetrating object such as a gunshot and can lead to serious vascular lesions including intracranial hemorrhage and traumatic aneurysms (Maas, Stocchetti et al. 2008).

1.2 Posttraumatic epilepsy

Posttraumatic epilepsy (PTE) is a long-term negative consequence of TBI in which recurrent spontaneous seizures occur after the initial head injury (Pitkänen and McIntosh 2006). PTE accounts for approximately 20% of symptomatic epilepsy (epilepsy that results from identifiable structural lesions in the brain (Engel 2001; Lowenstein 2009)) and 6% of all epilepsies (Hauser, Annegers et al. 1993). Epidemiologic studies show that PTE develops in 30% of individuals between the ages of 15 and 34, 14% of children under the age of 14, and 8% of adults over the age of 65 (Hauser, Annegers et al. 1993).

Studies investigating the development of epilepsy are critical because: 1) it is the most common form of acquired epilepsy; 2) treatment and management of PTE are

difficult; and 3) the probability of developing PTE after TBI is as high as 50% in some cases (Lowenstein 2009). In the remaining portion of this chapter, I will provide an overview of PTE beginning with a brief historical background about epilepsy after TBI. I will the follow upon this with discussions on the risk factors, treatments, and existing challenges and knowledge gaps in PTE.

1.2.1 The history of PTE

The correlation between epilepsy and TBI has been dated as far back as 3,000 B.C. Neurosurgical cases of ancient Egyptians have been documented in possibly the world's oldest medical text, The Edwin Smith Papyrus (Feldman and Goodrich 1999). Examples of surgical cases recorded include "A wound in the head, penetrating to the bone (incomplete)" and "A gaping wound in the head penetrating to the bone and splitting the skull " (Breasted 1930). Patients reported in the Edwin Smith Papyrus undoubtedly experienced epilepsy after a severe TBI. Indeed, in one case titled "A gaping wound in the head penetrating to the bone and perforating the sutures" the patient experienced symptoms described as "convulsions" or "delirium". In the case "Compound comminuted fracture of the skull displaying no visible external injury", a direct association between TBI and epilepsy is made clear in which the patient experienced "obscure convulsive action like symptoms accompanying injury to the brain" (Breasted 1930). Consistently, Hippocrates (460 – 377 B.C.) also documented seizures in his treatise "On Wounds in the Head." Interestingly, Hippocrates noted that patients with epidural or subdural hematomas over the temporal lobe have convulsions on the contralateral side of the body. In fact, "the father of medicine" considered convulsions as a poor prognostic outcome (Panourias, Skiadas et al. 2005). Evidence of PTE was also documented in the Middle Ages. As reported by Valescus de Tharanta (1382 – 1418 A.D.), the Portuguese physician

described a man with a penetrating head injury experiencing as many as eight epileptic attacks a day (Diamantis, Sidiropoulou et al. 2010). Thus, while evidence of seizures and epilepsy after a TBI has been historically documented, the pathophysiology of PTE is not understood.

1.2.2 Incidence and risk factors of PTE

A common set of definitions of PTE was established by investigators to distinguish seizures after TBI in the clinical and preclinical setting: 1) immediate seizures, which occur less than 24 hours after injury; 2) early seizures, which occur less than 1 week after injury; and 3) late seizures, which occur more than 1 week after injury and represent the diagnosis of PTE (Pitkänen and McIntosh 2006; Lowenstein 2009).

It is widely agreed that the severity of injury is strongly correlated with an increased risk of developing seizures (Jennett and Lewin 1960; Annegers, Hauser et al. 1998). A prospective, multicenter study showed that 16.8% of TBI patients with a GCS score of 3 – 8, 24.3% with GCS 9 – 12, and 8.0% GCS 13 – 15 developed late posttraumatic seizures 24 months after injury (Englander, Bushnik et al. 2003). Some examples of severe head injuries that have a clear association for late seizure development include penetrating head injuries, brain contusions, and/or subdural hematomas (Temkin 2003). In fact, the prevalence of PTE is ~50% in 20th century war veterans due to their increased exposure to penetrating head injuries (Salazar, Jabbari et al. 1985; Raymont, Salazar et al. 2010; Alder, Fujioka et al. 2011). However, military personnel from current conflicts in Iraq and Afghanistan, such as the recent Operation Enduring Freedom and Operation Iraqi Freedom, were found to be more prone to blast injuries and the incidence of PTE in these veterans remains to be determined (Lowenstein 2009; Chen, Baca et al. 2014)

The occurrence of early posttraumatic seizures has also been considered a risk factor for PTE. In one of the earlier PTE epidemiological studies, the authors found that patients with early posttraumatic seizures were four times more likely to develop late posttraumatic seizures (Jennett and Lewin 1960). In a separate study, the authors confirmed that increased prevalence of PTE is associated with early posttraumatic seizures, however, the correlation is much higher in children (De Santis, Sganzerla et al. 1992). Interestingly, using the Cox proportional hazards model, a study found that patients with early posttraumatic seizures with a single temporal or frontal brain lesion are 8.58 and 3.43 times more likely to develop PTE. (Angeleri, Majkowski et al. 1999).

1.2.3 Antiepileptogenic drugs for PTE

Because secondary injury after TBI can comprise a vast number of cellular and molecular events leading to further deleterious consequences, treating and managing PTE has proven extremely difficult. Although it is common practice to treat patients with antiepileptic drugs (AEDs) to prevent early posttraumatic seizures following a head injury, the effectiveness of current AEDs to treat epilepsy or even late seizures after a TBI have all proved unsuccessful. Phenytoin, a major anticonvulsant which selectively blocks Na^+ channels and suppresses high-frequency neuronal firing (Yaari, Selzer et al. 1986), was found to be ineffective in treating late posttraumatic seizures at 18 – 24 months after TBI (McQueen, Blackwood et al. 1983; Young, Rapp et al. 1983; Temkin, Dikmen et al. 1999). Moreover, seizure rates were found to be similar between phenytoin- and placebo-treated groups (Temkin, Dikmen et al. 1990). Valproate, another common AED, also failed to prevent late posttraumatic seizures 24 months post TBI (Temkin, Dikmen et al. 1999). Other drugs, such as phenobarbital and carbamazepine also did not exert an

antiepileptogenic effect after TBI (Temkin 2009). Thus, prophylactic antiepileptogenic therapy for PTE seizures remains unproven, at least with current AEDs.

1.2.4 Challenges and knowledge gaps in PTE

While PTE is clinically recognized, the pathophysiology of PTE is unknown and new treatment options for patients with PTE are required. A major obstacle in designing effective treatment options is the lack of understanding of the genesis of PTE after a head injury. Preclinical studies must use acceptable models of PTE that reliably reflect the human condition. Additionally, detailed evaluation of electrophysiological and histological changes is urgently needed not only to determine the cellular and molecular changes underlying PTE, but to also define biomarkers for new therapeutic treatment development. Thus, the challenge here is not to simply prevent posttraumatic seizures that arise after TBI, but to fully prevent post-TBI epileptogenesis. Therefore, in my studies, I aim to identify and characterize potential surrogate markers of PTE using *in vivo* optical imaging, long-term video-electroencephalography (vEEG) recordings, and immunohistochemistry and Western blot analysis. In “Chapter 2: Mouse model of PTE”, I review the three main types of preclinical PTE models and introduce my model of PTE using the controlled cortical impact (CCI) injury device. “Chapter 3: Optical biomarkers of PTE” describes different neuroimaging techniques used to identify PTE and my studies on utilizing optical coherence tomography (OCT) in defining optical biomarkers of PTE. In “Chapter 4: Electrographic biomarkers of PTE”, background on electrophysiological studies in preclinical models of PTE is discussed as well as my findings from long-term vEEG recordings. Immunohistochemical and Western blot analysis of aquaporin-4 (AQP4) and the inwardly rectifying K^+ channel, Kir4.1, key astrocytic proteins involved in modulating seizure activity, are discussed in “Chapter 5: Histological biomarkers of PTE”. Finally, in

“Chapter 6: Conclusions and future directions”, I give an overall summary of the findings regarding identification of biomarkers in a mouse model of PTE and future directions in the field of PTE.

1.3 References

Alder, J., Fujioka, W., et al. (2011). "Lateral fluid percussion: model of traumatic brain injury in mice." J Vis Exp(54).

Andriessen, T. M., Jacobs, B., et al. (2010). "Clinical characteristics and pathophysiological mechanisms of focal and diffuse traumatic brain injury." Journal of cellular and molecular medicine **14**(10): 2381-2392.

Angeleri, F., Majkowski, J., et al. (1999). "Posttraumatic Epilepsy Risk Factors: One-Year Prospective Study After Head Injury." Epilepsia **40**(9): 1222-1230.

Annegers, J. F., Hauser, W. A., et al. (1998). "A population-based study of seizures after traumatic brain injuries." N Engl J Med **338**(1): 20-24.

Breasted, J. H. (1930). The Edwin Smith Surgical Papyrus: published in facsimile and hieroglyphic transliteration with translation and commentary in two volumes, Chic. UP.

Chen, L. L., Baca, C. B., et al. (2014). "Posttraumatic epilepsy in operation enduring freedom/operation iraqi freedom veterans." Military medicine **179**(5): 492-496.

De Santis, A., Sganzerla, E., et al. (1992). Risk factors for late posttraumatic epilepsy. Neurotraumatology: Progress and Perspectives, Springer**:** 64-67.

Diamantis, A., Sidiropoulou, K., et al. (2010). "Epilepsy during the Middle Ages, the Renaissance and the Enlightenment." Journal of neurology **257**(5): 691-698.

Engel, J., Jr. (2001). "A proposed diagnostic scheme for people with epileptic seizures and with epilepsy: report of the ILAE Task Force on Classification and Terminology." Epilepsia **42**(6): 796-803.

Englander, J., Bushnik, T., et al. (2003). "Analyzing risk factors for late posttraumatic seizures: a prospective, multicenter investigation." Archives of physical medicine and rehabilitation **84**(3): 365-373.

Faul, M., Wald, M. M., et al. (2007). "Using a cost-benefit analysis to estimate outcomes of a clinical treatment guideline: testing the Brain Trauma Foundation guidelines for the treatment of severe traumatic brain injury." Journal of Trauma and Acute Care Surgery **63**(6): 1271-1278.

Faul M., Xu L., et al. (2010). "Traumatic brain injury in the United States: Emergency department visits, hospitalizations and deaths 2002 - 2006." Atlanta (GA): Centers for Disease Control and Prevention, National Center for Injury Prevention and Control.

Feldman, R. P. and Goodrich, J. T. (1999). "The edwin smith surgical papyrus." Child's Nervous System **15**(6-7): 281-284.

Grinberg, L. T., Anghinah, R., et al. (2016). "Chronic traumatic encephalopathy presenting as Alzheimer's disease in a retired soccer player." Journal of Alzheimer's disease **54**(1): 169-174.

Hauser, W. A., Annegers, J. F., et al. (1993). "Incidence of epilepsy and unprovoked seizures in Rochester, Minnesota: 1935-1984." Epilepsia **34**(3): 453-468.

Humphreys, I., Wood, R. L., et al. (2013). "The costs of traumatic brain injury: a literature review." ClinicoEconomics and outcomes research: CEOR **5**: 281.

Jennett, W. B. and Lewin, W. (1960). "Traumatic epilepsy after closed head injuries." Journal of neurology, neurosurgery, and psychiatry **23**(4): 295.

Konrad, C., Geburek, A. J., et al. (2011). "Long-term cognitive and emotional consequences of mild traumatic brain injury." Psychological medicine **41**(6): 1197-1211.

Kovacs, S. K., Leonessa, F., et al. (2014). "Blast TBI models, neuropathology, and implications for seizure risk." Frontiers in neurology **5**: 47.

Langlois, J. A., Rutland-Brown, W., et al. (2004). "Traumatic Brain Injury in the United States: Emergency Department Visits, Hospitalizations, and Deaths."

Langlois, J. A., Rutland-Brown, W., et al. (2006). "The Epidemiology and Impact of Traumatic Brain Injury: A Brief Overview." J Head Trauma Rehabil **21**(5): 375-378.

Ling, H., Morris, H. R., et al. (2017). "Mixed pathologies including chronic traumatic encephalopathy account for dementia in retired association football (soccer) players." Acta neuropathologica **133**(3): 337-352.

Lowenstein, D. H. (2009). "Epilepsy after head injury: an overview." Epilepsia **50 Suppl 2**: 4-9.

Maas, A. I., Menon, D. K., et al. (2014). "Collaborative European NeuroTrauma Effectiveness Research in Traumatic Brain Injury (CENTER-TBI) A Prospective Longitudinal Observational Study." Neurosurgery **76**(1): 67-80.

Maas, A. I., Stocchetti, N., et al. (2008). "Moderate and severe traumatic brain injury in adults." The Lancet Neurology **7**(8): 728-741.

McQueen, J. K., Blackwood, D. H., et al. (1983). "Low risk of late post-traumatic seizures following severe head injury: implications for clinical trials of prophylaxis." Journal of Neurology, Neurosurgery & Psychiatry **46**(10): 899-904.

Meythaler, J. M., Peduzzi, J. D., et al. (2001). "Current concepts: diffuse axonal injury–associated traumatic brain injury." Archives of physical medicine and rehabilitation **82**(10): 1461-1471.

Mez, J., Daneshvar, D. H., et al. (2017). "Clinicopathological evaluation of chronic traumatic encephalopathy in players of American football." Jama **318**(4): 360-370.

Panourias, I. G., Skiadas, P. K., et al. (2005). "Hippocrates: a pioneer in the treatment of head injuries." Neurosurgery **57**(1): 181-189.

Pitkänen, A. and McIntosh, T. K. (2006). "Animal models of post-traumatic epilepsy." J Neurotrauma **23**(2): 241-261.

Rao, V. and Lyketsos, C. (2000). "Neuropsychiatric sequelae of traumatic brain injury." Psychosomatics **41**(2): 95-103.

Ray, S. K., Dixon, C. E., et al. (2002). "Molecular mechanisms in the pathogenesis of traumatic brain injury." Histol Histopathol **17**(4): 1137-1152.

Raymont, V., Salazar, A. M., et al. (2010). "Correlates of posttraumatic epilepsy 35 years following combat brain injury." Neurology **75**(3): 224-229.

Rona, R. J. (2012). "Long-term consequences of mild traumatic brain injury." The British Journal of Psychiatry **201**(3): 172-174.

Salazar, A. M., Jabbari, B., et al. (1985). "Epilepsy after penetrating head injury. I. Clinical correlates A report of the Vietnam Head Injury Study." Neurology **35**(10): 1406-1406.

Salehi, A., Zhang, J. H., et al. (2017). "Response of the cerebral vasculature following traumatic brain injury." Journal of Cerebral Blood Flow & Metabolism **37**(7): 2320-2339.

Selassie, A. W., Zaloshnja, E., et al. (2008). "Incidence of long-term disability following traumatic brain injury hospitalization, United States, 2003." The Journal of head trauma rehabilitation **23**(2): 123-131.

Smith, D. H., Meaney, D. F., et al. (2003). "Diffuse axonal injury in head trauma." The Journal of head trauma rehabilitation **18**(4): 307-316.

Teasdale, G. and Jennett, B. (1974). "Assessment of coma and impaired consciousness. A practical scale." Lancet **2**(7872): 81-84.

Temkin, N. R. (2003). "Risk factors for posttraumatic seizures in adults." Epilepsia **44**: 18-20.

Temkin, N. R. (2009). "Preventing and treating posttraumatic seizures: the human experience." Epilepsia **50 Suppl 2**: 10-13.

Temkin, N. R., Dikmen, S. S., et al. (1999). "Valproate therapy for prevention of posttraumatic seizures: a randomized trial." Journal of neurosurgery **91**(4): 593-600.

Temkin, N. R., Dikmen, S. S., et al. (1990). "A randomized, double-blinded study of phenytoin for the prevention of post-traumatic seizures." The New England Journal of Medicine **323**(8): 497-502.

Warden, D. (2006). "Military TBI during the Iraq and Afghanistan wars." The Journal of head trauma rehabilitation **21**(5): 398-402.

Werner, C. and Engelhard, K. (2007). "Pathophysiology of traumatic brain injury." BJA: British Journal of Anaesthesia **99**(1): 4-9.

Xiong, Y., Mahmood, A., et al. (2013). "Animal models of traumatic brain injury." Nat Rev Neurosci **14**(2): 128-142.

Yaari, Y., Selzer, M. E., et al. (1986). "Phenytoin: mechanisms of its anticonvulsant action." Ann Neurol **20**(2): 171-184.

Young, B., Rapp, R. P., et al. (1983). "Failure of prophylactically administered phenytoin to prevent late posttraumatic seizures." Journal of neurosurgery **58**(2): 236-241.

Chapter 2: Mouse model of posttraumatic epilepsy

2.1 Abstract

The pathophysiology of posttraumatic epilepsy (PTE), in which trauma to the brain leads to spontaneous recurrent seizures, is poorly understood. Establishing clinically relevant models of PTE that recapitulate the human condition is essential for understanding the molecular and cellular mechanisms underlying the development of PTE. In the present study, the controlled cortical impact (CCI) injury model was used as a model of PTE. Adult CD1 wildtype (WT) and aquaporin-4 knockout (AQP4 KO) male mice were subjected to a single CCI injury over the right frontal cortex and ipsilateral hippocampal physiology was monitored at 14, 30, 60, and 90 days post injury (dpi) using video-electroencephalography (vEEG) recordings. In some mice, the dura was ruptured and severe bleeding and immediate brain swelling was observed. In other cases, the dura remained intact, however, subdural hematoma and hemorrhage was evident. Behavioral seizures observed after TBI were typically motor arrests with facial automatisms, behavior that is also commonly seen in human and other preclinical models of PTE. Interestingly, AQP4 KO mice exhibited more spontaneous seizures and longer seizure duration compared to WT mice, suggesting a role of AQP4 in seizure modulation after TBI. These findings suggest that this model exhibits similiarites to human PTE and thus serves as a useful model for studying PTE.

2.2 Introduction

From a modeling perspective, the pathophysiology and heterogeneity of traumatic brain injury (TBI) and epilepsy creates a tremendous challenge for researchers. Besides the aforementioned types of injury (see Chapter 1), other factors

that may contribute to the overall effect of a head injury include, but are not limited to age, sex, pre-existing conditions, and genetics (Pitkänen and McIntosh 2006). Although experimental models of PTE cannot entirely represent the human condition, they are valuable for studying the cellular and molecular aspects of posttraumatic epilepsy (PTE). Moreover, animal models can be utilized to develop and characterize new therapeutic strategies.

There are three widely used models of PTE: 1) fluid percussion injury (FPI), 2) controlled cortical impact (CCI) injury, and 3) weight-drop injury (Pitkänen and McIntosh 2006).

2.2.1 Fluid percussion injury model

The FPI model uses a pendulum, dropped from a predetermined height, to strike the piston of a cylindrical reservoir of fluid that generates a fluid pressure pulse onto the intact dura (McIntosh, Vink et al. 1989; Xiong, Mahmood et al. 2013). The degree of the injury depends on the pressure pulse which can be induced centrally, parasagitally, or laterally (Cernak 2005; Xiong, Mahmood et al. 2013). Historically, the FPI model was used in dogs, pigs, cats, rabbits, and sheep (McIntosh, Vink et al. 1989; Cernak 2005) and has more recently been adapted for use in rodents (McIntosh, Vink et al. 1989; Carbonell, Maris et al. 1998; Kabadi, Hilton et al. 2010; Alder, Fujioka et al. 2011). FPI is generally used to replicate the human closed head injury (Cernak 2005; Pitkänen and McIntosh 2006; Xiong, Mahmood et al. 2013) in which it produces a brief displacement and deformation of the brain (Xiong, Mahmood et al. 2013) and can result in behavioral and cognitive deficits (Xiong, Mahmood et al. 2013). A major drawback of FPI is its high mortality rate (30 – 40%), thus studies using the FPI model will require a large sample size to reach statistical power (Kharatishvili, Nissinen et al. 2006).

FPI has proven to be a useful model for PTE. In one study, epileptiform activity was observed in 92% of rats during normal awake behavior and electrocorticographic (ECoG) recordings revealed epileptiform activity near the site of injury spreading to adjacent areas of the neocortex (D'Ambrosio, Fairbanks et al. 2004). Subsequent studies from the same group showed spontaneous neocortical and limbic seizures after FPI from three different trauma sites with two injury severities, albeit with high variability between rats. Behaviorally, the rats displayed motor arrests (with and without facial automatisms) and loss of posture which was associated with cortical seizures (Curia, Levitt et al. 2010) In another study using two independent experimental groups, 50% and 43% of rats developed PTE after severe FPI in the parietal cortex at 11 months and 12 months, respectively with latency between 7 weeks – 1 year. Rats with PTE had secondarily generalized tonic-clonic seizures with focal onset in the ipsilateral ventral hippocampus that propagated to the contralateral parietal cortex (Kharatishvili, Nissinen et al. 2006). PTE after FPI has also been demonstrated in mice, although the prevalence of PTE in mice was lower compared with rats. Surprisingly, FPI in the parietotemporal cortex resulted in only 3% of mice experiencing late posttraumatic spontaneous seizures 6 months after injury even with 58% of mice exhibiting spontaneous epileptiform discharges (Bolkvadze and Pitkänen 2012).

2.2.2 Controlled cortical impact injury model

In the CCI model, the injury is delivered onto the intact dura using a pneumatically driven impactor. The advantage of CCI over FPI is that it allows the user to adjust mechanical factors such as velocity of impact, depth of impact, diameter of impactor tip, and duration of contact, which results in high reproducibility (Cernak 2005; Xiong, Mahmood et al. 2013) and low mortality rate (Dixon, Clifton et al. 1991). CCI

produces a more focal injury and can reproduce injuries similar to human TBI such as breakdown of the blood-brain barrier (BBB), diffuse axonal injury (DAI), brain edema, increased intracranial pressure, and coma (Cernak 2005; Xiong, Mahmood et al. 2013). Additionally, increasing severity of injury can produce long lasting neurological deficits and gross histopathologic changes in the brain at areas distant to the injury site (Dixon, Clifton et al. 1991).

The CCI model has also shown promise as a model of PTE after TBI. Studies utilizing this model have reported spontaneous seizures after injury. Tail and neck stiffness, head nodding, and freezing behavior have been previously reported after mild and severe CCI between 42 and 71 days after TBI, as well as spontaneous tonic-clonic seizures in a limited number of mice after severe CCI (Hunt, Scheff et al. 2009; Hunt, Scheff et al. 2010). Late spontaneous seizures have also been identified electrographically. In one study, late spontaneous seizures were detected 6 months after CCI with no progression of epilepsy or epileptiform spiking up to 9 months even with a pentylenezetratole (PTZ) challenge. In this study, CCI was induced at a depth of 0.5 mm, however the cortical lesion extended throughout the layers of the cortex and the hippocampus was damaged in 60% of mice (Bolkvadze and Pitkänen 2012). In another study, a 16-week video-electroencephalographic (vEEG) monitoring revealed low frequency spontaneous seizures (average 0.55 ± 0.16 seizures/day) in ~50% of mice subjected to a severe CCI (Guo, Zeng et al. 2013).

2.2.3 Weight drop model

The weight drop model can be performed on the skull with or without a craniotomy in which the injury is produced by a free-falling weight from a designated height. The level of injury is determined by the mass of the weight and height at which it

is released (Dixon, Clifton et al. 1991; Cernak 2005). Various extensions of the weight drop model include Feeny's weight drop and Marmarou's weight drop. In Feeny's weight drop model, a cortical contusion is produced and cortical cavitation is present over 2 weeks after injury (Cernak 2005). Marmarou's model, on the other hand, represents an acceleration model which results in diffuse axonal injury (Cernak 2005; Xiong, Mahmood et al. 2013).

Although no studies to date have used long-term vEEG recordings to monitor late posttraumatic seizures in a weight drop model, increased hyperexcitability and seizure susceptibility have been previously reported. In one of the earliest studies of epileptic seizures after weight drop, EEG demonstrated generalized seizure activity 2 hours after injury (Nilsson, Ronne-Engström et al. 1994). Additionally, rats with TBI from weight drop exhibited consistently enhanced seizure susceptibility after PTZ challenge 15 weeks after injury (Golarai, Greenwood et al. 2001).

While multiple models of PTE exist, the CCI model was chosen for this study primarily due to its high reproducibility and relative ease to adjust injury parameters. Moreover, CCI was selected as the TBI model of choice because, compared with FPI, more mice developed late spontaneous seizures after CCI injury (Bolkvadze and Pitkänen 2012).

2.3 Materials and methods

2.3.1 Animals

All experiments were conducted in accordance with the National Institutes of Health guidelines and approved by the University of California, Riverside Institutional Animal Care and Use Committee. CD1 wild-type (WT) and AQP4 knockout (AQP4 KO)

adult male mice between the ages of 8 – 10 week old were used for all experiments. The mice were housed under a 12-hour light/dark cycle with water and food provided *ad libitum*.

2.3.2 Study design

This study utilized multiple research techniques to fully understand the pathophysiology of PTE. To better understand the temporal progression of PTE, I chose experimental endpoints of 14, 30, 60, and 90 days post injury (dpi). At day 0, mice received a moderate-severe TBI in the right frontal cortex and a thinned skull over the parietal bone for optical coherence tomography (OCT) imaging (Chapter 3). 10 days before each final time point, mice underwent its final OCT imaging and an indwelling EEG implanted in the ipsilateral hippocampus. After recovery of 3 days, mice underwent continuous vEEG recording for 1 week (Chapter 4). At the final experimental endpoint, electrographic seizure threshold (EST) and duration (ESD) was assessed (Chapter 4). Mice were then sacrificed for immunohistochemistry (IHC) or Western blot analysis (Chapter 5). A summary of the study design is shown in Figure 2.1.

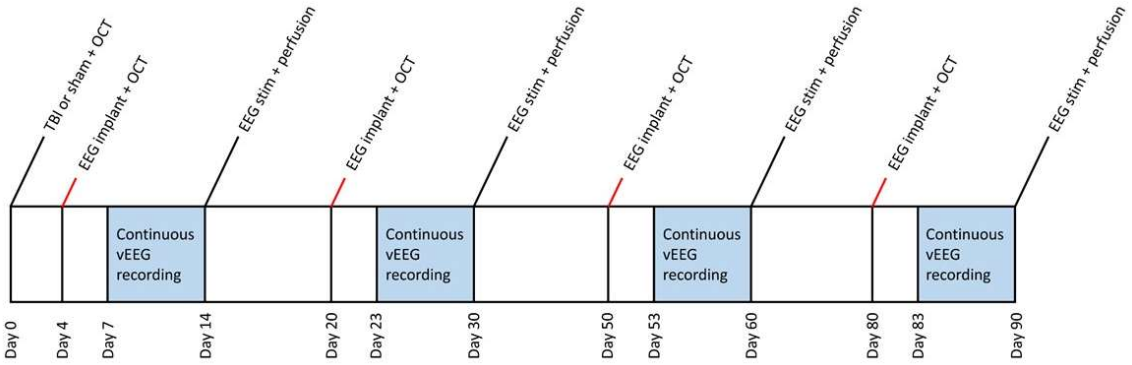

Figure 2.1 Summary of study design.

2.3.3 Surgery

Mice were anesthetized with an intraperitoneal (i.p.) injection of ketamine and xylazine (80 mg/kg ketamine, 10 mg/kg xylazine). Additional anesthesia was administered only when necessary. Once an adequate plane of anesthesia was achieved, the hairs on the scalp was removed using clippers and depilatory cream. The scalp was then disinfected with betadine solution and cleaned with 70% ethanol. Mice were then mounted onto a stereotactic frame and a midline incision was made and reflected. The fascia was gently removed and the skull was cleaned with normal saline and cotton swabs.

2.3.4 Induction of traumatic brain injury using controlled cortical impactor

The CCI model (Leica Biosystems) was used in this study. A craniotomy of ~ 2 × 2 mm^2 was created over the right frontal cortex with the dura intact (Figure 2.2). A moderate-severe TBI was then induced onto the exposed brain with a 2 mm flat impactor tip at a velocity of 5 m/s, a depth of 1 mm, and a contact time of 200 ms. After injury, the skull flap was carefully replaced and the incision was sutured. Mice were then allowed to recover over a temperature-controlled heating pad. Sham controls received a craniotomy only.

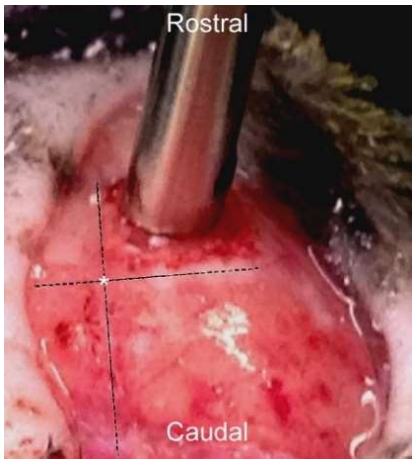

Figure 2.2 CCI model of TBI. The CCI model of TBI was used in this study. Injury was induced in the right frontal cortex with a 2 mm flat impactor tip at a velocity of 5 m/s, a depth of 1 mm, and a contact time of 200 ms onto the exposed dura. * = bregma.

2.3.5 Electrode preparation

A 3-channel two twisted stainless steel electrode (Plastics One) was used for all EEG surgeries and prepared as previously described (Lapato, Szu et al. 2017). The twisted bipolar wires were cut to 2 mm for implanting into the dorsal hippocampus and the untwisted wire was cut ~ 0.5 mm to ground in the dura. To ensure high-fidelity EEG recordings, ~ 0.5 mm of the insulating coat was removed at the distal tip of all wires. The electrodes were then sterilized with 70% ethanol and the ground position on top of the implant pedestal was marked to ensure proper placement of the pins during EEG acquisition.

2.3.6 Electrode implantation

Mice underwent EEG implant surgery 10 days prior to their final time point (14, 30, 60 and 90 dpi). Mice were immobilized in the stereotactic frame and the skull was cleaned with normal saline and cotton swabs. To create greater surface area for cementing the electrode, etching gel was applied to the skull for ~10 seconds and washed 2 – 3 times with normal saline. Stereotaxic coordinates of the hippocampus were identified (Paxinos and Franklin 2001) and a craniotomy of ~ 2 mm in diameter (to accommodate the distance between the recording and ground wires) was created with a high speed surgical hand drill with a ¼ mm HP-sized carbide bur (SS White). The skull flap was then removed and bone dust was washed off with normal saline and cotton swabs. The dura was then carefully detached using a 27 G needle. Bonding agent (Clearfil photobond) was then applied onto the skull with a microbrush (without contact to the exposed brain) and light cured for 20 seconds. Using a side clamp, the pedestal of the electrode was secured onto a probe holder and the implant was slowly lowered into the hippocampus (AP = -1.8 mm, ML = +1.6 mm from bregma) until the implant pedestal

contacted the top of the skull (~ 2 mm length of the recording wires). To secure the electrode in place, dental cement (Panavia SA cement) was applied across the skull surface and surrounding the implant and light cured for 20 seconds, followed by additional cement as necessary. After surgery completion, the animals recovered for 3 days.

2.3.7 Continuous vEEG acquisition

vEEG acquisition began 3 days after electrode implantation and lasted 7 days. During vEEG recording, mice were single housed with access to food and water *ad libitum* and freely moving. Behavioral activity was video monitored with a megapixel IP camera (HD 1080P) with infrared LED for night time recording (ELP1 CCTV) and time synced with EEG recording. Mice were recorded using either our customized wireless EEG sensor (BioPac) or a tethered system (BioPac). For wireless EEG recordings, a wireless transmitter (Epoch) was attached to the implanted EEG pedestal and the cage was placed on top of a receiving tray (Figure 2.3A). For tethered EEG recordings, mice were connected to the acquisition system via a commutator to allow for freedom of motion (Figure 2.3B). Both wireless and tethered EEG recordings were obtained using a digital acquisition system (MP150 or MP160, Acqknowledge 4.4 or Acqknowledge 5 software). Normal EEG output was amplified with a gain of 5000 and bandpass filtered from 0.1 – 35 Hz, and digitized at 625 samples/s.

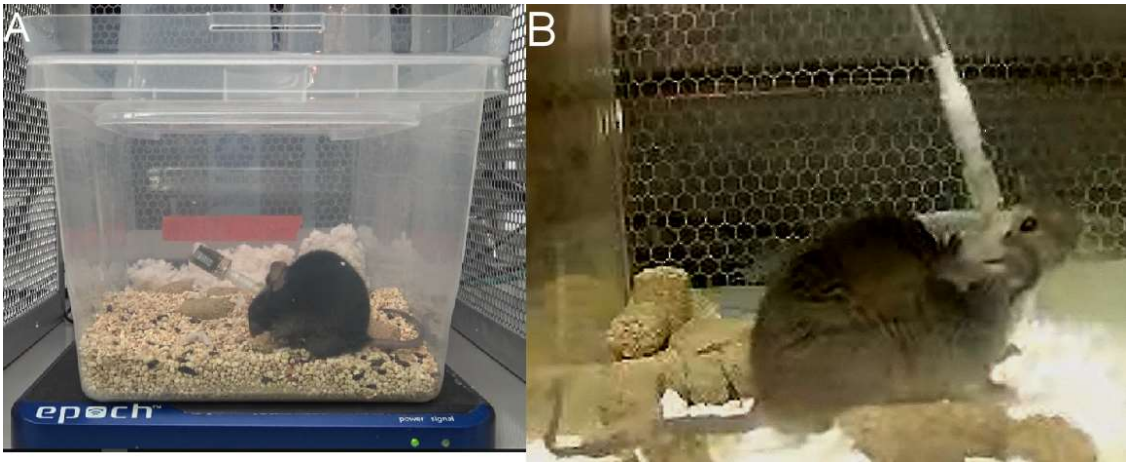

Figure 2.3 vEEG set up for chronic recording. A) Example of a mouse wearing a customized wireless EEG transmitter. The cage was then placed on top of a receiving tray for EEG recording. **B)** Example of a mouse on the EEG tethered set up. Here, a tether was connected from the EEG pedestal to a commutator to allow freedom of motion during EEG recording.

2.3.8 Confirmation of spontaneous seizures and posttraumatic epilepsy

Electrographic spontaneous seizures from the 1-week vEEG recordings were manually identified and confirmed by two blinded observers. Spontaneous seizures were defined as spiking epileptiform activity lasting continuously for at least 5 seconds at a frequency of ≥ 3Hz and double the amplitude compared to baseline. Electrographic seizures were also correlated with corresponding time-synced video for behavioral assessment. Mice with two or more spontaneous seizures were classified as having PTE.

2.3.9 Statistical analysis

A Student's t-test was performed to compare spontaneous seizure duration between WT *vs.* AQP4 KO mice and a p value of < 0.05 was deemed significant. Error bars are reported as standard error of the mean (SEM). Fisher's exact test was used to compare percent of total mice with PTE in WT and AQP4 KO mice and a p value of < 0.05 was deemed significant.

2.4 Results

2.4.1 Injury severity after TBI

This CCI model of TBI induces a moderate-severe injury. In some mice, the dura was ruptured which resulted in substantial bleeding and immediate brain swelling, indicative of vasogenic edema. In cases where the dura was not ruptured, subdural hematoma and hemorrhage were evident (Figure 2.4). One intriguing observation was that AQP4 KO mice oftentimes exhibited less bleeding and dura rupture after CCI.

Figure 2.4 Injury severity after CCI. In this example, the dura is intact and subdural hematoma and hemorrhage can be seen immediately after TBI. In other cases, dura rupture, severe bleeding, and immediate brain swelling indicative of vasogenic edema can be seen (data not shown).

2.4.2 Spontaneous seizures after TBI

To establish a working model of PTE, spontaneous recurrent seizures must be observed at least 1 week after the initial trauma. Electrographic spontaneous seizures were detected at each time point after TBI in both genotypes and correlated with corresponding video for behavioral assessment. Nonconvulsive seizures were observed that correlated with the electrographic seizures. Behaviorally, seizures were characterized primarily by motor arrest with occasional facial clonus based on the modified Racine scale (Table 2.1) (Ihara, Tomonoh et al. 2016). In rare cases, mice exhibited tail stiffness, limb clonus, and incessant grooming. A single WT mouse exhibited early posttraumatic seizures during handling where immobility, jumping, rearing, and falling behavior were observed. Sham mice remained seizure-free with the

exception of one mouse in each genotype which displayed a single seizure at 60 days (WT) and 14 days (AQP4 KO) post craniotomy. No sham mice exhibited PTE.

Score	Behavioral stage
0	No behavioral change
1	Sudden behavioral arrest with orofacial automatism
2	Head nodding
3	Forelimb clonus with lordotic posture
4	Forelimb clonus with rearing and falling
5	Generalized tonic-clonic activity with loss of postural tone

Table 2.1 Modified Racine scale for classification of behavioral seizures.

Electrographically, most seizure onset was sudden with increased frequency and amplitude (fast polyspike) followed by return to baseline. Other seizures initiated from a ramp-up of baseline and developed into a full seizure or spikes of at least 3 Hz was observed. Figure 2.5 shows different electrographic seizure morphologies captured during the 1-week vEEG recording.

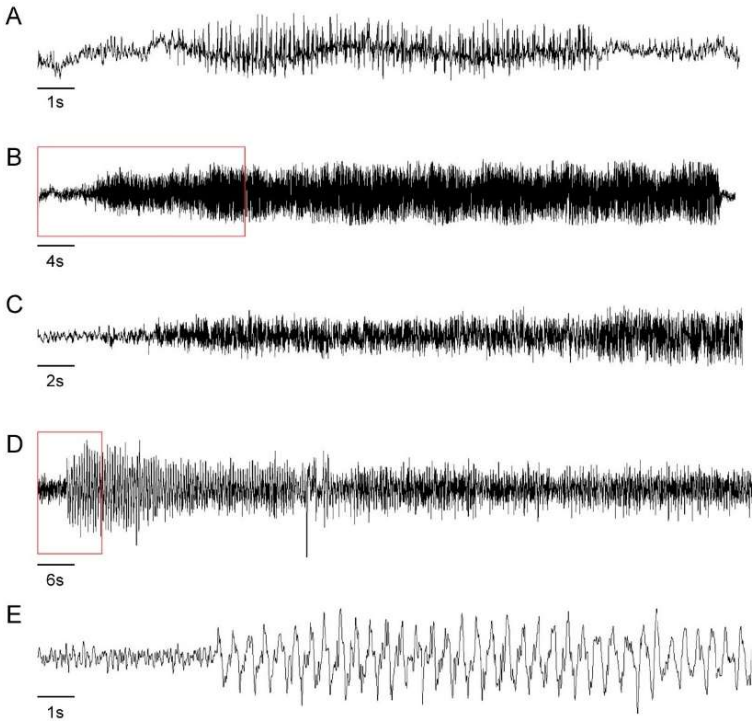

Figure 2.5 Morphology of spontaneous seizures. Examples of different electrographic seizure morphology. **A)** Typical spontaneous seizure with increased frequency and amplitude (fast polyspike) followed by return to baseline. **B)** A seizure initiated from a ramp-up of baseline and developed into full seizure. **C)** Expanded EEG from red boxed area in B demonstrating baseline gradually increasing in amplitude and developing into a full seizure. **D)** A seizure exhibiting 3 Hz spikes. **E)** Expanded EEG from red boxed area in D.

Interestingly, AQP4 KO mice exhibited more spontaneous seizures after TBI compared with WT mice. The number of WT mice that developed spontaneous seizures are 1/8 (13%), 3/10 (30%), 4/12 (33%), and 2/7 (29%) at 14, 30, 60, and 90 dpi, respectively. The total number of seizures in WT mice are 4, 8, 20, and 6 at 14, 30, 60, and 90 dpi, respectively. The number of AQP4 KO mice that developed spontaneous seizures are 4/7 (57%), 5/13 (38%), 3/6 (50%), and 0/4 (0%) at 14, 30, 60, and 90 dpi, respectively. The total number of seizures in WT mice are 4, 8, 20, and 6 at 14, 30, 60, and 90 dpi, respectively. The total number of seizures in AQP4 KO mice are 19, 26, and 11, and 0 at 14, 30, and 60 dpi, respectively (Table 2.2). Additionally, seizure duration in AQP4 KO mice (24.27 ± 2.832 s) were remarkably longer compared with WT mice (15.26 ± 1.847 s) after TBI (Figure 2.6A).

Genotype	Timepoint	Number of mice with seizures	Number of seizures	Number of mice with PTE
WT	14D	1/8 (13%)	4	1/8 (13%)
	30D	3/10 (30%)	8	2/10 (20%)
	60D	4/11 (36%)	20	3/11 (27%)
	90D	2/7 (29%)	6	1/7 (14%)
Total		**10/36 (28%)**	**38**	**6/36 (17%)**
AQP4 KO	14D	4/7 (57%)	19	2/7 (29%)
	30D	5/13 (38%)	26	4/13 (31%)
	60D	3/6 (50%)	11	2/6 (33%)
	90D	0/4 (0%)	0	0/4 (0%)
Total		**12/30 (40%)**	**56**	**8/30 (27%)**

Table 2.2 Spontaneous seizures observed after TBI.

It is expected that not all TBI will result in the development of PTE. Thus, the total number of mice that developed PTE was also calculated. Although not statistically significant, the development of PTE was higher in AQP4 KO mice (8/30, 27%) compared with WT mice (6/36, 17%; Figure 2.6B). In WT mice, the number of mice that developed

PTE are 1/8 (13%), 2/10 (20%), 3/11 (27%), and 1/7 (14%) at 14, 30, 60, and 90 dpi, respectively. In AQP4 KO mice, the number of that developed PTE are 2/7 (29%), 4/13 (31%), 2/6 (33%), and 0/4 (0%) at 14, 30, 60, and 90 dpi, respectively (Table 2.2).

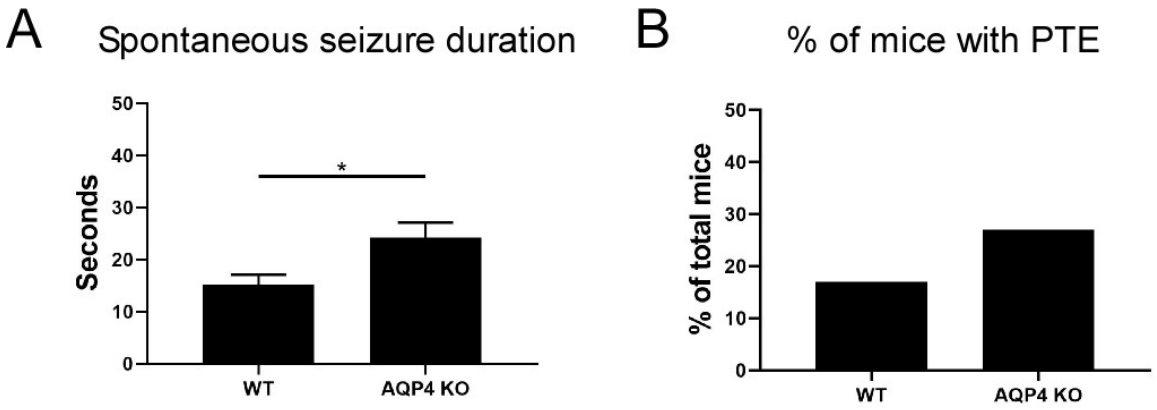

Figure 2.6 AQP4 KO mice have longer seizure duration and greater incidence of PTE. A) AQP4 KO mice had significantly longer seizure duration (24.24 ±2.832 seconds) compared with WT mice (15.26 ± 1.847 seconds) after TBI (Student's t-test, p = 0.0177). **B)** A greater percentage of AQ4 KO mice (27%) developed PTE compared with WT mice (17%) (Fisher's exact test, p = 0.6127).

2.5 Discussion

The present study was designed to provide a model of PTE for potential biomarker development. The frontal lobe was chosen as the location for the TBI due its impact on epileptogenesis. Human and preclinical studies have shown frontal lesions as a significant risk factor for PTE (Pohlmann-Eden and Bruckmeir 1997; Hudak, Trivedi et al. 2004; D'Ambrosio, Fender et al. 2005; Curia, Levitt et al. 2010). In a unilateral contusion, the probability of late posttraumatic seizures from frontal, temporal, and parietal locations was 20%, 16%, and 19%, respectively; whereas in bilateral contusions, the risk for epilepsy from frontal, temporal and parietal locations was 26%, 31%, and 66%, respectively (Englander, Bushnik et al. 2003). Additionally, compared with injury induced in the medial-parietal and caudal-parietal cortex, FPI in the rostral-parietal cortex resulted in higher seizure frequency (Curia, Levitt et al. 2010). Based on these

findings, it is expected that animals in my studies would have a higher probability of developing epilepsy from a brain injury arising in the frontal cortex.

The CCI injury model used in this study induced a moderate-severe focal contusion with dura rupture and subdural hemorrhage. In this model, animals displayed nonconvulsive subclinical seizures. Behaviorally, the mice showed motor arrests with facial automatisms. Nonconvulsive spontaneous seizures have also been previously reported in humans with moderate-severe TBI (Vespa, Nuwer et al. 1999) and rodent models of PTE (Curia, Levitt et al. 2010; Rodgers, Dudek et al. 2015), thus supporting the translational aspect of this model. Immobility observed during seizure activity could also correlate with loss of consciousness. Unfortunately, loss of consciousness cannot be graded or scored in animal models but has been seen in patients with temporal lobe epilepsy (TLE). vEEG studies in patients with TLE reported motionless staring, oral automatisms, and loss of consciousness (Escueta, Kunze et al. 1977; Maldonado, Delgado-Escueta et al. 1988).

Seizures in TLE are generally characterized as either complex-partial seizure or simple-partial seizures. Interestingly, complex-partial seizures are associated with impaired consciousness, inhibition of motor activity, and automatisms associated with unresponsiveness (ILAE 1981; ILAE 1989) and have been shown to be an important component of PTE (Becker, Grossman et al. 1979; D'Ambrosio and Miller 2010; Raymont, Salazar et al. 2010). Loss of consciousness can also be correlated with large-amplitude cortical oscillations in the neocortex. Indeed, TLE patients with complex-partial seizures not only showed fast polyspike seizures in the temporal lobe, but also large amplitude slow activity in the frontoparietal neocortices. These slow waves continued into the postictal period and during impaired consciousness (Blumenfeld,

Rivera et al. 2004). While the mechanisms underlying this phenomenon remain unknown, a “network inhibition” hypothesis has been postulated suggesting that seizures from the temporal lobe propagates to subcortical structures leading to cortical deactivation and subsequent inhibition of consciousness (Norden and Blumenfeld 2002). Therefore, in this study, when the mice are experiencing a non-convulsive seizure in the hippocampus, the seizure may potentially spread to nearby cortical structures to inhibit its level of consciousness. Future studies utilizing multiple electrodes in various areas of the brain may help in validating the network inhibition hypothesis.

Experimental studies have also found that the frontal cortex is highly susceptible to seizures regardless of injury location. After FPI in the rostral-parietal cortex, the incidence and severity of seizures arising from the frontal cortex were higher compared to seizures in the parietal or occipital cortices. Furthermore, limbic seizures were found to proceed more slowly (several months after TBI) than cortical seizures (D'Ambrosio, Fender et al. 2005; Curia, Levitt et al. 2010). In my study, a single electrode was used to monitor for hippocampal seizures after TBI in the frontal cortex. Although spontaneous seizures were observed as early 14 days after TBI, the majority of the seizures in both genotypes were seen at 60 dpi (33% in WT mice and 50% in AQP4 KO mice, Table 2.2). An explanation for this may be the fact that the hippocampus is distant from the injury site (frontal cortex) and the injury sustained in the hippocampus is mild. Thus, seizures generating from the hippocampus may not be evident until later. Another possibility is that focal seizures that begin in the frontal neocortex can spread and kindle the hippocampus (D'Ambrosio, Fender et al. 2005; Curia, Levitt et al. 2010) via cortico-cortico or cortico-subcortical pathways (D'Ambrosio, Fender et al. 2005). Thus, in this model, seizures may possibly initiate from the perilesional cortex (adjacent to the impact

site) and spread to subcortical areas that would ultimately kindle connections to the hippocampus, making the hippocampus more susceptible to seizures at later times after injury.

Based on my findings, most of the hippocampal spontaneous seizures occurred at the 30- and 60-day time points. WT mice exhibited 8 seizures at 30 dpi and 20 seizures at 60 dpi. On the other hand, AQP4 KO mice had 26 seizures at 30 dpi and only 11 seizures at 60 dpi. By 90 days, only 6 seizures were observed in WT mice while APQ4 KO mice, surprisingly, did not have any spontaneous seizures by 90 dpi. Interestingly, studies utilizing the CCI model of PTE in mice showed ~ 8 – 9 % spontaneous cortical seizures 6 months after injury and no spontaneous cortical seizures 9 months after injury even with a PTZ challenge within 6 months after CCI (Bolkvadze and Pitkänen 2012). In this case, CCI was induced at a depth of 0.5 mm over the parieto-temporal cortex where the underlying hippocampus is particularly vulnerable to injury even at a shallow impact. Unfortunately, hippocampal EEG recordings were not performed in that study and thus it is not clear whether hippocampal seizures were also occurring at 6 or 9 months post injury.

In a separate study, 36 – 40% spontaneous seizures were reported in mice after CCI (Hunt, Scheff et al. 2009; Hunt, Scheff et al. 2010). The percentage of spontaneous seizures related to late posttraumatic seizures (seizures that occur at least 1 week after the initial TBI and represents the true manifestation of PTE) remains unclear. This is primarily due to lack of EEG recordings and only random visual observation for spontaneous seizures in 1 – 2 hour intervals up to 10 weeks post injury (Hunt, Scheff et al. 2009; Hunt, Scheff et al. 2010). Similar to many experimental models of PTE, the TBI was also performed over the parietotemporal cortex where the underlying hippocampus

is highly susceptible to injury. Indeed, the authors reported increased excitatory postsynaptic current (EPSC) from hippocampal slices with overt mossy fiber sprouting (MFS), suggesting newly formed excitatory networks between the dentate granule cells and the injured cortex (Hunt, Scheff et al. 2010). Therefore, in my studies, spontaneous hippocampal seizures may be caused by newly formed excitatory connections induced by the injury in the frontal cortex.

In total, AQP4 KO mice developed more posttraumatic seizures (56 seizures) compared with WT mice (39 seizures) and a higher percentage of AQP4 KO mice developed PTE compared with WT mice (Figure 2.6B). This was an unanticipated finding because TBI induced in most AQP4 KO mice was less severe which hinted at the possibility of WT mice exhibiting more PTE compared with AQP4 KO mice. Interestingly, in an intrahippocampal kainic acid (IHKA) model of temporal lobe epilepsy (TLE), AQP4 KO mice exhibited more spontaneous seizures during the epileptogenic period compared with WT mice (Lee, Hsu et al. 2012). In the same model, a dramatic increase in AQP4 protein level was observed 30 days after induction of status epilepticus (SE) (Hubbard, Szu et al. 2016). In the present study, WT mice had 5, 8, 20, and 6 spontaneous seizures 14, 30, 60 and 90 dpi, respectively, while AQP4 KO mice had 19, 26, and 11 spontaneous seizures 14, 30, and 60 dpi, respectively, and no seizures at 90 dpi (Table 2.2). This suggests that AQP4 may play a neuroprotective role in the development of PTE, particularly at the 30-day time point. However, the numbers of seizures decreased by 60 dpi (20 seizures in WT mice and 11 seizures in AQP4 KO mice) suggests that compensatory mechanisms in AQP4 KO mice may be present at later time points to attenuate seizures.

Altered expression and subcellular localization of AQP4 was found in postmortem sclerotic hippocampi from patients with mesial TLE (Eid, Lee et al. 2005) and in IHKA (Alvestad, Hammer et al. 2013) and pilocarpine-induced epilepsy models (Kim, Ryu et al. 2009; Kim, Yeo et al. 2010). Although an overall increased AQP4 expression was found in the sclerotic hippocampus in human TLE (Lee, Eid et al. 2004), reduction in perivascular AQP4 was observed (Eid, Lee et al. 2005). Furthermore, levels of AQP4 in astrocytic endfeet facing capillaries were reduced 14 days and 11 weeks after induction of SE (Alvestad, Hammer et al. 2013). This suggests that loss of AQP4 polarization at the endfeet begins as early as 14 dpi leading to overall mislocalization of AQP4 and increased number of seizures by 60 dpi. However, by 90 dpi, compensatory mechanisms in the hippocampus (such as remodeling of inhibitory hippocampal circuits) may transpire to reduce neuronal hyperexcitability leading to decreased numbers of spontaneous seizures.

Overall, findings from this study support this model as a useful and translational tool for studying PTE in the preclinical context. Specifically, this model has the highest yield for PTE after CCI in mice and. suggests an altered network connectivity between the frontal cortex and the hippocampus after TBI.

2.6 References

Alder, J., Fujioka, W., et al. (2011). "Lateral fluid percussion: model of traumatic brain injury in mice." J Vis Exp(54).

Alvestad, S., Hammer, J., et al. (2013). "Mislocalization of AQP4 precedes chronic seizures in the kainate model of temporal lobe epilepsy." Epilepsy research **105**(1-2): 30-41.

Becker, D. P., Grossman, R. G., et al. (1979). "Head injuries—panel 3." Archives of neurology **36**(12): 750-758.

Blumenfeld, H., Rivera, M., et al. (2004). "Ictal neocortical slowing in temporal lobe epilepsy." Neurology **63**(6): 1015-1021.

Bolkvadze, T. and Pitkänen, A. (2012). "Development of post-traumatic epilepsy after controlled cortical impact and lateral fluid-percussion-induced brain injury in the mouse." J Neurotrauma **29**(5): 789-812.

Carbonell, W. S., Maris, D. O., et al. (1998). "Adaptation of the fluid percussion injury model to the mouse." J Neurotrauma **15**(3): 217-229.

Cernak, I. (2005). "Animal models of head trauma." NeuroRx **2**(3): 410-422.

Curia, G., Levitt, M., et al. (2010). "Impact of injury location and severity on posttraumatic epilepsy in the rat: role of frontal neocortex." Cerebral cortex **21**(7): 1574-1592.

D'Ambrosio, R., Fender, J. S., et al. (2005). "Progression from frontal–parietal to mesial–temporal epilepsy after fluid percussion injury in the rat." Brain **128**(1): 174-188.

D'Ambrosio, R., Fairbanks, J. P., et al. (2004). "Post-traumatic epilepsy following fluid percussion injury in the rat." Brain **127**(2): 304-314.

D'Ambrosio, R. and Miller, J. W. (2010). "What is an epileptic seizure? Unifying definitions in clinical practice and animal research to develop novel treatments." Epilepsy currents **10**(3): 61-66.

Dixon, C. E., Clifton, G. L., et al. (1991). "A controlled cortical impact model of traumatic brain injury in the rat." J Neurosci Methods **39**(3): 253-262.

Eid, T., Lee, T.-S. W., et al. (2005). "Loss of perivascular aquaporin 4 may underlie deficient water and K+ homeostasis in the human epileptogenic hippocampus." Proceedings of the National Academy of Sciences **102**(4): 1193-1198.

Englander, J., Bushnik, T., et al. (2003). "Analyzing risk factors for late posttraumatic seizures: a prospective, multicenter investigation." Archives of physical medicine and rehabilitation **84**(3): 365-373.

Escueta, A. V., Kunze, U., et al. (1977). "Lapse of consciousness and automatisms in temporal lobe epilepsy A videotape analysis." Neurology **27**(2): 144-144.

Golarai, G., Greenwood, A. C., et al. (2001). "Physiological and structural evidence for hippocampal involvement in persistent seizure susceptibility after traumatic brain injury." Journal of Neuroscience **21**(21): 8523-8537.

Guo, D., Zeng, L., et al. (2013). "Rapamycin attenuates the development of posttraumatic epilepsy in a mouse model of traumatic brain injury." PLoS One **8**(5): e64078.

Hubbard, J. A., Szu, J. I., et al. (2016). "Regulation of astrocyte glutamate transporter-1 (GLT1) and aquaporin-4 (AQP4) expression in a model of epilepsy." Experimental neurology **283**: 85-96.

Hudak, A. M., Trivedi, K., et al. (2004). "Evaluation of seizure-like episodes in survivors of moderate and severe traumatic brain injury." J Head Trauma Rehabil **19**(4): 290-295.

Hunt, R. F., Scheff, S. W., et al. (2009). "Posttraumatic epilepsy after controlled cortical impact injury in mice." Exp Neurol **215**(2): 243-252.

Hunt, R. F., Scheff, S. W., et al. (2010). "Regionally localized recurrent excitation in the dentate gyrus of a cortical contusion model of posttraumatic epilepsy." J Neurophysiol **103**(3): 1490-1500.

Ihara, Y., Tomonoh, Y., et al. (2016). "Retigabine, a Kv7. 2/Kv7. 3-channel opener, attenuates drug-induced seizures in knock-in mice harboring Kcnq2 mutations." PloS one **11**(2): e0150095.

ILAE (1981). "Proposal for revised clinical and electroencephalographic classification of epileptic seizures." Epilepsia **22**(4): 489-501.

ILAE (1989). "Proposal for revised classification of epilepsies and epileptic syndromes." Epilepsia **30**(4): 389-399.

Kabadi, S. V., Hilton, G. D., et al. (2010). "Fluid-percussion-induced traumatic brain injury model in rats." Nat Protoc **5**(9): 1552-1563.

Kharatishvili, I., Nissinen, J., et al. (2006). "A model of posttraumatic epilepsy induced by lateral fluid-percussion brain injury in rats." Neuroscience **140**(2): 685-697.

Kim, J.-E., Ryu, H., et al. (2009). "Differential expressions of aquaporin subtypes in astroglia in the hippocampus of chronic epileptic rats." Neuroscience **163**(3): 781-789.

Kim, J. E., Yeo, S. I., et al. (2010). "Astroglial loss and edema formation in the rat piriform cortex and hippocampus following pilocarpine-induced status epilepticus." Journal of Comparative Neurology **518**(22): 4612-4628.

Lapato, A. S., Szu, J. I., et al. (2017). "Chronic demyelination-induced seizures." Neuroscience **346**: 409-422.

Lee, D. J., Hsu, M. S., et al. (2012). "Decreased expression of the glial water channel aquaporin-4 in the intrahippocampal kainic acid model of epileptogenesis." Experimental neurology **235**(1): 246-255.

Lee, T. S., Eid, T., et al. (2004). "Aquaporin-4 is increased in the sclerotic hippocampus in human temporal lobe epilepsy." Acta neuropathologica **108**(6): 493-502.

Maldonado, H., Delgado-Escueta, A., et al. (1988). "Complex partial seizures of hippocampal and amygdalar origin." Epilepsia **29**(4): 420-433.

McIntosh, T. K., Vink, R., et al. (1989). "Traumatic brain injury in the rat: characterization of a lateral fluid-percussion model." Neuroscience **28**(1): 233-244.

Nilsson, P., Ronne-Engström, E., et al. (1994). "Epileptic seizure activity in the acute phase following cortical impact trauma in rat." Brain research **637**(1-2): 227-232.

Norden, A. D. and Blumenfeld, H. (2002). "The role of subcortical structures in human epilepsy." Epilepsy & Behavior **3**(3): 219-231.

Paxinos, G. and Franklin, K. (2001). "The mouse brain atlas in stereotaxic coordinates." San Diego, CA: Academic.

Pitkänen, A. and McIntosh, T. K. (2006). "Animal models of post-traumatic epilepsy." J Neurotrauma **23**(2): 241-261.

Pohlmann-Eden, B. and Bruckmeir, J. (1997). "Predictors and dynamics of posttraumatic epilepsy." Acta neurologica scandinavica **95**(5): 257-262.

Raymont, V., Salazar, A. M., et al. (2010). "Correlates of posttraumatic epilepsy 35 years following combat brain injury." Neurology **75**(3): 224-229.

Rodgers, K. M., Dudek, F. E., et al. (2015). "Progressive, Seizure-Like, Spike-Wave Discharges Are Common in Both Injured and Uninjured Sprague-Dawley Rats: Implications for the Fluid Percussion Injury Model of Post-Traumatic Epilepsy." J Neurosci **35**(24): 9194-9204.

Vespa, P. M., Nuwer, M. R., et al. (1999). "Increased incidence and impact of nonconvulsive and convulsive seizures after traumatic brain injury as detected by continuous electroencephalographic monitoring." Journal of neurosurgery **91**(5): 750-760.

Xiong, Y., Mahmood, A., et al. (2013). "Animal models of traumatic brain injury." Nat Rev Neurosci **14**(2): 128-142.

Chapter 3: Optical biomarkers of posttraumatic epilepsy

3.1 Abstract

Posttraumatic epilepsy (PTE) is a serious neurological consequence of traumatic brain injury (TBI) and accounts for approximately 4% of focal epilepsy in the general population. Unfortunately, no treatments exist for PTE and accurate characterization and identification of PTE markers are needed. Neuroimaging is one approach to identify predictors of PTE, however, human and animal imaging studies are lacking. Here, optical coherence tomography (OCT) imaging was employed to quantitatively assess the optical attenuation coefficient (μ) in the brain 4, 20, 50, and 80 days after TBI in wildtype (WT) and aquaporin-4 knockout (AQP4 KO) mice. In this study, WT and AQP4 KO mice were subjected to a severe TBI in the right frontal cortex using the controlled cortical impact (CCI) injury device and OCT imaging was performed in the parietal cortex over a thinned skull. No significant differences in μ between sham and TBI were observed at all timepoints in both WT and AQP4 KO mice. However, in the sham groups, AQP4 KO mice exhibited higher μ compared with WT mice. Future OCT studies with greater sensitivity and specificity will allow more detailed analysis of the hippocampus and other regions of the brain for direct correlation with mice that developed PTE.

3.2 Introduction

PTE is a serious neurological consequence of TBI and accounts for approximately 4% of focal epilepsy in the general population (Kumar, Gupta et al. 2003; Gupta, Sayed et al. 2014). Although factors contributing to the onset of PTE remain unclear, it is generally accepted that risks of developing PTE include early posttraumatic

seizures, prolonged unconsciousness, and severity of injury (Kumar, Gupta et al. 2003; Gupta, Saksena et al. 2005).

In some cases, PTE is medically refractory (Kumar, Gupta et al. 2003; Kharatishvili, Immonen et al. 2007; Gupta, Sayed et al. 2014) and prophylactic antiepileptic treatments have proven to be unsuccessful (Temkin, Dikmen et al. 1990; Temkin, Dikmen et al. 1999). Thus, accurate characterization and identification of PTE markers must be defined for the successful treatment and management of patients after a TBI to prevent the development of epilepsy.

The use of neuroimaging techniques has been one approach to identify new risk factors and predictors of PTE. Depending on the type of injury, mechanisms of TBI may include events such as hemoglobin breakdown, axonal injury, gliosis, and cell death (Diaz-Arrastia, Agostini et al. 2000). These pathological features may be detected by imaging modalities such as magnetic resonance imaging (MRI). Indeed, studies have shown that hemosiderin deposits can be detected with MRI (Angeleri, Majkowski et al. 1999; Wilde, Hunter et al. 2005) and the presence of iron and other metals have been linked to PTE (Willmore, Sypert et al. 1978; Angeleri, Majkowski et al. 1999). Extensions of MRI such as magnetization transfer (MT) MRI and diffusion tensor imaging (DTI) have also been employed to image patients with PTE. In a study on TBI patients with and without seizures 1 – 10 years after head trauma, T1-weighted MT MRI showed significantly higher intractable seizure (12 out of 13 patients) in delayed PTE that was associated with gliosis around the hemosiderin deposit (Kumar, Gupta et al. 2003). In another study, DTI was performed in chronic TBI patients with and without epilepsy. Interestingly, the mean regional fractional anisotropy was significantly lower in patients

with PTE than patients without PTE, suggesting increased gliosis (Gupta, Saksena et al. 2005).

MRI has also been utilized to develop potential imaging biomarkers of PTE in animal models. In a quantitative MRI study using a lateral fluid percussion injury (FPI) TBI model in rats, the authors showed that the average diffusion coefficient (Dav) in the hippocampus ipsilateral to injury was positively correlated with the density of mossy fiber sprouting and increased seizure susceptibility 11 months after TBI (Kharatishvili, Immonen et al. 2007). In a later study, the same group extended the MRI analysis on the existing data and saw that a change in interaction between water and macromolecules in the perilesional cortex demonstrated the greatest predictive value for seizure susceptibility at 9 and 23 days after TBI, whereas the Dav in the thalamus 2 months after TBI was the best biomarker. However, the greatest predictive value of all biomarkers was attained by combining the Dav values in the perilesional cortex and the thalamus 2 months after TBI (Immonen, Kharatishvili et al. 2013).

While MRI has been the imaging modality of choice in studying PTE, other imaging techniques can also be applied to identify potential predictors of PTE. Optical imaging approaches have emerged as a promising tool to image the brain *in vivo* and are based on the interaction between light and the living tissue. When the brain is illuminated, the intrinsic optical signal (IOS) reflects less light in active areas compared to nonactive areas (Frostig, Masino et al. 1995) and is thought to be generated by hemodynamic responses (Haglund and Hochman 2004). Analysis of the IOS has been investigated in human (Haglund and Hochman 2004; Zhao, Suh et al. 2007) and animal models of epilepsy (Bahar, Suh et al. 2006). In human epilepsy studies, IOS detected and localized the largest blood volume changes in the seizure focus (Haglund and

Hochman 2004; Zhao, Suh et al. 2007) which was consistent in a rat model of focal seizures (Bahar, Suh et al. 2006). Although IOS imaging shows promise in measuring brain activity, various drawbacks of this technique limit enthusiasm. First, IOS imaging has a shallow imaging range (~ 600 μm) (Frostig, Masino et al. 1995), thus restricting imaging in deeper cortical layers or brain regions. Second, signals produced by IOS rely on changes in hemodynamic responses which requires imaging at multiple wavelengths. For instance, blood volume changes requires the wavelength of 570 nm, whereas alterations in oximetry utilizes the wavelength of 600 nm (Frostig, Masino et al. 1995).

An alternative approach to IOS imaging is OCT, a minimally invasive imaging technique capable of producing cross-sectional images of the biological sample with micrometer resolution and an imaging depth in the order of millimeters (Rodriguez, Szu et al. 2014). Since its inception in the early 1990s, applications of OCT have evolved drastically. From ophthalmic and arterial imaging, extensions of OCT have been adapted for various functions such as optical biopsy and medical diagnostics (Fujimoto, Pitris et al. 2000). Due to its distinctive advantages over other imaging modalities, applications of OCT in neuroimaging are emerging.

In previous studies, I demonstrated the ability of OCT to reliably detect intrinsic optical changes in the mouse cortex using seizure and cerebral edema models *in vivo*. In the generalized seizure model, OCT was able to detect a decrease in intensity after injection of pentylenetetrazole (PTZ) prior to the clinical manifestation of the seizure (Eberle, Reynolds et al. 2012). These preliminary findings were extended in a later study using both a generalized and focal seizure model to analyze changes in optical attenuation coefficient (μ) in the mouse cortex *in vivo*. In these studies, OCT was able to differentiate between focal and generalized seizures and localize depth dependent

changes in attenuation after induction of focal seizures (Eberle, Hsu et al. 2015). Furthermore, in a water intoxication model of cytotoxic edema, OCT detected a decrease in intensity ~7 minutes after induction of cerebral edema which was positively correlated with an increase in brain water content (Rodriguez, Szu et al. 2014).

Thus, with previous successful applications of OCT in models of focal and generalized seizure and cerebral edema, I hypothesized that OCT can identify potential biomarkers of PTE in a mouse model. In these studies, I used OCT to investigate changes in optical properties of the mouse cortex over time after injury. OCT imaging was performed at various time points after injury in wildtype (WT) and aquaporin-4 knockout (AQP4 KO) mice and μ was examined and quantified. Thus, OCT derived optical signals have the potential to contribute to the understanding of: 1) how the brain changes structurally and functionally after injury; 2) how AQP4 contributes to alterations in the brain after TBI; and 3) how changes in the mouse cortex after injury contributes to the development of epilepsy.

3.3 Materials and methods

3.3.1 Animals

All experiments were conducted in accordance with the National Institutes of Health guidelines and approved by the University of California, Riverside Institutional Animal Care and Use Committee. CD1 WT and AQP4 KO adult male mice between the ages of 8 – 10 weeks old were used for all experiments. The mice were housed under a 12-hour light/dark cycle with water and food provided *ad libitum*. Please refer to Chapter 2 for experimental methods regarding the injury model and a summary of the study design.

3.3.2 Surgery

3.3.2.1 Thinned skull cranial window for optical imaging

On day 0, prior to the induction of TBI, a thinned skull cranial window was created to obtain baseline OCT images. Mice were anesthetized with an intraperitoneal (i.p.) injection of ketamine and xylazine (80 mg/kg ketamine, 10 mg/kg xylazine) and additional anesthesia was administered as needed. Once an adequate plane of anesthesia was achieved, the hairs on the scalp were removed using clippers and depilatory cream and the scalp was disinfected with betadine solution and cleaned with 70% ethanol. Mice were then mounted onto a stereotactic frame and a midline incision was made and reflected. Using various dental burs a 4 × 4 mm^2 thinned skull cranial window was created over the parietal bone as previously described (Szu, Eberle et al. 2012). The thinned skull allowed for greater light depth penetration and preserved the natural state of the brain.

3.3.3 Optical coherence tomography imaging

Mice were subjected to 2 OCT imaging: 1) baseline OCT imaging at day 0 and 2) final OCT imaging 10 days prior to the experimental endpoint (14, 30, 60, and 90 days post injury; dpi). For the final OCT imaging, mice were anesthetized as described above and the sutures were carefully removed. Using normal saline and cotton swabs, the underlying soft scar tissue was then gently isolated from the previously thinned skull. Animals were then immobilized on a stereotactic frame and placed under the OCT objective for imaging.

A spectral-domain OCT system centered at 1300 nm was used to image the mouse brain *in vivo* (Figure 3.1). The light source consisted of two superluminescent

diodes with a combined center wavelength of 1298 nm with a 120 nm full-width half maximum bandwidth (Thorlabs, Inc.). Light was sent through a fiberoptic circulator and split with an 80/20 fiber coupler between the sample and reference arms. The reflected light from both the sample and reference arms was recombined at the splitter, dispersed by a grating (1100 lines per mm, Wasatch Photonics), and detected on the 1024-pixel line scan camera (Goodrich SUI SU-LDH linear digital high speed InGaAs camera). The imaging system has an axial imaging depth of ~2 mm in the biological sample, and axial and lateral resolutions of 8 and 20 μm, respectively. OCT volumetric data were acquired with 2048 A-lines and 250 images were used to render a single volume. One OCT volume was obtained during each imaging session.

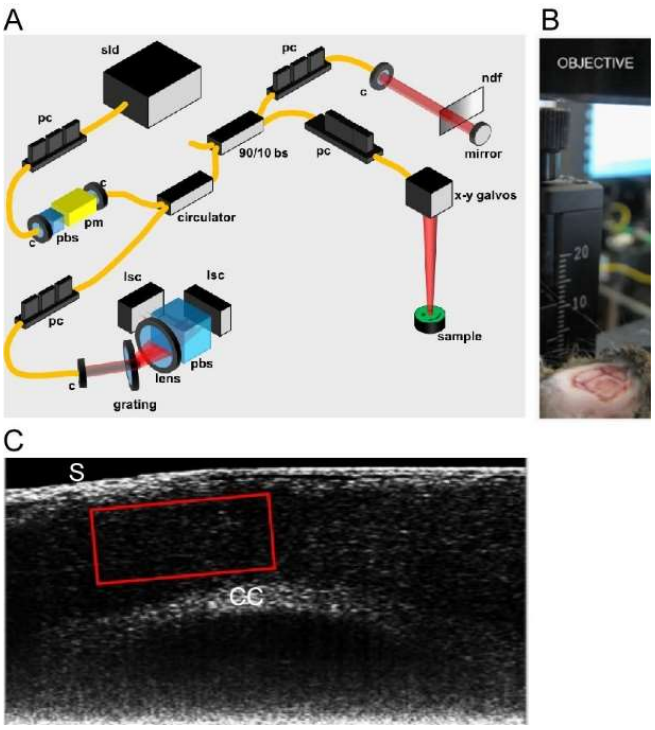

Figure 3.1 In vivo OCT imaging. A) Schematic of OCT system. sld = super-luminescent diodes, pc = polarization controller, c = collimator, pbs = polarization beam splitter, pm = polarization modulator, bs = beam splitter, ndf = neutral density filter, lsc = line scan cameras. **B)** The mouse brain is placed under the OCT objective for in vivo OCT imaging. **C)** In vivo sagittal attenuation image of the mouse brain. S = surface of the thinned skull, CC = corpus callosum, and red box delineates the ROI used for quantifying attenuation coefficient values

3.3.3.1 Analysis of optical attenuation coefficient

As coherent light travels through a sample its power is attenuated due to scattering and absorption. Attenuation coefficient, or μ, is an optical property of a sample and describes how strongly it scatters and absorbs light and thus, can provide information regarding the composition of the sample (Vermeer, Mo et al. 2014). In this study, the average attenuation of the cortex was quantified to determine the effects of trauma. An attenuation image was created from an OCT intensity image and μ was calculated on a pixel-by-pixel basis as previously described (Vermeer, Mo et al. 2014). All pixels within the region of interest (ROI) was included in the calculation (Figure 3.1C).

3.4 Statistical analysis

Comparison of sham and TBI groups at each time point for each genotype was performed using one-way ANOVA with Tukey's multiple comparison test. Comparison of sham *vs*. TBI at each time point between WT and AQP4 KO was performed using two-way ANOVA with Bonferroni's *post hoc* multiple comparison test. All error bars are represented as mean ± standard error of the mean (SEM). Differences were considered statistically significant when p value < 0.05. N's for all time points are the following: WT sham 0 day = 45, 4 day = 9, 20 day = 9, 50 day = 17, 80 day = 10; WT TBI day 0 = 58, day 4 = 9, day 20 = 9, day 50 = 17, day 80 = 10; AQP4 KO sham day 0 = 37, day 4 = 7, day 20 = 11, day 50 = 11, day 80 = 7; AQP4 KO TBI day 0 = 39, day 4 = 12, day 20 = 11, day 50 = 6, day 80 = 10. Day 0 n's is the sum of each time point for each treatment. All statistical analysis was performed using GraphPad Prism 8.

3.5 Results

3.5.1 Significant increase in μ in AQP4 KO mice after craniotomy

The average μ between sham and TBI was compared for both WT and AQP4 KO mice at all time points was analyzed for each treatment at all time points. No significant changes in μ were observed between sham and TBI groups for WT and AQP4 KO mice

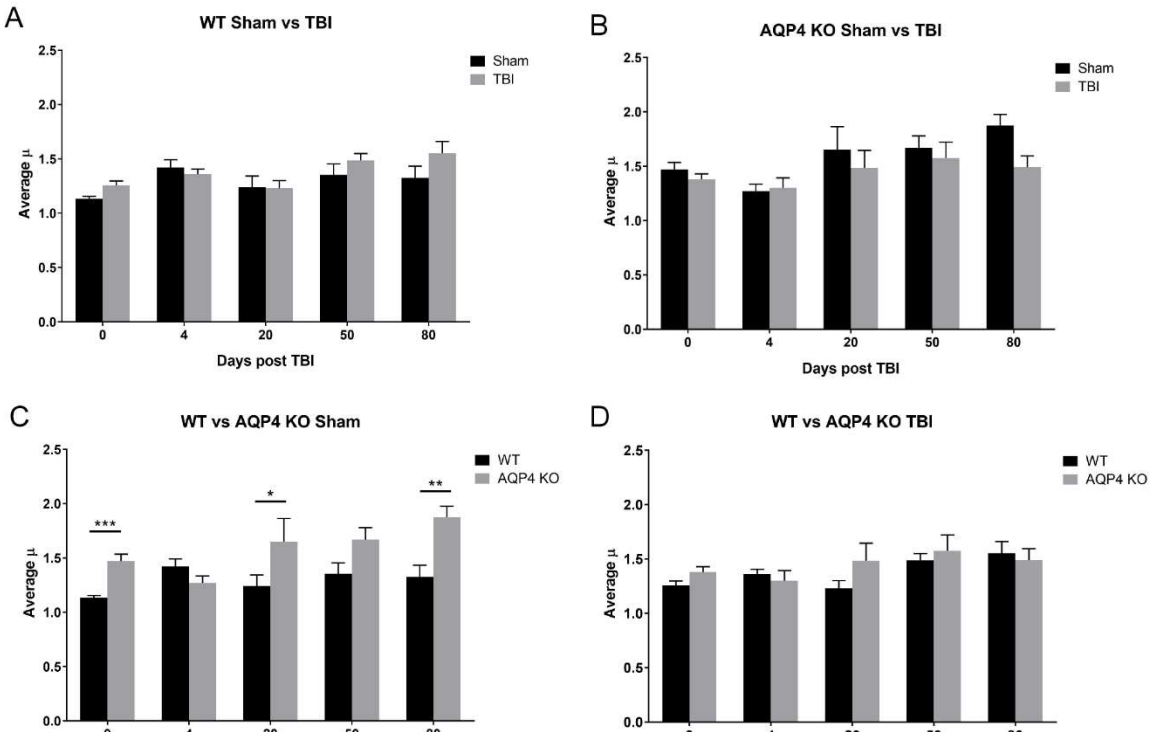

Figure 3.2 TBI does not induce alterations in μ. A-B. No significant changes in μ were observed between sham and TBI groups for both WT and AQP4 KO mice. **C.** AQP4 KO mice displayed significant increases in μ at baseline (day 0) and 20 and 80 days after craniotomy compared with WT mice. **D.** No significant differences in μ were observed after TBI between WT and AQP4 KO mice. Statistical assessment of sham groups between WT and AQP4 KO mice was performed with two-way ANOVA with Bonferroni *post hoc* analysis which revealed a significant interaction between genotype ($F(1,153) = 19.68$, $p < 0.0001$) and time ($F(4,153) = 0.9584$, $p = 0.0053$). * $p < 0.05$, ** $p < 0.01$, *** $p < 0.001$. Error bars are SEM.

(Figure 3.2 A-B). When comparing only sham groups between genotypes, a significant increase in average μ was observed at baseline (day 0), 20 and 80 days after craniotomy (Figure 3.2C). No significant differences were detected when comparing TBI groups between WT and AQP4 KO mice (Figure 3.2D).

3.6 Discussion

In the present study, OCT imaging was performed to quantitatively determine optical signal changes after TBI. I hypothesized that alterations in intrinsic optical signals in the parietal cortex can be detected with OCT after TBI in the frontal cortex. The major findings of this study are: 1) TBI does not induce alterations in intrinsic optical signals; and 2) in sham groups, AQP4 KO mice had a higher average μ compared with WT mice at baseline (day 0),20, and 80 days after craniotomy.

A serious consequence following a severe TBI is the development of cerebral edema. There are two major types of edema: 1) vasogenic edema which results from a compromised blood-brain barrier (BBB); and 2) cytotoxic edema which results from intracellular accumulation of water (Unterberg, Stover et al. 2004; Papadopoulos and Verkman 2007). The type of cerebral edema formed may depend on the type of the injury. In cerebral contusions, such as those produced by CCI, edema formation and progression can be seen in the hemorrhagic core. Traditionally, it was thought that vasogenic edema was the primary form of brain edema following a TBI due to breakdown of the BBB in and around contusions. However, many studies have challenged this notion and have shown that cytotoxic edema is the predominant form of brain swelling in a contusion model and that traumatic brain edema can not only be focal and perifocal, but can also diffuse to different areas of the brain (Unterberg, Stover et al. 2004).

In experimental models, swelling is observed in the primary lesion area (Soares, Thomas et al. 1992; Kiening, van Landeghem et al. 2002; McBride, Szu et al. 2014) and can also be detected in the hippocampus (Soares, Thomas et al. 1992). Previous studies have shown that brain swelling can begin as early as 1 hour after injury (Bareyre,

Wahl et al. 1997) and is at a maximal 24 – 48 hours after TBI (Soares, Thomas et al. 1992; Bareyre, Wahl et al. 1997; Kiening, van Landeghem et al. 2002) which resolves by 7 dpi (Bareyre, Wahl et al. 1997). However, to my knowledge, time course imaging studies at chronic time points after TBI, particularly up to 90 dpi, have not been performed previously.

I have previously demonstrated the ability of OCT to detect optical signal changes in a mouse model of cerebral edema. Using a water intoxication model of cytotoxic edema, OCT was able to identify a significant decrease in μ ~7 minutes after water injection that continued to decline until the animal expired. Additionally, post-mortem brain water content analysis confirmed the presence of increased brain water content in mice injected with water compared with controls (Rodriguez, Szu et al. 2014). Thus, I hypothesized that OCT can detect optical changes that may possibly correlate with cerebral edema after TBI. Indeed, immediate swelling of the frontal cortex was qualitatively observed after induction of TBI. However, unlike anticipated, changes in μ were not observed after TBI at all time points in both WT and AQP4 KO mice, suggesting that cerebral edema did not diffuse caudally from the injury location and may primarily be present in the contusional and peri-contusional cortex or that swelling at distant regions was present at earlier time points Interestingly, most AQP4 KO mice exhibited less bleeding and swelling at the time of injury. This was a surprising qualitative observation that may explain the lack of optical signal changes after injury in the AQP4 KO group. Indeed, previous studies have shown that AQP4 KO mice are protected from cytotoxic edema (Manley, Fujimura et al. 2000). Furthermore, studies have shown that compared with WT mice, AQP4 KO mice exhibited decreased injury volume by 7 days, reduced hemispheric enlargement by 3 days, and lower intracranial

pressure by 6 hours after TBI (Yao, Uchida et al. 2015). These studies suggest that AQP4 KO mice may be more resilient to injury and that lack of AQP4 have neuroprotective effects after TBI.

Previous studies have also shown swelling in the ipsilateral hippocampus after TBI (Bareyre, Wahl et al. 1997) and MRI studies have confirmed ipsilateral hippocampal lesions after injury (Kharatishvili, Immonen et al. 2007; Kharatishvili, Sierra et al. 2009). Unfortunately, due to the limited depth penetration of OCT (~2 mm), the optical properties of the hippocampus cannot be determined. However, one way to overcome this limitation is to increase the excitation wavelength. By using a super continuum light source at 1.7 μm, the hippocampus of mice was able to be visualized with OCT (Chong, Merkle et al. 2015). Therefore, if a longer wavelength were used in these studies, optical signal changes in the hippocampus after TBI might have been detected, especially since hippocampal spontaneous seizures were detected after TBI in both WT and AQP4 KO mice at all time points. Indeed, previous studies performed in our laboratory demonstrated the capability of OCT to detect cortical changes in μ in acute models of focal and generalized seizures (Eberle, Reynolds et al. 2012; Eberle, Hsu et al. 2015). Lack of changes in μ from these studies suggest that spontaneous seizures in this model may be mostly hippocampal or that cortical seizures were not detected at the time of OCT imaging. Moreover, OCT imaging over the lesion or perilesional cortex may yield greater changes in μ and provide important information regarding structural and functional changes in the brain after TBI. However, OCT imaging around these areas can only be employed when bleeding from the injury is minimal as blood is highly scattering and depth penetration from OCT will be even more limited. Additionally, in the experimental studies previously mentioned, moderate-severe TBI was induced in the

cortical region directly above the hippocampus (Bareyre, Wahl et al. 1997; Kharatishvili, Nissinen et al. 2006; Kharatishvili, Immonen et al. 2007; Kharatishvili, Sierra et al. 2009) rendering the hippocampus more vulnerable to injury. Thus, it is not surprising that swelling and MRI signals of the hippocampus were more pronounced. If MRI imaging was performed in brain regions distant to the injury site (similar to my studies) then it may be possible that MRI signals may be small or not significant.

Interestingly, compared with WT mice, AQP4 KO mice displayed a significantly higher average μ during baseline (day 0), 20, and 80 days after craniotomy (Figure 3.2C). One possible explanation may be due to the process of aging. Indeed, OCT imaging with 1.7 μm wavelength revealed a significantly lower attenuation value in younger mice (5 weeks old) compared with older mice (5 months old) in which the authors attributed to increased scattering (Chong, Merkle et al. 2015). Furthermore, it is known that brain activity declines with normal aging and functional MRI studies have shown reduced resting-state activity in older adults compared to younger subjects (Damoiseaux, Beckmann et al. 2007). As previously mentioned, the basic principles of optical imaging rely on the interaction between light and brain tissue and more active tissue will reflect less light (Frostig, Masino et al. 1995). Therefore, decreased brain activity (as related to age) will result in increased scattering which may be correlated with the increased attenuation observed in the mice imaged at later time points.

Unlike AQP4 KO sham mice, WT sham mice did not exhibit similar trends. In fact, in the context of aging, AQP4 was shown to be developmentally regulated (Hsu, Seldin et al. 2011; Gupta and Kanungo 2013) and a surprising enhancement of AQP4 was observed in 70 week old mice (Gupta and Kanungo 2013). The extracellular space (ECS) in the brain is enriched with neurotransmitters, ions, peptides, and extracellular

matrix molecules that are critical for glial-neuronal interactions (Binder, Papadopoulos et al. 2004). Furthermore, studies have indicated that the ECS undergoes volume changes during neuronal activity and ECS constriction has been implicated in neurological diseases such as epilepsy (Traynelis and Dingledine 1989; Schwartzkroin, Baraban et al. 1998; Binder, Papadopoulos et al. 2004). In aged rats, the ECS volume was found to be significantly decreased and diffusion was slowed (Syková, Mazel et al. 1998) which makes the brain particularly vulnerable to anoxia (Papadopoulos, Koumenis et al. 1997; Syková, Mazel et al. 1998). Therefore, AQP4 may be upregulated as a response to aging to maintain proper ion and water homeostasis. While these studies provide some clues into why an increase in optical attenuation coefficient was observed, it remains unclear as to why AQP4 KO sham mice exhibited higher attenuation values compared to WT sham mice and the association between aging and AQP4 requires further investigation.

Another possible factor contributing to the changes in attenuation coefficient may be due to the surgery alone. In both treatment groups, mice received a thinned skull cortical window for OCT imaging. Although a relatively quick process (less than 5 minutes), thinning of the skull can result in minor brain trauma due to the vibration and the heat generated from the drilling. Although bleeding in the brain was not observed after skull thinning, possible microbleeds can occur that cannot be viewed with the naked eye. Because blood is highly scattering (Fujimoto 2003), even small amount of blood leaking from broken vessels may cause a change in attenuation values. Interestingly, AQP4 has been shown to play a role in BBB maintenance (Nico, Frigeri et al. 2001; Nicchia, Nico et al. 2004; Zhou, Kong et al. 2008). In adult mice, AQP4 deletion resulted in ultrastructural changes in microvessels and increased BBB

permeability (Zhou, Kong et al. 2008). Thus, the skull thinning process may potentially cause more microtrauma in AQP4 KO mice resulting in leaky BBB leading to a higher μ values compared to WT mice.

The observation that there were no significant differences in μ were detected between sham and TBI groups in both genotypes across time suggests that TBI alone did not induce changes in intrinsic optical signals. While altered μ was observed in WT TBI mice, the changes seen can be attributed to skull aberrations. Uniform skull thinning is essential in this study to increase imaging depth penetration and I have previously shown that differences in skull thickness can affect imaging quality and analysis (Szu, Eberle et al. 2012). After thinning, the skull may attempt to regenerate or heal itself and the newly synthesized skull may be uneven and irregular. In this study, all mice received a thinned skull at day 0. Due to regrowth of the skull, a small cohort of older mice at later time points (50- and 80-day time points) were subjected to re-thinning of the skull to allow better OCT penetration. Attenuation coefficient from these mice were compared with mice that did not undergo re-thinning and μ values were not statistically different (data not shown).

Unfortunately, due to limited OCT depth penetration, changes in attenuation coefficient of the hippocampus cannot be ascertained in the present studies. However, OCT imaging was able to capture the entire corpus callosum and analysis of OCT-derived signals from the corpus callosum could potentially serve as a biomarker for PTE. White matter structural abnormalities have been well documented in imaging studies of both experimental and human TBI (Bramlett and Dietrich 2002; Wilde, Chu et al. 2006; Rutgers, Fillard et al. 2008; Rodriguez-Grande, Obenaus et al. 2018; Wendel, Lee et al. 2018). Furthermore, due to its role in connecting the two hemispheres, abnormalities in

the corpus callosum can potentially lead to circuit dysfunction as seen in epilepsy. In the present study, each mouse served as its own internal control with two OCT imaging sessions. Due to skull aberrations at chronic time points (50 and 80 days), the corpus callosum cannot be viewed as clearly, and thus, analysis of the corpus callosum was excluded in these studies. Future studies utilizing a separate cohort of mice for control and experimental groups to quantify attenuation coefficient of the corpus callosum may show more promise in identifying potential biomarkers for PTE.

Despite the fact that development of PTE after TBI is clinically accepted, the lack of available studies in humans and animals represent a severe impediment to the advancement in this field. Unfortunately, due to heterogeneity of epilepsy and TBI itself, studies of PTE are not only difficult to conduct but may also yield inconclusive or controversial results. In human studies, low sample size in recruiting patients due to specific inclusion and exclusion criteria raises challenges in properly characterizing and defining imaging biomarkers. For instance, the variability of head injury and the latency to the onset of epilepsy creates a tremendous obstacle in accurately identifying predictors of PTE. Therefore, while human and animal studies of PTE have attempted to develop imaging biomarkers of PTE, the potential of these biomarkers to accurately predict the development of PTE remains to be elucidated.

In conclusion, minimally invasive OCT imaging shows promise in potentially identifying biomarkers in the brain after TBI in the preclinical context. Importantly, my study is the first to use OCT imaging in a chronic time course study after TBI. Here, OCT was able to detect changes in the optical attenuation after craniotomy in AQP4 KO mice, however changes in μ were not observed after TBI. To expand the current findings, future studies will require an OCT system with higher sensitivity and specificity

to better characterize OCT signals in various regions of the brain to accurately detect pathology and correlate with clinical outcome.

3.7 References

Angeleri, F., Majkowski, J., et al. (1999). "Posttraumatic Epilepsy Risk Factors: One-Year Prospective Study After Head Injury." Epilepsia **40**(9): 1222-1230.

Bahar, S., Suh, M., et al. (2006). "Intrinsic optical signal imaging of neocortical seizures: the 'epileptic dip'." Neuroreport **17**(5): 499-503.

Bareyre, F., Wahl, F., et al. (1997). "Time course of cerebral edema after traumatic brain injury in rats: effects of riluzole and mannitol." J Neurotrauma **14**(11): 839-849.

Binder, D. K., Papadopoulos, M. C., et al. (2004). "In vivo measurement of brain extracellular space diffusion by cortical surface photobleaching." Journal of Neuroscience **24**(37): 8049-8056.

Bramlett, H. M. and Dietrich, D. W. (2002). "Quantitative structural changes in white and gray matter 1 year following traumatic brain injury in rats." Acta neuropathologica **103**(6): 607-614.

Chong, S. P., Merkle, C. W., et al. (2015). "Noninvasive, in vivo imaging of subcortical mouse brain regions with 1.7 μm optical coherence tomography." Optics letters **40**(21): 4911-4914.

Damoiseaux, J., Beckmann, C., et al. (2007). "Reduced resting-state brain activity in the "default network" in normal aging." Cerebral cortex **18**(8): 1856-1864.

Diaz-Arrastia, R., Agostini, M. A., et al. (2000). "Neurophysiologic and neuroradiologic features of intractable epilepsy after traumatic brain injury in adults." Archives of neurology **57**(11): 1611-1616.

Eberle, M. M., Hsu, M. S., et al. (2015). "Localization of cortical tissue optical changes during seizure activity in vivo with optical coherence tomography." Biomedical optics express **6**(5): 1812-1827.

Eberle, M. M., Reynolds, C. L., et al. (2012). "In vivo detection of cortical optical changes associated with seizure activity with optical coherence tomography." Biomedical optics express **3**(11): 2700-2706.

Frostig, R. D., Masino, S. A., et al. (1995). "Using light to probe the brain: Intrinsic signal optical imaging." International Journal of Imaging Systems and Technology **6**(2-3): 216-224.

Fujimoto, J. G. (2003). "Optical coherence tomography for ultrahigh resolution in vivo imaging." Nature biotechnology **21**(11): 1361.

Fujimoto, J. G., Pitris, C., et al. (2000). "Optical coherence tomography: an emerging technology for biomedical imaging and optical biopsy." Neoplasia **2**(1-2): 9-25.

Gupta, P. K., Sayed, N., et al. (2014). "Subtypes of post-traumatic epilepsy: clinical, electrophysiological, and imaging features." J Neurotrauma **31**(16): 1439-1443.

Gupta, R. K. and Kanungo, M. (2013). "Glial molecular alterations with mouse brain development and aging: up-regulation of the Kir4. 1 and aquaporin-4." Age **35**(1): 59-67.

Gupta, R. K., Saksena, S., et al. (2005). "Diffusion tensor imaging in late posttraumatic epilepsy." Epilepsia **46**(9): 1465-1471.

Haglund, M. M. and Hochman, D. W. (2004). "Optical imaging of epileptiform activity in human neocortex." Epilepsia **45**(s4): 43-47.

Hsu, M. S., Seldin, M., et al. (2011). "Laminar-specific and developmental expression of aquaporin-4 in the mouse hippocampus." Neuroscience **178**: 21-32.

Immonen, R., Kharatishvili, I., et al. (2013). "MRI biomarkers for post-traumatic epileptogenesis." J Neurotrauma **30**(14): 1305-1309.

Kharatishvili, I., Immonen, R., et al. (2007). "Quantitative diffusion MRI of hippocampus as a surrogate marker for post-traumatic epileptogenesis." Brain **130**(12): 3155-3168.

Kharatishvili, I., Nissinen, J., et al. (2006). "A model of posttraumatic epilepsy induced by lateral fluid-percussion brain injury in rats." Neuroscience **140**(2): 685-697.

Kharatishvili, I., Sierra, A., et al. (2009). "Quantitative T2 mapping as a potential marker for the initial assessment of the severity of damage after traumatic brain injury in rat." Experimental neurology **217**(1): 154-164.

Kiening, K. L., van Landeghem, F. K., et al. (2002). "Decreased hemispheric Aquaporin-4 is linked to evolving brain edema following controlled cortical impact injury in rats." Neuroscience letters **324**(2): 105-108.

Kumar, R., Gupta, R. K., et al. (2003). "Magnetization transfer MR imaging in patients with posttraumatic epilepsy." American journal of neuroradiology **24**(2): 218-224.

Manley, G. T., Fujimura, M., et al. (2000). "Aquaporin-4 deletion in mice reduces brain edema after acute water intoxication and ischemic stroke." Nature medicine **6**(2): 159.

McBride, D. W., Szu, J. I., et al. (2014). "Reduction of cerebral edema after traumatic brain injury using an osmotic transport device." J Neurotrauma **31**(23): 1948-1954.

Nicchia, G., Nico, B., et al. (2004). "The role of aquaporin-4 in the blood–brain barrier development and integrity: studies in animal and cell culture models." Neuroscience **129**(4): 935-944.

Nico, B., Frigeri, A., et al. (2001). "Role of aquaporin-4 water channel in the development and integrity of the blood-brain barrier." Journal of cell science **114**(7): 1297-1307.

Papadopoulos, M., Koumenis, I., et al. (1997). "Increasing vulnerability of astrocytes to oxidative injury with age despite constant antioxidant defenses." Neuroscience **82**(3): 915-925.

Papadopoulos, M. C. and Verkman, A. S. (2007). "Aquaporin-4 and brain edema." Pediatric nephrology **22**(6): 778-784.

Rodriguez-Grande, B., Obenaus, A., et al. (2018). "Gliovascular changes precede white matter damage and long-term disorders in juvenile mild closed head injury." Glia.

Rodriguez, C. L., Szu, J. I., et al. (2014). "Decreased light attenuation in cerebral cortex during cerebral edema detected using optical coherence tomography." Neurophotonics **1**(2): 025004.

Rutgers, D., Fillard, P., et al. (2008). "Diffusion tensor imaging characteristics of the corpus callosum in mild, moderate, and severe traumatic brain injury." American Journal of Neuroradiology **29**(9): 1730-1735.

Schwartzkroin, P. A., Baraban, S. C., et al. (1998). "Osmolarity, ionic flux, and changes in brain excitability." Epilepsy research **32**(1-2): 275-285.

Soares, H. D., Thomas, M., et al. (1992). "Development of prolonged focal cerebral edema and regional cation changes following experimental brain injury in the rat." Journal of neurochemistry **58**(5): 1845-1852.

Syková, E., Mazel, T., et al. (1998). "Diffusion constraints and neuron–glia interaction during aging." Experimental gerontology **33**(7-8): 837-851.

Szu, J. I., Eberle, M. M., et al. (2012). "Thinned-skull cortical window technique for in vivo optical coherence tomography imaging." J Vis Exp(69): e50053.

Temkin, N. R., Dikmen, S. S., et al. (1999). "Valproate therapy for prevention of posttraumatic seizures: a randomized trial." Journal of neurosurgery **91**(4): 593-600.

Temkin, N. R., Dikmen, S. S., et al. (1990). "A randomized, double-blinded study of phenytoin for the prevention of post-traumatic seizures." The New England Journal of Medicine **323**(8): 497-502.

Traynelis, S. F. and Dingledine, R. (1989). "Role of extracellular space in hyperosmotic suppression of potassium-induced electrographic seizures." Journal of Neurophysiology **61**(5): 927-938.

Unterberg, A., Stover, J., et al. (2004). "Edema and brain trauma." Neuroscience **129**(4): 1019-1027.

Vermeer, K., Mo, J., et al. (2014). "Depth-resolved model-based reconstruction of attenuation coefficients in optical coherence tomography." Biomedical optics express **5**(1): 322-337.

Wendel, K. M., Lee, J. B., et al. (2018). "Corpus callosum vasculature predicts white matter microstructure abnormalities following pediatric mild traumatic brain injury." Journal of neurotrauma(ja).

Wilde, E. A., Chu, Z., et al. (2006). "Diffusion tensor imaging in the corpus callosum in children after moderate to severe traumatic brain injury." Journal of neurotrauma **23**(10): 1412-1426.

Wilde, E. A., Hunter, J. V., et al. (2005). "Frontal and temporal morphometric findings on MRI in children after moderate to severe traumatic brain injury." J Neurotrauma **22**(3): 333-344.

Willmore, L. J., Sypert, G. W., et al. (1978). "Recurrent seizures induced by cortical iron injection: a model of posttraumatic epilepsy." Ann Neurol **4**(4): 329-336.

Yao, X., Uchida, K., et al. (2015). "Mildly reduced brain swelling and improved neurological outcome in aquaporin-4 knockout mice following controlled cortical impact brain injury." J Neurotrauma **32**(19): 1458-1464.

Zhao, M., Suh, M., et al. (2007). "Focal increases in perfusion and decreases in hemoglobin oxygenation precede seizure onset in spontaneous human epilepsy." Epilepsia **48**(11): 2059-2067.

Zhou, J., Kong, H., et al. (2008). "Altered blood–brain barrier integrity in adult aquaporin-4 knockout mice." Neuroreport **19**(1): 1-5.

Chapter 4: Hippocampal electrographic biomarkers of posttraumatic epilepsy

4.1 Abstract

Posttraumatic epilepsy (PTE) is a serious neurological consequence that develops over an unknown latent period following a traumatic brain injury (TBI). Clinical studies have shown that PTE can manifest as temporal lobe epilepsy (TLE) in which recurrent spontaneous seizures arise from the temporal lobe. While studies have attempted to identify electrographic changes in the brain after TBI, long-term *in vivo* electrophysiological changes in the hippocampus after head trauma are not well characterized. In this study, adult male CD1 wildtype (WT) and aquaporin-4 knockout (AQP4 KO) mice were subjected to a single moderate-severe TBI in the frontal cortex and underwent *in vivo* video-electroencephalographic (vEEG) recordings and intrahippocampal electrical stimulation for the quantitative assessment of electrographic seizure threshold (EST) and duration (ESD) in the ipsilateral hippocampus. Power spectral density (PSD) analysis revealed alterations in power at specific EEG frequencies at various times after injury and Morlet wavelet analysis detected specific patterns in power between mice with and without PTE. No significant differences in EST were observed between sham and TBI mice at all time points in both genotypes; however, ESD was consistently higher in AQP4 KO mice compared with WT mice. These findings suggest that specific EEG phenotypes can be detected between WT and AQP4 KO mice which may serve as EEG biomarkers for PTE.

4.2 Introduction

Posttraumatic epilepsy (PTE) is a serious neurological consequence that develops over a latent period following a traumatic brain injury (TBI). Clinical studies

have shown that PTE can manifest as temporal lobe epilepsy (TLE) (Santhakumar, Ratzliff et al. 2001) in which recurrent spontaneous seizures arise from the temporal lobe (Hubbard, Hsu et al. 2013). Indeed, several studies have demonstrated that patients can develop TLE after a TBI (Mathern, Babb et al. 1994; Diaz-Arrastia, Agostini et al. 2000), particularly when injury occurred early in life (age <5 years) (Mathern, Babb et al. 1994; Diaz-Arrastia, Agostini et al. 2000). Seizures in TLE include both simple and complex partial seizures. Various psychic, gustatory, olfactory, and autonomic symptoms can be seen in patients with simple partial seizures. On the other hand, patients with complex partial seizures can experience loss of awareness accompanied by facial automatisms including lip smacking and chewing. Generalized convulsions can also occur in TLE patients (Wiebe, Blume et al. 2001).

The pathology of TLE is characterized by hippocampal sclerosis including cell loss and mossy fiber sprouting (Golarai, Greenwood et al. 2001; Hunt, Scheff et al. 2009; Hubbard, Hsu et al. 2013) which leads to altered structural and functional hippocampal networks. In fact, hippocampal circuitry reorganization has been shown in animal models of PTE *in vitro*. For instance, the development of spontaneous and hilar-evoked epileptiform activity was observed in hippocampal slices from mice 6 months after controlled cortical impact (CCI) injury which was associated with TLE pathology (Hunt, Scheff et al. 2009; Hunt, Scheff et al. 2010). Additionally, rats that underwent fluid percussion injury (FPI) displayed granule cell hyperexcitability 1 week after TBI with recovery by 1 month and a long-term decrease in seizure threshold in the hippocampus after high frequency stimulation (Santhakumar, Ratzliff et al. 2001). In another study, rats with TBI from the weight drop model showed persistent hyperexcitability in the dentate gyrus (DG), specifically in the granule and molecular cell layer (Golarai,

Greenwood et al. 2001). These studies demonstrate the significance of the temporal lobe, particularly the hippocampus, and its susceptibility to neuronal hyperexcitability after injury.

Despite these fundamental studies, *in vivo* electrophysiological changes in the hippocampus after experimental head injury have not been well characterized. In most animal models of PTE, injury is impacted in an area directly above the hippocampus and electrocorticographic (ECoG) recordings were employed to detect and monitor spontaneous seizures after TBI (D'Ambrosio, Fairbanks et al. 2004; Bolkvadze and Pitkänen 2012; Rodgers, Dudek et al. 2015). In one study, two cortical screw electrodes and one depth electrode in the ventral hippocampus was used to record and monitor for late spontaneous seizures in rats after lateral FPI. Interestingly, late spontaneous electrographic seizures were first detected in the ipsilateral ventral hippocampus which then propagated to the uninjured contralateral parietal cortex (Kharatishvili, Nissinen et al. 2006). However, in this study, vEEG began 7 weeks after TBI, therefore whether the seizure initiated from the ipsilateral ventral hippocampus or in other brain regions remains unknown.

While the studies mentioned above have confirmed that spontaneous seizures and epilepsy can develop after TBI, electroencephalographic (EEG) biomarkers remain to be identified. Indeed, current animal models of PTE have detected electrographic spontaneous seizures at various time points after TBI (D'Ambrosio, Fairbanks et al. 2004; Kharatishvili, Nissinen et al. 2006; Kharatishvili, Immonen et al. 2007; Bolkvadze and Pitkänen 2012; Guo, Zeng et al. 2013; Kelly, Miller et al. 2015); however, EEG analysis of such recordings generally does not go beyond counting the frequency of spontaneous seizures, electrographic discharges (ED), and latency to first seizure

(Kharatishvili, Nissinen et al. 2006; Bolkvadze and Pitkänen 2012; Guo, Zeng et al. 2013). Thus, comprehensive analysis from video-EEG (vEEG) recordings must be analyzed thoroughly to evaluate specific electrographic characteristics that may pertain to PTE so that a unifying agreement regarding EEG biomarkers can be defined.

In the PTE studies described above, hippocampal pathology, and subsequently, altered hippocampal networks, were evident primarily because the injury affected the underlying hippocampus. In this study, I aimed to determine whether a single episode of TBI in the frontal cortex could lead to spontaneous seizures in the hippocampus, and ultimately, the development of PTE. Specifically, I focused on the following questions: 1) is EEG power altered at different times after a TBI; 2) are there changes in EEG power prior to seizure onset; 3) can TBI result in a decrease in seizure threshold; and 4) how does AQP4 modulate seizure activity after TBI?

4.3 Materials and methods

4.3.1 Animals

All experiments were conducted in accordance with the National Institutes of Health guidelines and approved by the University of California, Riverside Institutional Animal Care and Use Committee. CD1 wild-type (WT) and AQP4 knockout (AQP4 KO) adult male mice between the ages of 8 – 10 weeks old were used for all experiments. The mice were housed under a 12-hour light/dark cycle with water and food provided *ad libitum*. Please refer to Chapter 2 for experimental methods regarding the injury model and for a summary of the study design.

4.3.2 Surgical preparation

Mice were anesthetized with an intraperitoneal (i.p.) injection of ketamine and xylazine (80 mg/kg ketamine, 10 mg/kg xylazine). Additional anesthesia was administered only when necessary. Once an adequate plane of anesthesia was achieved, the hairs on the scalp was removed using clippers and depilatory cream. The scalp was then disinfected with 3 alternating swipes of betadine solution and cleaned with 70% ethanol. Mice were then mounted onto a stereotactic frame and a midline incision was made and reflected. The fascia was gently removed and the skull was cleaned with normal saline and cotton swabs.

4.3.3 Electrode preparation

A 3-channel two twisted bipolar stainless steel electrode (Plastics One) was used for all EEG surgeries and prepared as previously described (Lapato, Szu et al. 2017). The twisted bipolar wires were cut to 2 mm for implanting in the dorsal hippocampus and the untwisted wire was cut ~ 0.5 mm to ground in the dura. To ensure high-fidelity EEG recordings, a scalpel was used to remove ~ 0.5 mm of the insulating coat at the distal tip of twisted recording wires and all of the insulating coat was on the ground wire. The electrodes were then sterilized with 70% ethanol and the ground position on top of the implant pedestal was marked to ensure proper placement of the pins during EEG acquisition.

4.3.4 Electrode implantation

Mice underwent EEG implant surgery 10 days prior to their final time point (14, 30, 60, and 90 days post injury (dpi)) immediately after obtaining their final optical coherence tomography imaging (OCT). Mice were immobilized in the stereotactic frame

and the skull was cleaned with normal saline and cotton swabs. To create greater surface area for cementing the electrode, etching gel was applied to the skull for ~10 seconds and washed 2 – 3 times with normal saline. Stereotaxic coordinates of the hippocampus were identified (Paxinos and Franklin 2001) and a craniotomy of ~ 2 mm in diameter (to accommodate the distance between the recording and ground wires) was created with a high speed surgical hand drill with a ¼ HP-sized carbide bur (SS White). The skull flap was then isolated and placed aside and bone dust was removed with normal saline and cotton swabs. The dura was then carefully removed using a 27G needle. Bonding agent (Clearfil photobond) was then applied onto the skull with a microbrush without contact to the exposed brain and light cured for 20 seconds. The pedestal of the electrode was then secured onto a probe holder with a side clamp and the implant was slowly lowered into the ipsilateral (to the injury) dorsal hippocampus (AP = -1.8 mm, ML = +1.6 mm from bregma) until the implant pedestal contacted the top of the skull (~ 2 mm length of the recording wires). To secure the electrode in place, dental cement (Panavia SA cement) was applied across the skull surface and surrounding the implant and light cured for 20 seconds, followed by additional cement as necessary. After surgery completion, the animals recovered for 3 days.

4.3.5 Continuous vEEG data monitoring

vEEG acquisition began 3 days after electrode implantation. Mice were recorded using either our customized wireless EEG sensor (Epoch) or a tethered system (BioPac). For wireless EEG recording, the implant pedestal was connected to a wireless transmitter (Epoch) and the cage was placed on top of a receiving tray. For tethered EEG recording, mice were connected to the acquisition system via a commutator to allow for freedom of motion during acquisition. Both wireless and tethered EEG

recordings were acquired using a digital acquisition system (MP150 or MP160, Acqknowledge 4.4 or 5 software). Normal EEG output was amplified with a gain of 5000 and bandpass filtered from 0.1 – 35 Hz, and digitized at 625 samples/s. Behavioral activity was monitored and recorded with a high definition USB dome camera with infrared LED night vision.

4.3.6 Power spectral density analysis of long-term vEEG recordings

Resting EEG data acquired during the 1-week period was extracted from Acqknowledge software (Biopac) and power spectral density (PSD) was analyzed using BrainVision Analyzer 2.1 (Brain Products GmbH). Due to the large number of datasets, random 20-hour bins were selected from each EEG recording for analysis. Artifacts were removed with semi-automatic procedure in BrainVision Analyzer 2.1 software based on max-min, low activity, and amplitude criteria. EEG signals were then divided into 10 second segments and Fast Fourier Transform (FFT) was performed on each segment at 1 Hz resolution from 1 – 35 Hz to generate frequency values. EEG frequency bands were determined as the following: delta (1 – 4 Hz), theta (4 – 7 Hz), alpha (7 – 15 Hz), and beta (15 – 35 Hz). FFT results were then extracted from BrainVision and averaged using MatLab (Mathworks).

4.3.7 Morlet wavelet analysis

Spontaneous seizures were first analyzed manually from the 1-week vEEG recording period and confirmed by two blinded observers. Electrographic seizures were defined as lasting ≥ 5 seconds with ≥ 3 Hz and at least double the amplitude compared to baseline. Mice with two or more spontaneous seizures were defined as having PTE. Confirmed seizures were processed for Morlet wavelets from 1 – 35 Hz using power

density (μV/Hz) 10 seconds before and after seizure onset using BrainVision Analyzer 2.1 (Brain Products GmbH). A Morlet parameter of 15 was used to provide the most optimal frequency/power discrimination. Grand averages of Morlet wavelets were performed for all seizures at each time point for both genotypes. Additionally, grand averages of Morlet wavelets were also obtained for mice that developed PTE *vs.* mice that did not develop PTE for both genotypes.

4.3.8 Intrahippocampal electrical stimulation and analysis

After completion of vEEG recording, mice underwent *in vivo* intrahippocampal electrical stimulation for the quantitative assessment of electrographic seizure threshold (EST) and electrographic seizure duration (ESD) at each experimental endpoint (14, 30, 60, and 90 dpi). Here, mice were connected to a tethered EEG system as previously described and electrical stimulations were delivered with a stimulus isolator (World Precision Instruments Linear Stimulus Isolator A395). A 15 minute EEG baseline was acquired followed by electrical stimulation as previously described (Binder, Yao et al. 2006). Each electrical stimulation consisted of a 60 Hz, 1 s train of 1 ms biphasic rectangular pulses. Stimulation intensity was increased incrementally by 20 μA every 2 minutes starting at 20 μA. EST was recorded as the threshold in which a hippocampal afterdischarge (seizure) of at least 5 seconds was detected. ESD was recorded as the total duration of the electrographic seizure at the determined EST.

4.3.9 Statistical analysis

4.3.9.1 Power spectral density

Comparisons of EEG power spectral density at specific EEG frequency ranges between sham *vs.* TBI at all time points were performed for each genotype using two-

way ANOVA with Bonferroni's *post hoc* analysis. All error bars are represented as mean ± standard error of the mean (SEM) and differences were considered statistically significant when p value < 0.05. N's for all time points are the following: WT sham day 14 = 47, day 30 = 32, day 60 = 30, day 90 = 8; WT TBI day 14 = 38, day 30 = 42, day 60 = 78, day 90 = 19; AQP4 KO sham day 14 = 30, day 30 = 35, day 60 = 17, day 90 = 28; AQP4 KO TBI day 14 = 30, day 30 = 29, day 60 = 31, day 90 = 16. All statistical analysis was performed using GraphPad Prism 8.

4.3.9.2 Electrographic seizure threshold and duration

Comparisons between treatments and genotypes were performed with two-way ANOVA with Bonferroni's *post hoc* analysis. All error bars are represented as mean ± standard error of the mean (SEM) and differences were considered statistically significant when p value < 0.05. N's for all time points are the following: WT sham day 14 = 7, day 30 = 5, day 60 = 5, day 90 = 7; WT TBI day 14 = 9, day 30 = 6, day 60 = 12, day 90 = 11; AQP4 KO sham day 14 = 5, day 30 = 6, day 60 = 5, day 90 = 12; and AQP4 KO TBI day 14 = 7, day 30 = 7, day 60 = 7, day 90 = 13. All statistical analysis was performed using GraphPad Prism 8.

4.4 Results

4.4.1 Altered EEG power after TBI

EEG frequency bins were determined to be the following: delta (1 – 4 Hz), theta (4 – 7 Hz), alpha (7 – 15 Hz), and beta (15 – 35 Hz). In WT mice, significant increases in EEG power were observed in the delta and beta frequencies 14 and 30 dpi, respectively, after TBI (Figure 4.1). In AQP4 KO mice, significant increases in EEG

power were observed in delta and theta frequencies 14 dpi and in theta and alpha frequencies 90 dpi (Figure 4.2).

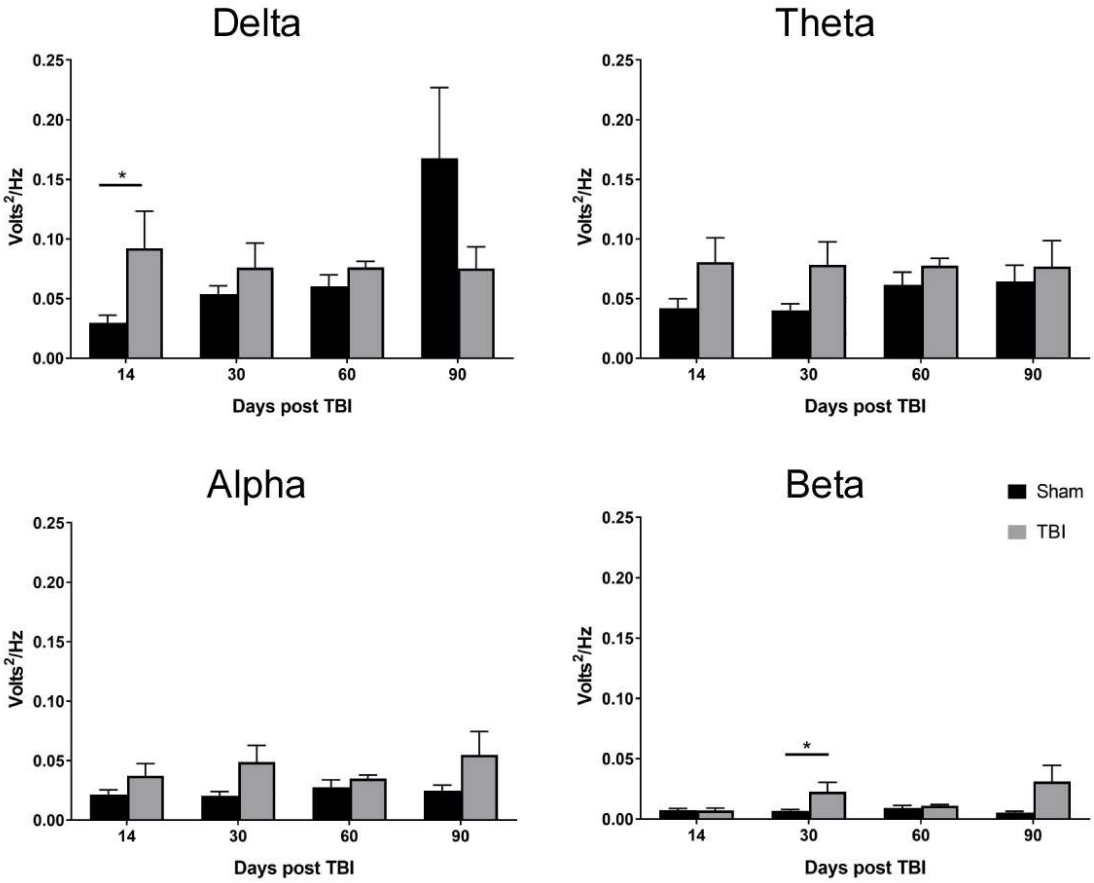

Figure 4.1 Changes in EEG power after TBI in WT mice. A significant increase in EEG power was observed in the delta and beta frequency 14 dpi and 30 dpi, respectively. No significant differences in EEG power was observed in the theta and alpha frequency after TBI. Comparisons between sham and TBI at each EEG frequency was evaluated with one-way ANOVA with Tukey's multiple comparison test. In the delta frequency, a significant interaction was detected ($F(3,286) = 3.693$, $p = 0.0123$) and in the beta frequency, main effect of treatment (sham vs TBI) was significant ($F(1,186) = 8.843$, $p = 0.0032$). * $p < 0.05$, ** $p < 0.01$, *** $p < 0.001$. Error bars are SEM.

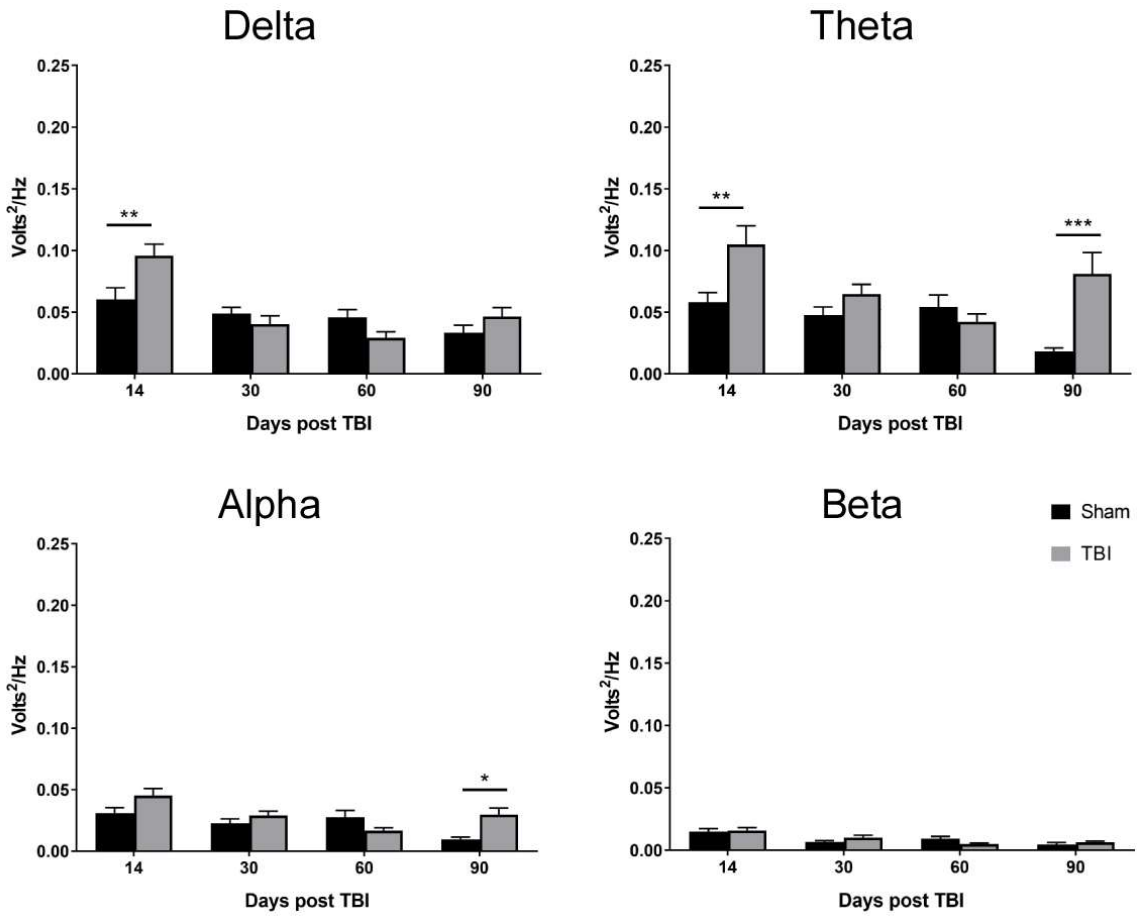

Figure 4.2 Changes in EEG power after TBI in AQP4 KO mice. A significant increase in EEG power was observed in the delta and theta frequencies at 14 dpi and in the theta and alpha frequencies 90dpi. Comparisons between sham vs. TBI at each EEG frequency was evaluated with one-way ANOVA with Tukey's multiple comparison test. In the delta frequency, a significant interaction ($F(3,207) = 5.208$, $p = 0.0017$) and time ($F(3,207) = 13.90$, $p < 0.0001$) was detected. In the theta frequency, significant interaction ($F(3, 228) = 4.714$, $p = 0.0033$), time ($F(3,228) = 4.893$, $p = 0.0026$), and treatment ($F(1,228) = 16.24$, $p < 0.0001$) was revealed. In the alpha frequency, significant interaction ($F(3, 228) = 3.985$, $p = 0.0086$), time ($F(3,228) = 7.067$, $p = 0.0001$), and treatment ($F(1,228) = 5.734$, $p = 0.0174$) was revealed. * $p < 0.05$, ** $p < 0.01$, *** $p < 0.001$. Error bars are SEM.

4.4.2 Morlet wavelet analysis

Morlet wavelets revealed different EEG power patterns at each time point in both WT and AQP4 KO mice. EEG power was seemingly consistent at all time points in AQP4 KO mice, whereas EEG power was uniquely different at all time points in WT

mice. Specifically, a higher EEG power in the lower frequencies (~5 – 10 Hz) was detected ~ 5 seconds prior to seizure onset at 14 dpi in WT mice that was not present in AQP4 KO mice. At 30 dpi, lower EEG power was consistent across time and frequency in WT. At 60 and 90 dpi, lower EEG power was more apparent at frequencies between 20 – 35 Hz (Figure 4.3).

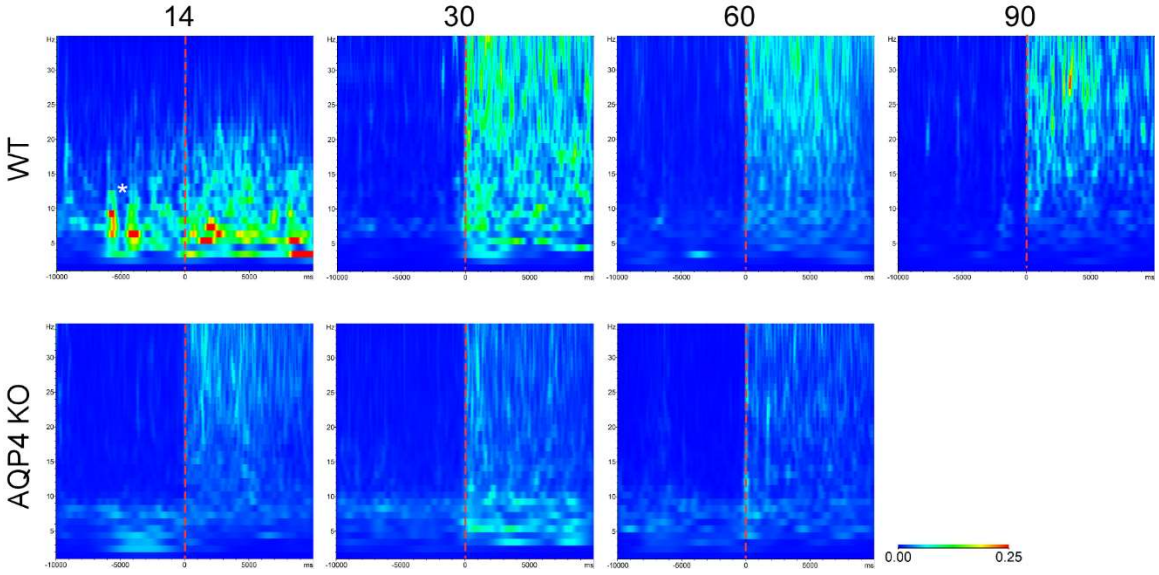

Figure 4.3 Morlet wavelet grand averages at each time point for WT and AQP4 KO mice. Morlet wavelet analysis revealed different EEG patterns between WT and AQP4 KO mice at each time point. Increased power was observed at lower frequencies (~5 – 10 Hz) ~ 5 seconds prior to seizure onset (white asterisk) at 14 dpi in WT mice. Dashed red line = seizure onset.

Analysis of each individual Morlet wavelets was then performed for all individual seizures for both genotypes which revealed that the higher power wavelet pattern detected ~5 seconds prior to seizure onset in WT mice at 14 dpi (Figure 4.3) was due to spike artifact (Figure 4.4). Additionally, individual Morlet wavelet analysis revealed heterogeneity of EEG power for different seizure morphologies. “3 Hz spikes” seizure type exhibited Morlet wavelets with decreased EEG power at the lower frequencies that was consistent with each spike (Figure 4.4 A). On the other hand, “fast polyspikes” seizure type exhibited Morlet wavelets with different patterns including increased power

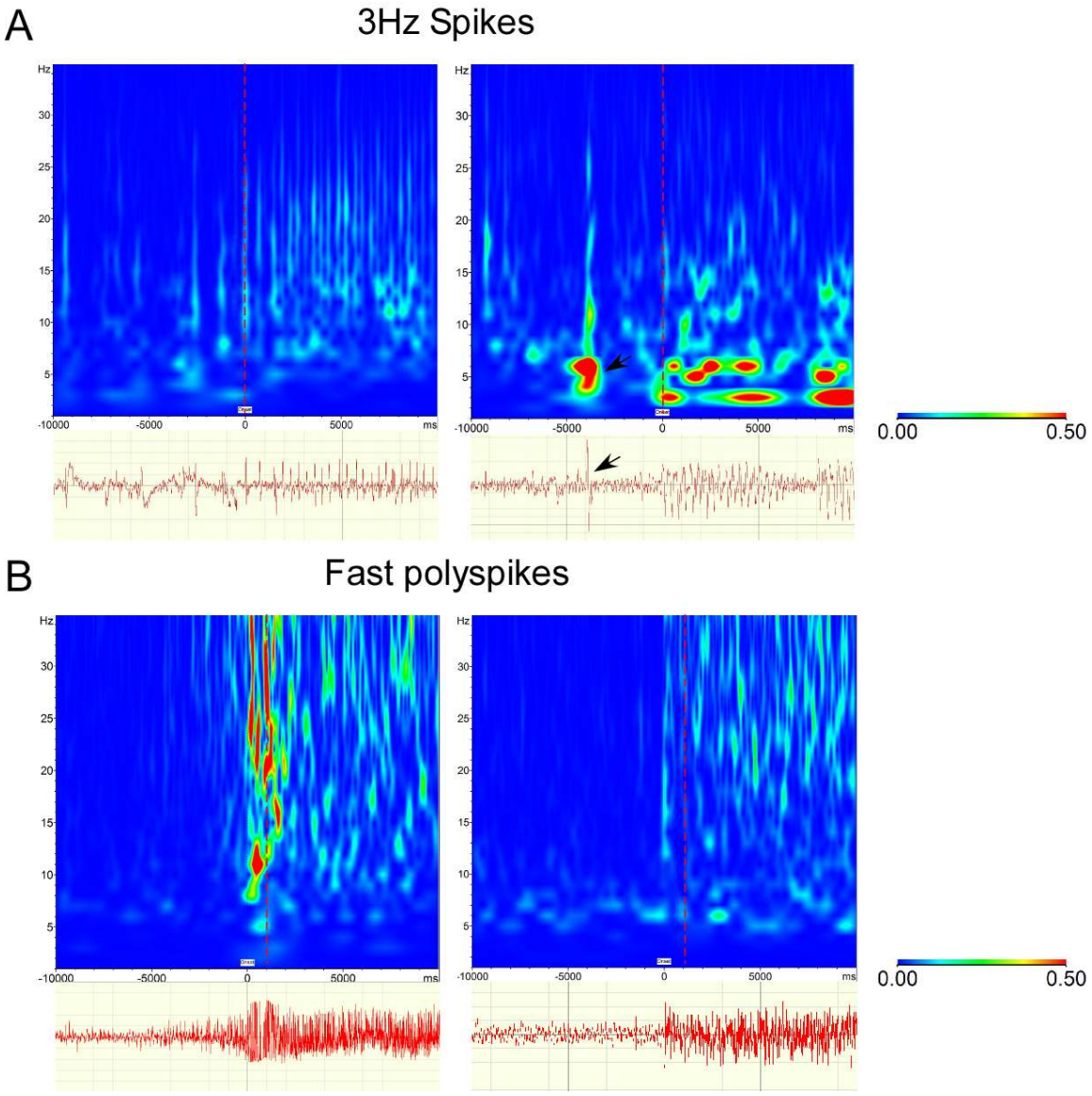

Figure 4.4 Representative Morlet wavelets for different seizure morphologies. A) Morlet wavelets for 3 Hz spikes. An increase in power ~ 5 seconds prior to seizure onset was revealed to be due to a spike artifact (black arrow) that was detected in the Morlet wavelet grand average of WT mice at 14 dpi (Figure 4.3). **B)** Morlet wavelets also revealed different patterns in EEG power in seizures with fast polyspikes. Dashed red line = seizure onset.

in the beginning of a seizure (Figure 4.4B left) or lower EEG power that was constant throughout time and frequency (Figure 4.4B right). Wavelet analysis of the single seizures detected in WT and AQP4 KO sham mice at 60 and 14 dpi, respectively, displayed varying power. WT sham mouse seizure had lower EEG power predominantly

at higher frequencies while AQP4 KO sham mouse exhibited somewhat similar EEG power across time and frequency (Figure 4.5 left). Specifically, in the AQP4 KO sham mouse, the Morlet wavelet did not display a distinct seizure onset (Figure 4.5 right). Finally, Morlet wavelets showed different EEG power in mice with and without PTE. Surprisingly, for both genotypes, mice with PTE had lower power across frequency and time, whereas mice without PTE had higher power across frequency and time. Furthermore, WT mice had overall higher EEG power compared with AQP4 KO mice (note differences in scale bar; Figure 4.6).

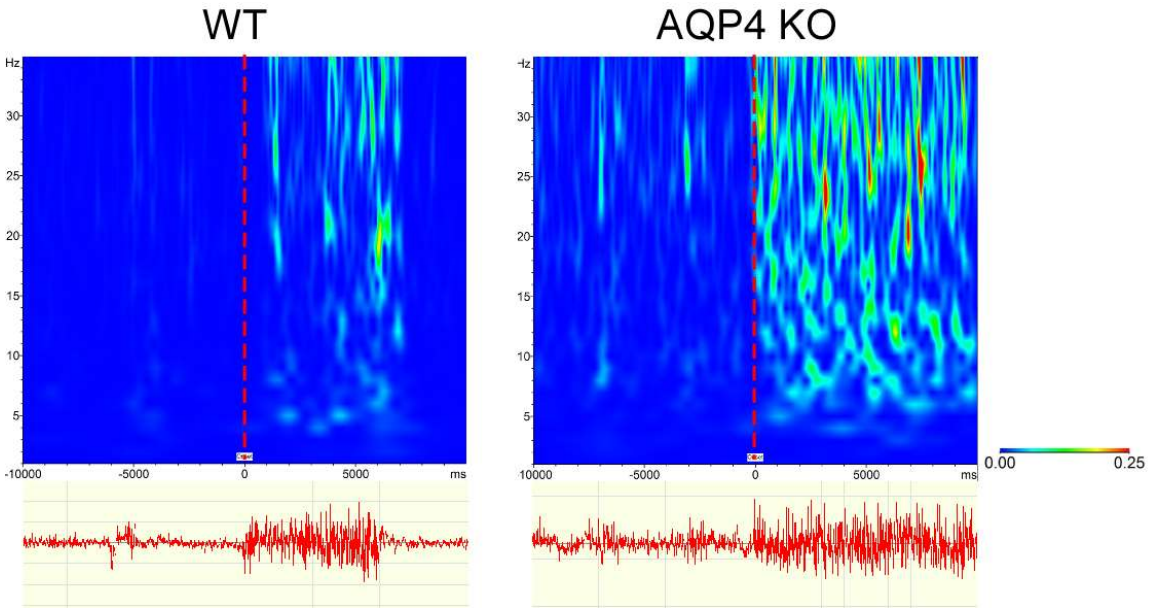

Figure 4.5 Morlet wavelets of sham seizures. Morlet wavelets with corresponding EEG of seizures detected in WT and AQP4 KO mice at 60 and 14 days post craniotomy, respectively. Dashed red line = seizure onset.

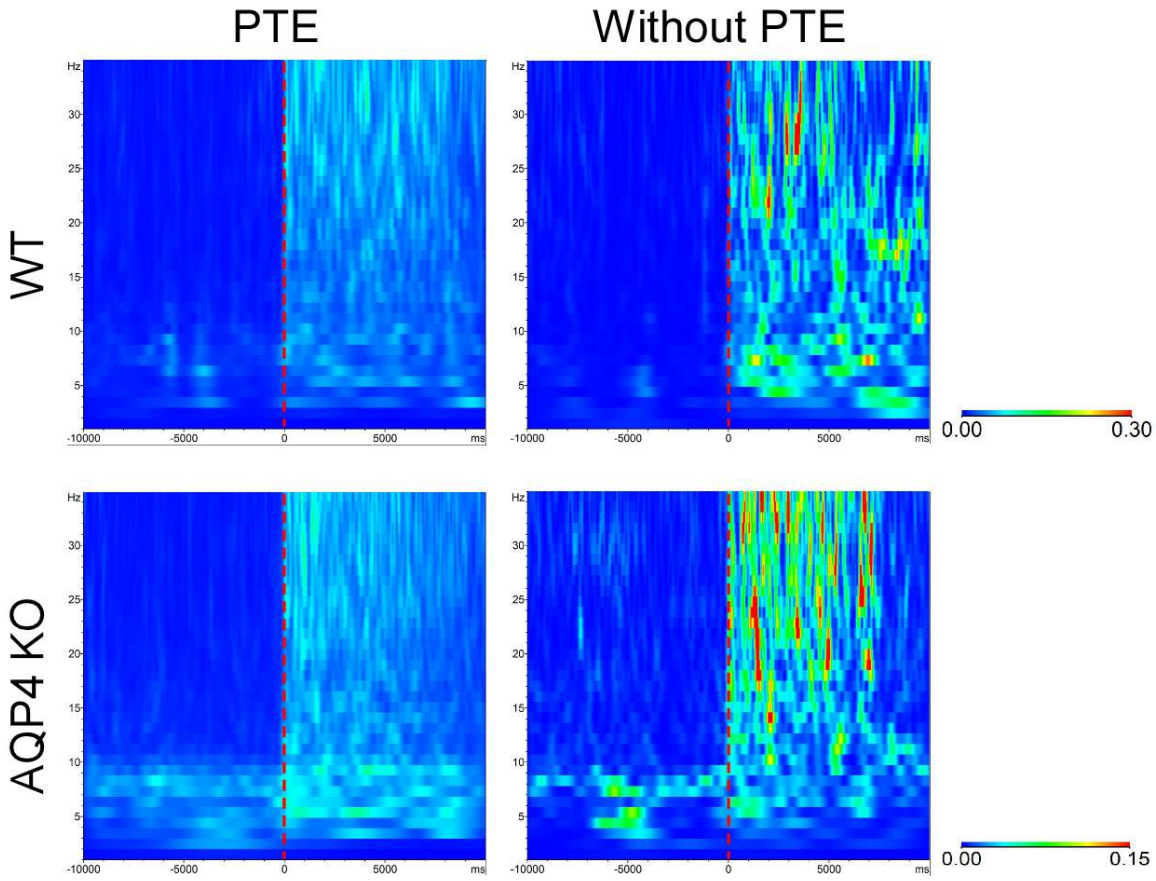

Figure 4.6 Morlet wavelet grand averages of seizures in mice with and without PTE. Seizures from mice with PTE have lower EEG power while seizures from mice without PTE have higher EEG power. WT mice also have overall higher EEG power compared with AQP4 KO mice (note the difference in scale). Dashed red line = seizure onset.

4.4.3 Electrographic seizure threshold and duration

No significant differences in EST and ESD were observed between sham *vs.* TBI at all time points in both WT (Figure 4.7A) and AQP4 KO mice (Figure 4.7B). No significant differences in EST and ESD were observed in sham and TBI groups between WT and AQP4 KO mice (data not shown). AQP4 KO mice exhibited significantly longer ESD at 14 and 90 days in the sham groups and at 30 and 90 days in the TBI groups, compared with WT mice (Figure 4.7C).

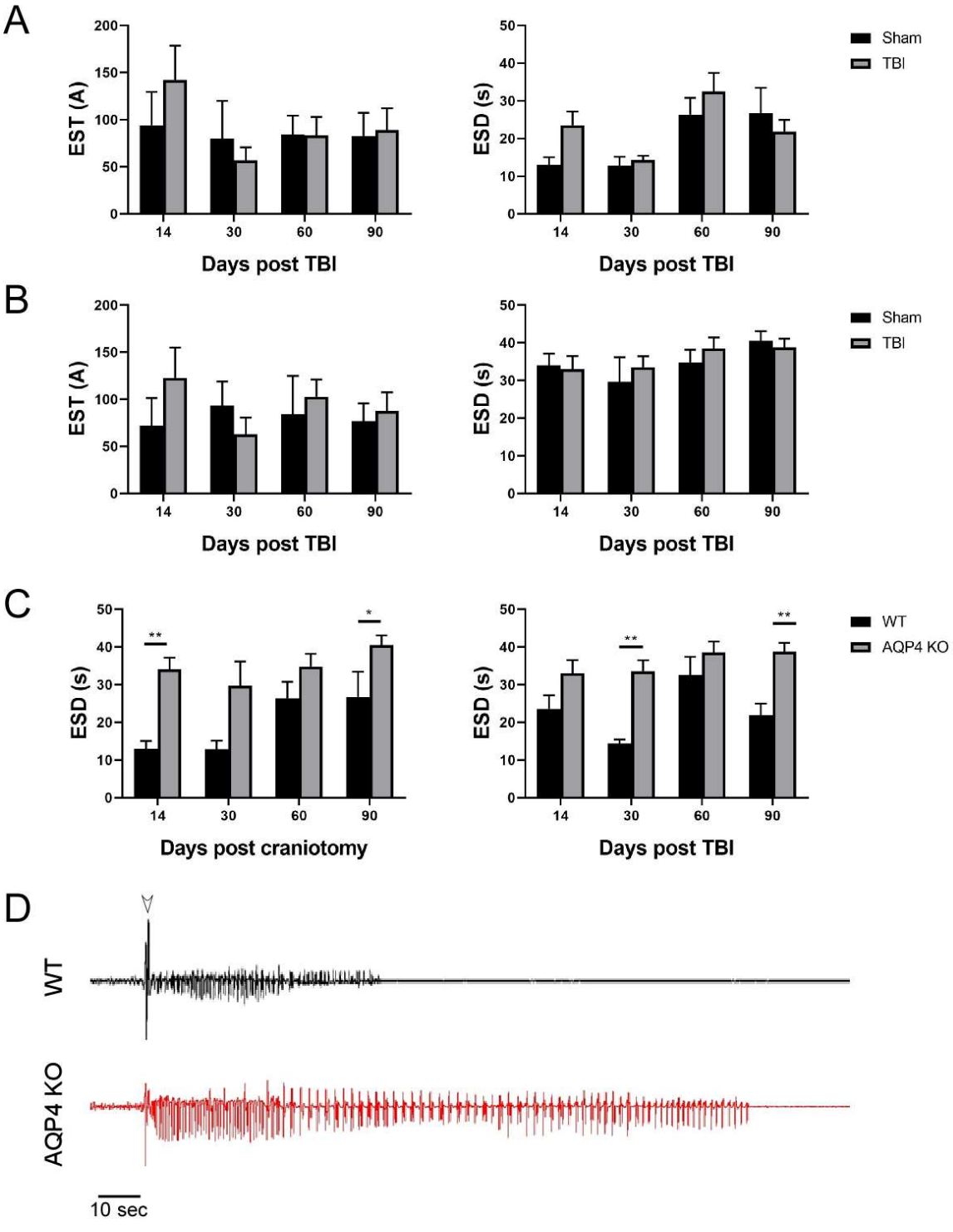
A
EST (A)
200
150
100
50
0
14
30
60
90
Days post TBI
ESD (s)
50
40
30
20
10
0
Sham
TBI
B
C
**
*
Days post craniotomy
WT
AQP4 KO
D
WT
AQP4 KO
10 sec

Figure 4.7 Electrographic seizure threshold and duration after TBI. **A)** No significant differences in EST (left) and ESD (right) were observed in WT mice. **B)** No significant differences in EST (left) and ESD (right) were observed in AQP4 KO mice. **C)** AQP4 KO mice exhibited significantly longer ESD in sham groups at 14 and 90 days after craniotomy (left) and 30 and 90 days after TBI (right) compared with WT mice. **D)** Representative EEG from WT and AQP4 KO mice 90 dpi showing dramatically longer stimulation-induced seizure duration in AQP4 KO mice. WT seizure was 37 seconds long and AQP4 KO seizure was 96 seconds long. Arrow heard = stimulation artifact. ESD comparisons between WT *vs.* AQP4 KO mice in sham and TBI groups were analyzed with two-way ANOVA with Bonferroni's *post hoc* analysis. In the sham group, significant time ($F(3,44) = 3.868$, $p = 0.0154$) and genotype ($F(1,44) = 23.05$, $p < 0.0001$) were detected. In the TBI group, significant time ($F(3,64) = 3.132$, $p = 0.0316$) and genotype ($F(1,64) = 24.57$, $p < 0.0001$) was detected. * $p < 0.05$, ** $p < 0.01$. Error bars are SEM.

4.4 Discussion

PTE refers to the development of spontaneous seizures after TBI and accounts for 20% of all epilepsies (Engel 2001; Lowenstein 2009). Current experimental models of PTE have focused on testing seizure susceptibility pharmacologically and injured animals were shown to be more predisposed to generalized seizures. These studies, however, lack chronic detailed EEG analysis. In the present study, I have shown that a single TBI in the frontal cortex can induce delayed onset of spontaneous hippocampal seizures. *In vivo* electrophysiological techniques and complex EEG analysis were employed to determine changes in EEG power, seizure threshold, and seizure duration at various time points after injury. Results from these studies also further elucidated the role of AQP4 in seizure modulation after a brain injury. These findings helped address the proposed questions and may also be a step forward in identifying potential electrographic biomarkers after TBI.

In "Chapter 2: Mouse model of PTE", I discussed the interesting findings of AQP4 KO mice exhibiting remarkably longer seizures compared with the seizure duration of WT mice. These findings correlate with the longer seizure duration observed after electrical intrahippocampal stimulation in sham and TBI AQP4 KO (Figure 4.7C). Increased hippocampal seizure duration have been previously reported in AQP4 KO

mice after induction of status epilepticus (SE) with kainic acid (Lee, Hsu et al. 2012) and after intrahippocampal electrical stimulation (Binder, Yao et al. 2006) in naïve mice, further corroborating findings from this study. One explanation for increased seizure duration can be due to impaired K^+ reuptake observed in AQP4 KO mice. During enhanced neuronal activity, K^+ is released into the ECS and taken up by astrocytes via Kir4.1 to restore electrochemical equilibrium. However, in the absence of AQP4, extracellular K^+ clearance was found to be slowed (Binder, Yao et al. 2006; Strohschein, Hüttmann et al. 2011). Because AQP4 and Kir4.1 are found to be colocalized (Nagelhus, Mathiisen et al. 2004) it is thought that water and K^+ influx are coupled and contribute to activity-induced glial cell swelling (Walz 1992). Thus, in the present study, AQP4 KO mice may have altered baseline K^+ kinetics but also potential subcellular mislocalization of Kir4.1. Therefore, during seizure activity, lack of proper K^+ reuptake and buffering by Kir4.1 in AQP4 KO mice may result in heightened concentrations of extracellular K^+ leading to further depolarization of neurons and ultimately increasing seizure duration.

EEG is the gold standard in detecting seizures in the brain however, detailed EEG analysis of seizures after head trauma has not been extensively implemented. Simple visual analysis of raw EEG recordings can be unreliable and crucial information regarding brain function can be overlooked. Thus, EEG signals should be extracted and analyzed in detail so that EEG can provide useful information for accurate diagnostic purposes. Here, changes in EEG were, analyzed for the 1-week vEEG recording. To identify any differences between sham and TBI mice, PSD was first performed at each EEG frequency range for all timepoints in both WT and AQP4 KO mice. After TBI, an increase in delta and beta was observed 14 and 30 dpi, respectively in WT mice (Figure

4.1). In AQP4 KO mice, an increase in delta and theta was observed 14 dpi and an increase in theta and alpha was observed 90 dpi (Figure 4.2). One would expect that an increase in PSD at higher frequencies such as alpha and beta would indicate more seizure activity. However, this was not observed in AQP4 KO mice where an increase in alpha was detected 90 dpi but no spontaneous seizures were detected. Furthermore, PSD analysis was performed for the 1-week recording which can include all behavioral activity of the mice such as sleeping, eating, exploratory, and grooming behaviors. Thus, alterations in PSD can reflect all behavioral activities.

In early findings, hippocampal slow waves were found to be present during slow wave sleep (non-REM sleep) (Leung, Da Silva et al. 1982) which is thought to be important for memory consolidation (Marshall and Born 2007). In WT mice, an increase in delta 14 dpi may associated with increased non-REM sleep. Behavioral correlates of hippocampal fast rhythms, such as alpha and beta, have been conflicting. Studies have found hippocampal fast rhythms between 20 – 70 Hz associated with immobility, walking, and REM sleep (Leung, Da Silva et al. 1982; Leung 1992). Unfortunately, hippocampal EEG bands, specifically delta, alpha, and beta, are not well defined, thus, interpretation of PSD analysis in this model is challenging.

One of the most well-studied hippocampal EEG frequencies is the hippocampal theta pattern. Hippocampal theta has been correlated with voluntary movement, learning and memory, and REM sleep (Winson 1974; Bland 1986; Buzsáki 2002; Hasselmo 2005). Loss of hippocampal theta would thus be expected after TBI as sleep disturbances (Verma, Anand et al. 2007; Orff, Ayalon et al. 2009) and memory deficits have been previously reported (Vakil 2005; McAllister, Flashman et al. 2006). Indeed, an association between impaired memory function and attenuated hippocampal theta

was observed after FPI (Fedor, Berman et al. 2010). However, in the present study, an increase in theta was observed. Previous studies have identified two types of hippocampal theta: type 1, which is related to voluntary movement; and type 2, which is present in complete lack of movement (Bland 1986). Therefore, the increase in theta observed 14 dpi in AQP4 KO mice may be related to immobility or type 2 theta. Indeed, motor arrests were associated with electrographic seizures and AQP4 KO mice had more seizures (57%) compared with WT mice (13%) at 14 dpi. Increased theta pattern was also observed 90 dpi in AQP4 KO mice, however, no seizures were detected at this time point. Instead, theta increase at 90 dpi may be more closely related to aging. In fact, previous reports have shown that aged rodents have increased in type 2 theta (Cooper, Prinz et al. 1975; Abe and Toyosawa 1999). Changes in theta power have been also previously implicated in a model of PTE. In one study, rats underwent a severe FPI and ECoG was recorded 14 dpi. Interestingly, FFT analysis of an epileptic seizure revealed suppression of theta immediately before seizure onset, followed by an increased theta power during the ictal event, which was proceeded by theta attenuation at seizure termination (D'Ambrosio, Fairbanks et al. 2004). Therefore, the significant increase in theta observed 14 dpi in AQP4 KO mice may also reflect the higher number of seizures recorded.

Because FFT assumes that EEG signals are stationary, the resulting data obtained is solely a representation of the frequency domain. EEG signals, however, are dynamic. Therefore, Morlet wavelet analysis, which identify changes in EEG power across frequency and time (Cohen 2014), was applied to each electrographic seizure. Morlet wavelets detected heterogeneous EEG power patterns in all seizures even when seizure morphology was similar (Figure 4.4). Remarkably, Morlet wavelet patterns were

unique in mice with and without PTE in which lower EEG power was revealed in mice with PTE and higher EEG power was detected in mice without PTE across both time and frequency (Figure 4.6). The lower EEG power in mice with PTE can be attributed to the significant increase in delta and theta power after TBI as identified by PSD analysis. This further indicates that Morlet wavelet analysis can be a powerful tool to discriminate between epileptic and nonepileptic seizures and can potentially serve to categorize seizures in fuller detail than raw EEG or EEG power analyses, and potentially also as an EEG biomarker for PTE.

In summary, I have developed an *in vivo* model of PTE that results in specific electrographic phenotypes that may serve as potential biomarkers of PTE. Additionally, EEG differences between WT and AQP4 KO mice suggest a critical role of AQP4 in modulating seizures in the hippocampus at various time points after injury. These findings are the first to be reported in an animal model of PTE and future studies utilizing this model can help in defining the mechanisms underlying PTE.

4.5 References

Abe, Y. and Toyosawa, K. (1999). "Age-related changes in rat hippocampal theta rhythms: a difference between type 1 and type 2 theta." Journal of veterinary medical science **61**(5): 543-548.

Binder, D. K., Yao, X., et al. (2006). "Increased seizure duration and slowed potassium kinetics in mice lacking aquaporin-4 water channels." Glia **53**(6): 631-636.

Bland, B. H. (1986). "The physiology and pharmacology of hippocampal formation theta rhythms." Progress in neurobiology **26**(1): 1-54.

Bolkvadze, T. and Pitkänen, A. (2012). "Development of post-traumatic epilepsy after controlled cortical impact and lateral fluid-percussion-induced brain injury in the mouse." J Neurotrauma **29**(5): 789-812.

Buzsáki, G. (2002). "Theta oscillations in the hippocampus." Neuron **33**(3): 325-340.

Cohen, M. X. (2014). Analyzing neural time series data: theory and practice, MIT press.

Cooper, R. L., Prinz, P. N., et al. (1975). "Age-dependent changes in hippocampal theta." Experimental aging research **1**(1): 91-98.

D'Ambrosio, R., Fairbanks, J. P., et al. (2004). "Post-traumatic epilepsy following fluid percussion injury in the rat." Brain **127**(2): 304-314.

Diaz-Arrastia, R., Agostini, M. A., et al. (2000). "Neurophysiologic and neuroradiologic features of intractable epilepsy after traumatic brain injury in adults." Archives of neurology **57**(11): 1611-1616.

Engel, J., Jr. (2001). "A proposed diagnostic scheme for people with epileptic seizures and with epilepsy: report of the ILAE Task Force on Classification and Terminology." Epilepsia **42**(6): 796-803.

Fedor, M., Berman, R. F., et al. (2010). "Hippocampal theta dysfunction after lateral fluid percussion injury." Journal of neurotrauma **27**(9): 1605-1615.

Golarai, G., Greenwood, A. C., et al. (2001). "Physiological and structural evidence for hippocampal involvement in persistent seizure susceptibility after traumatic brain injury." Journal of Neuroscience **21**(21): 8523-8537.

Guo, D., Zeng, L., et al. (2013). "Rapamycin attenuates the development of posttraumatic epilepsy in a mouse model of traumatic brain injury." PLoS One **8**(5): e64078.

Hasselmo, M. E. (2005). "What is the function of hippocampal theta rhythm?—Linking behavioral data to phasic properties of field potential and unit recording data." Hippocampus **15**(7): 936-949.

Hubbard, J. A., Hsu, M. S., et al. (2013). "Glial cell changes in epilepsy: overview of the clinical problem and therapeutic opportunities." Neurochem Int **63**(7): 638-651.

Hunt, R. F., Scheff, S. W., et al. (2009). "Posttraumatic epilepsy after controlled cortical impact injury in mice." Exp Neurol **215**(2): 243-252.

Hunt, R. F., Scheff, S. W., et al. (2010). "Regionally localized recurrent excitation in the dentate gyrus of a cortical contusion model of posttraumatic epilepsy." J Neurophysiol **103**(3): 1490-1500.

Kelly, K. M., Miller, E. R., et al. (2015). "Posttraumatic seizures and epilepsy in adult rats after controlled cortical impact." Epilepsy research **117**: 104-116.

Kharatishvili, I., Immonen, R., et al. (2007). "Quantitative diffusion MRI of hippocampus as a surrogate marker for post-traumatic epileptogenesis." Brain **130**(12): 3155-3168.

Kharatishvili, I., Nissinen, J., et al. (2006). "A model of posttraumatic epilepsy induced by lateral fluid-percussion brain injury in rats." Neuroscience **140**(2): 685-697.

Lapato, A. S., Szu, J. I., et al. (2017). "Chronic demyelination-induced seizures." Neuroscience **346**: 409-422.

Lee, D. J., Hsu, M. S., et al. (2012). "Decreased expression of the glial water channel aquaporin-4 in the intrahippocampal kainic acid model of epileptogenesis." Experimental neurology **235**(1): 246-255.

Leung, L.-W. S., Da Silva, F. L., et al. (1982). "Spectral characteristics of the hippocampal EEG in the freely moving rat." Electroencephalography and clinical neurophysiology **54**(2): 203-219.

Leung, L. S. (1992). "Fast (beta) rhythms in the hippocampus: a review." Hippocampus **2**(2): 93-98.

Lowenstein, D. H. (2009). "Epilepsy after head injury: an overview." Epilepsia **50 Suppl 2**: 4-9.

Marshall, L. and Born, J. (2007). "The contribution of sleep to hippocampus-dependent memory consolidation." Trends in cognitive sciences **11**(10): 442-450.

Mathern, G. W., Babb, T. L., et al. (1994). "Traumatic compared to non-traumatic clinical-pathologic associations in temporal lobe epilepsy." Epilepsy Res **19**(2): 129-139.

McAllister, T. W., Flashman, L. A., et al. (2006). "Mechanisms of working memory dysfunction after mild and moderate TBI: evidence from functional MRI and neurogenetics." Journal of neurotrauma **23**(10): 1450-1467.

Nagelhus, E., Mathiisen, T., et al. (2004). "Aquaporin-4 in the central nervous system: cellular and subcellular distribution and coexpression with KIR4. 1." Neuroscience **129**(4): 905-913.

Orff, H. J., Ayalon, L., et al. (2009). "Traumatic brain injury and sleep disturbance: a review of current research." The Journal of head trauma rehabilitation **24**(3): 155-165.

Paxinos, G. and Franklin, K. (2001). "The mouse brain atlas in stereotaxic coordinates." San Diego, CA: Academic.

Rodgers, K. M., Dudek, F. E., et al. (2015). "Progressive, Seizure-Like, Spike-Wave Discharges Are Common in Both Injured and Uninjured Sprague-Dawley Rats: Implications for the Fluid Percussion Injury Model of Post-Traumatic Epilepsy." J Neurosci **35**(24): 9194-9204.

Santhakumar, V., Ratzliff, A. D., et al. (2001). "Long-term hyperexcitability in the hippocampus after experimental head trauma." Ann Neurol **50**(6): 708-717.

Strohschein, S., Hüttmann, K., et al. (2011). "Impact of aquaporin-4 channels on K+ buffering and gap junction coupling in the hippocampus." Glia **59**(6): 973-980.

Vakil, E. (2005). "The effect of moderate to severe traumatic brain injury (TBI) on different aspects of memory: a selective review." Journal of clinical and experimental neuropsychology **27**(8): 977-1021.

Verma, A., Anand, V., et al. (2007). "Sleep disorders in chronic traumatic brain injury." Journal of Clinical Sleep Medicine **3**(04): 357-362.

Walz, W. (1992). "Mechanism of rapid K+-induced swelling of mouse astrocytes." Neuroscience letters **135**(2): 243-246.

Wiebe, S., Blume, W. T., et al. (2001). "A randomized, controlled trial of surgery for temporal-lobe epilepsy." N Engl J Med **345**(5): 311-318.

Winson, J. (1974). "Patterns of hippocampal theta rhythm in the freely moving rat." Electroencephalography and clinical neurophysiology **36**: 291-301.

Chapter 5: Histological biomarkers of posttraumatic epilepsy

5.1 Abstract

It is now well documented that changes in astrocytes and astrocytic molecules play critical roles in the development of epilepsy. Specifically, alterations in the astrocytic water channel aquaporin-4 (AQP4) and the inwardly-rectifying potassium channel Kir4.1 have been shown in human and experimental models of epilepsy and traumatic brain injury (TBI). However, the roles of AQP4 and Kir4.1 are ill-defined in posttraumatic epilepsy (PTE). In this study, I aimed to determine if changes in these astrocyte channels contribute to epileptogenesis after TBI. Adult male CD1 wildtype (WT) and aquaporin-4 knockout (AQP4 KO) mice were subjected to a moderate-severe TBI in the right frontal cortex. Changes in astrocytes, AQP4, and Kir4.1 was determined using immunohistochemistry and Western blot analysis in the frontal cortex and the hippocampus. A significant increase in AQP4 was detected in the ipsilateral frontal cortex and hippocampus of WT mice that developed PTE compared with mice that did not develop PTE. Additionally, a significant increase in Kir4.1 in the hippocampus was observed in WT mice without PTE compared with AQP4 KO mice without PTE. These findings suggest that AQP4 and Kir4.1 are distinctly regulated and contribute to the pathogenesis of PTE.

5.2 Introduction

5.2.1 Astrocytes

Historically thought to act only as support cells, astrocytes and their dynamic functions have emerged over the past decade. It is now well recognized that astrocytes

are involved in multiple functions in the central nervous system (CNS) such as providing metabolic and structural support through water and ion homeostasis, maintaining the blood-brain barrier (BBB), and regulating synaptic transmission (Oberheim, Wang et al. 2006; Fiacco, Agulhon et al. 2009; Sofroniew and Vinters 2010; Szu and Binder 2016). Thus, it is now well recognized that astrocyte dysfunction is an essential component of CNS disorder pathology.

Since the late 19th century, astrocytes were broadly categorized into two groups: 1) protoplasmic astrocytes which are found in the gray matter and make close contact with neuronal cell bodies and synapses; and 2) fibrous astrocytes which are found in the white matter and are associated with neuronal axons (Reichenbach and Wolburg 2005; Allen and Barres 2009; Sofroniew and Vinters 2010). Besides their anatomical location and their cellular morphology, astrocyte heterogeneity also exists. For example, Müller glia are found in the retina, Bergmann glia are expressed in the cerebellum, and tanycytes are located in the third ventricle (Reichenbach and Wolburg 2005; Sofroniew and Vinters 2010). Not only are there different astrocyte types, these cells also express different molecules and functions (Sofroniew and Vinters 2010). For example, two distinct hippocampal astroglial glutamate transporters and receptors were identified using transgenic mice with GFAP promoter-controlled enhanced green fluorescent protein (EGFP) expression. Functionally, astrocyte expressing glutamate receptors were closely matched with AMPA receptors and were characterized by voltage-dependent outward K^+ currents, whereas astrocyte expressing glutamate transporters were exhibited glutamate uptake currents and inward K^+ currents (Matthias, Kirchhoff et al. 2003). These findings indicate that specific astrocyte subtypes can modulate neuronal activity using different mechanisms.

Similar to neurons, astrocytes express K^+ and Na^+ channels (Fiacco, Agulhon et al. 2009), however, unlike neurons, astrocytes are not electrically excitable (Parpura, Basarsky et al. 1994). Interestingly, astrocytes can communicate with each other through Ca^{2+} waves (Allen and Barres 2009; Fiacco, Agulhon et al. 2009; Sofroniew and Vinters 2010), the main form of astrocyte "excitability". Increases in intracellular astrocyte Ca^{2+} levels have been shown to modulate critical functions such as synaptic transmission, long-term potentiation, and cerebral blood flow coupling (Fiacco, Agulhon et al. 2009). Termed "gliotranmission", astrocytes have been shown to release glutamate, ATP, and D-serine in a calcium dependent-manner (Parpura, Basarsky et al. 1994; Fiacco, Agulhon et al. 2009).

5.2.1.1 Reactive astrocytes

In response to CNS insults such as trauma, ischemia, and infection, astrocytes become reactive in which their morphology and molecular expression are altered (Sofroniew 2009). Reactive astrocytosis, or astrogliosis, represents a spectrum of molecular, cellular, and functional changes in response to all levels of severities in a graded fashion (Sofroniew 2009; Sofroniew and Vinters 2010; Pekny and Pekna 2016). In the normal healthy CNS, astrocytes are restricted to their own domain, however, after insult, reactive astrocytes lose their individual domain and their processes extends to neighboring astrocytes (Oberheim, Tian et al. 2008; Sofroniew and Vinters 2010; Pekny and Pekna 2016). Expression of glial fibrillary acidic protein (GFAP), the main intermediate filament of astrocytes, has become the hallmark for astrogliosis in neurological disease and can be observed in even mild insults (Pekny and Nilsson 2005; Sofroniew and Vinters 2010; Pekny and Pekna 2016). However, it is important to point out that upregulation of GFAP can be detected even in healthy CNS leading to the false

impression of astrocyte proliferation (Sofroniew and Vinters 2010). In more severe injuries, there is substantial upregulation of GFAP, cell hypertrophy and proliferation, and glial scar formation. These changes are associated with tissue reorganization that may persist long after the initial insult (Sofroniew and Vinters 2010).

5.2.1.2 Reactive astrocytes in posttraumatic epilepsy

Not surprisingly, reactive astrocytes have been reported in both animal and human studies of posttraumatic epilepsy (PTE). Gliosis was observed in neocortical tissue specimen collected from patients with head trauma and a risk factor for epilepsy (Swartz, Houser et al. 2006). In a lateral fluid percussion injury model (FPI), GFAP immunoreactivity was observed 9 – 16 weeks after injury and correlated with the presence of epilepsy. Interestingly, FPI rats that developed PTE showed glial reactivity in the temporal cortex, while a single FPI rat that did not develop epilepsy did not show glial reactivity in the temporal focus (D'Ambrosio, Fairbanks et al. 2004).

5.2.1.3 Functional roles of reactive astrocytes after CNS insult

While it is acknowledged that reactive astrocytes develop after an insult, their function remains open to debate. Genetic ablation of astrocyte intermediate filaments (such as GFAP) in various CNS disease models has been used to study the roles of reactive astrocytes, however, the results remains conflicting as reactive astrocytes have been shown to exert both protective and damaging roles. For instance, ablation of reactive astrocytes in a spinal cord injury model shows lack of BBB repair, cell death, leukocyte infiltration, severe demyelination, and motor impairments (Faulkner, Herrmann et al. 2004). Moreover, in a model of experimental autoimmune encephalitis (EAE), wildtype mice with EAE showed reactive astrocytes surrounding infiltrating leukocytes,

reminiscent of a glial scar. On the other hand, increased inflammatory cells such as leukocytes, macrophages, T lymphocytes, and neutrophils, were observed in mice lacking reactive astrocytes (Voskuhl, Peterson et al. 2009). Thus, these studies show the beneficial roles of reactive astrocytes after CNS insults.

On the other hand, negative effects of reactive astrocytes have also been observed after CNS insult. It is well known that axon regeneration after CNS injury is inhibited by glial scar formation (Sofroniew 2005). Indeed, studies ablating reactive astrocytes in a stab injury model demonstrated increased nerve fiber growth around the injury site (Bush, Puvanachandra et al. 1999). Similarly, mice lacking GFAP and vimentin showed increased axonal sprouting and significant improvement in locomotor functions after spinal cord injury (Menet, Prieto et al. 2003). Interestingly, ablating reactive astrocytes increased hippocampal neurogenesis after injury suggesting that reactive astrocytes negatively regulate neurogenesis (Wilhelmsson, Faiz et al. 2012) even in old age (Larsson, Wilhelmsson et al. 2004).

Thus, whether or not reactive astrocytes are beneficial or harmful after a CNS insult remains to be elucidated. However, studies utilizing these transgenic models agree that reactive astrocytes may play more of a beneficial role during the acute stage of the injury and a detrimental role during the chronic phase (Sofroniew and Vinters 2010; Pekny, Wilhelmsson et al. 2014).

5.2.2 Aquaporin-4

The aquaporins (AQP) are a family of small (~ 30 kDa/monomer), hydrophobic, integral membrane proteins with at least 13 AQPs identified in mammals (Verkman and Mitra 2000; Verkman 2005). These proteins are ubiquitously expressed throughout the mammalian tissue, however, only a subset of AQPs are found in the CNS (Badaut,

Fukuda et al. 2014). Aquaporin-4 (AQP4) is primarily expressed in both brain and spinal cord astrocytes (Manley, Binder et al. 2004; Verkman, Binder et al. 2006) and facilitates the bidirectional transport of water in response to an osmotic gradient (Tait, Saadoun et al. 2008). Due to its role in water transport, AQP4 is found highly polarized to astrocytic endfeet in contact with blood vessels (Verkman, Binder et al. 2006; Nagelhus and Ottersen 2013) and is involved in water movement between blood and brain and brain and cerebrospinal fluid (CSF) compartments (Manley, Binder et al. 2004).

To further identify the role of AQP4 in physiology and disease, AQP4 knockout (AQP4 KO) mice were generated and characterized using a targeting vector for homologous recombination. Initial findings from AQP4 deletion showed normal development, growth, and survival in mice, however, a small deficit in urinary concentration was observed (Ma, Yang et al. 1997). Additionally, studies have detected no differences in brain morphology and BBB integrity (Saadoun, Tait et al. 2009). However, AQP4 KO mice exhibited hearing deficits (Li and Verkman 2001), mildly impaired retinal function (Li, Patil et al. 2002), and a decreased osmotic water permeability (Solenov, Watanabe et al. 2004).

Additional roles of AQP4 beyond that of maintaining water homeostasis have also been identified. One function includes astrocyte migration, which is critical after injury particularly for glial scar formation. After a stab injury, glial scar formation was significantly further from the wound in AQP4-null mice indicating slower migration of astrocytes to form a glial scar (Saadoun, Papadopoulos et al. 2005). Interestingly, AQP4 has been recently found to play a role in synaptic plasticity which is correlated with memory and cognitive functions (Szu and Binder 2016). In one study, mice lacking AQP4 exhibited deficits in brain-derived neurotrophic factor (BDNF)-dependent long-

term potentiation (LTP) and spatial memory impairments (Skucas, Mathews et al. 2011). Additionally, AQP4 has also been shown to regulate brain extracellular space (ECS) (Binder, Papadopoulos et al. 2004) and modulate potassium homeostasis (Binder, Yao et al. 2006) functional properties that are critical in epilepsy (Binder, Nagelhus et al. 2012). For example, AQP4 deletion in mice displayed increased ECS space (Binder, Papadopoulos et al. 2004), impaired K^+ homeostasis, and increased electrical stimulation-induced seizures (Binder, Yao et al. 2006).

5.2.3 Kir4.1

The inwardly rectifying potassium channels (Kir) are a functionally diverse family of ion channels. Kir channels are unique in that they show greater inward current flow into the cell rather than outward (Hibino, Inanobe et al. 2010), are primarily responsible for high K^+ permeability, and maintaining resting membrane potential close to the equilibrium potential of K^+ (Butt and Kalsi 2006). Kir channels are categorized based on their molecular and electrophysiological properties (Butt and Kalsi 2006) and to date, 15 Kir subunit genes have been identified (Hibino, Inanobe et al. 2010) and classified into seven subfamilies (Kir1.x – Kir7.x) (Butt and Kalsi 2006; Hibino, Inanobe et al. 2010).

Kir4.1 is localized to astrocytes, oligodendrocytes, Müller glia, and cochlear epithelium (Kofuji, Ceelen et al. 2000; Marcus, Wu et al. 2002; Olsen and Sontheimer 2008; Seifert, Hüttmann et al. 2009). K^+ homeostasis maintenance is critical for normal brain functions. Clearance of extracellular K^+ released during neuronal activity is essential as even small elevations in extracellular K^+ concentrations can lead to abnormal neuronal firing (Rutecki, Lebeda et al. 1985; Traynelis and Dingledine 1988; Traynelis and Dingledine 1989; Olsen and Sontheimer 2008). In astrocytes, Kir4.1 maintains K^+ homeostasis by either net uptake or spatial buffering mechanism

(MacAulay and Zeuthen 2012; Steinhäuser, Seifert et al. 2012; Cheung, Sibille et al. 2015). In the K^+ spatial buffering model, locally released K^+ following neuronal activity are taken up by astrocytes, redistributed across the astroglial syncytium via gap junctions, and transferred to areas of low K^+ concentration (Orkand 1986; Kofuji and Newman 2004).

To further investigate the role of Kir4.1 in astrocyte physiology, conditional knockout (cKO) of Kir4.1 was generated. These genetically modified mice have further demonstrated the significance of this channel's role in potassium homeostasis in the CNS. Kir4.1 cKO mice died prematurely, displayed severe ataxia, and stress-induced seizures. Electrophysiologically, Kir4.1 cKO hippocampal slices displayed glial membrane depolarization, impaired K^+ and glutamate uptake, and enhanced synaptic potentiation (Djukic, Casper et al. 2007). Moreover, mice lacking Kir4.1 exhibited spongiform vacuolization and demyelination in the spinal cord (Neusch, Rozengurt et al. 2001). Given its important in the auditory system, it is not surprising that hearing impairments were also noted in mice where Kir4.1 was knocked out (Marcus, Wu et al. 2002).

5.2.4 AQP4 and Kir4.1 colocalization

Direct interaction of AQP4 and Kir4.1 have been previously suggested. Double immunogold labeling of AQP4 and Kir4.1 were shown in close proximity of each other, and in some cases, superimposed on one another (Nagelhus, Mathiisen et al. 2004; Masaki, Wakayama et al. 2010). Moreover, AQP4 and Kir4.1 were found to be enriched in the perivascular membranes where the endfeet of astrocytes are in contact with blood vessels (Nagelhus, Horio et al. 1999; Nagelhus, Mathiisen et al. 2004; Ruiz-Ederra, Zhang et al. 2007; Masaki, Wakayama et al. 2010). Immunoprecipitation studies further

demonstrated that Kir4.1 co-precipitates with AQP4, expanding on the idea that AQP4 and Kir4.1 are intimately localized with each other (Connors and Kofuji 2006). These findings indicate that AQP4 and Kir4.1 are colocalized and may work in concert with one another during neuronal activity or even be a part of the same supramolecular complex (Amiry-Moghaddam, Frydenlund et al. 2004; Nagelhus, Mathiisen et al. 2004). While these findings are certainly convincing, other studies have demonstrated that AQP4 and Kir4.1 function independently of one another.

Thus, based on their cellular and subcellular localization, functional coupling between water transport and potassium clearance has been hypothesized in CNS disorders. For example, impaired astrocyte-dependent water homeostasis has been implicated in epilepsy. In brief, during neuronal activity, extracellular potassium is taken up by Kir4.1 accompanied by water entry through AQP4 to maintain osmotic balance. Potassium is then redistributed via potassium spatial buffering and water is released into the perivascular space through AQP4 expressed at astrocytic endfeet. In an epileptic brain, perivascular AQP4 is mislocalized to the neuropil, thus, resulting in astrocytic swelling, decreased ECS, and increased ephaptic interactions (Wetherington, Serrano et al. 2008). Indeed, patients with mesial temporal lobe epilepsy (TLE) displayed loss of AQP4 (Eid, Lee et al. 2005) and Kir4.1 (Heuser, Eid et al. 2012) at the perivascular endfeet. Interestingly, loss of perivascular AQP4 was also observed in an experimental model of TBI (Ren, Iliff et al. 2013) suggesting that mislocalization of AQP4 can contribute to further CNS pathology. Thus, evidence proving functional interaction between AQP4 and Kir4.1 is critical in understanding the mechanisms underlying neurological disorders such as PTE.

Interestingly, electrophysiological evidence using AQP4 null mice or inhibition of Kir4.1 by barium or RNAi knock-down have suggested that functional interactions between AQP4 and Kir4.1 are not dependent on one another (Ruiz-Ederra, Zhang et al. 2007; Zhang and Verkman 2008). For instance, no significant differences in membrane potential, barium-sensitive Kir4.1 potassium currents, or current-voltage curves were observed using whole-cell patch clamp and single-channel patch-clamp. No changes in Kir4.1 unitary conductance from glial cells isolated from wildtype (WT) and AQP4 null mice were detected as well (Ruiz-Ederra, Zhang et al. 2007; Zhang and Verkman 2008). Moreover, inhibition of Kir4.1 did not alter AQP4 dependent water permeability (Zhang and Verkman 2008). These findings support the hypothesis that AQP4 and Kir4.1 are functionally independent.

5.2.5 Changes in AQP4 and Kir4.1 in PTE

While accumulating evidence have demonstrated the significance of astrocytes and its molecular components, AQP4 and Kir4.1, in epilepsy and TBI, they have not been explored in detail in models of PTE. In one study, seizure severity after pentylenetetrazole (PTZ) administration was significantly worse in AQP4 KO mice compared with WT mice 1 month after CCI suggesting that AQP4 reduces seizure susceptibility by promoting a glial scar (Lu, Zador et al. 2011). In a rostral parasagittal fluid percussion injury (FPI) model, rats not only developed chronic seizures, but these seizures were associated with impaired inwardly rectifying K^+ currents. An unexpected finding was that loss of these Kir currents were more pronounced in the perilesional cortex than the hippocampus at acute time points which recovered 1 month after injury and that Kir4.1 expression was depleted particularly in the astrocytic foot processes (Stewart, Eastman et al. 2010) suggesting mislocalization of Kir4.1 after TBI. Despite

these crucial findings, further studies investigating the roles of AQP4 and Kir4.1 are needed. In the present study, immunohistochemistry (IHC) and Western blot analysis are used to investigate histological changes in astrocytes, AQP4, and Kir4.1 during the development of PTE.

5.3 Materials and methods

5.3.1 Animals

All experiments were conducted in accordance with the National Institutes of Health guidelines and approved by the University of California, Riverside Institutional Animal Care and Use Committee. Adult CD1 WT and AQP4 KO male mice between the ages of 8 – 10 weeks old were used for all experiments. The mice were housed under a 12-hour light/dark cycle with water and food provided *ad libitum*. Please refer to Chapter 2 for experimental methods regarding the injury model and a summary of the study design.

5.3.2 Immunohistochemistry

5.3.2.1 AQP4, Kir4.1, and GFAP immunoreactivity in the hippocampus

IHC analysis was performed on sham and injured mice at 14, 30, 60, and 90 days post injury (dpi). Mice were deeply anesthetized with an intraperitoneal (i.p.) injection of sodium pentobarbital (200 mg/kg) and transcardially perfused with ice-cold phosphate-buffered saline (PBS; pH 7.4) followed by 4% paraformaldehyde (PFA; pH 7.4). Brains were rapidly dissected, postfixed in 4% PFA overnight at 4 °C followed by cryoprotection in 30% sucrose in PBS at 4 °C. Brains were then frozen with ice-cold isopentane and stored in -80 °C until they were cut into 50 µm coronal sections using a

cryostat (Leica CM 1950, Leica Microsystems). Sections were stored in PBS at 4 °C and all slices were processed simultaneously. Alternating sections away from the electrode track mark were chosen for staining. Sections were blocked with 5% normal goat serum in 0.1 M PBS for 1 hour and incubated with primary antibody to AQP4 (1:200, Millipore AB2218), Kir4.1 (1:100 Alomone, APC-035), and glial acidic fibrillary protein (GFAP) (1:200, Millipore MAB360) in 0.3% Triton X-100 overnight at 4 °C. After washing with PBS, sections were incubated with species-specific secondary antibody conjugated with Alexa 488 or Alexa 594 (Life Technologies) for visualization and then mounted in ProLong Antifade kit with DAPI (Invitrogen). 5X images of both ipsilateral and contralateral hippocampus were obtained on a fluorescence microscope (Leica DFC345 FX).

5.3.2.2 AQP4, Kir4.1, and GFAP immunoreactivity in the frontal cortex

IHC analysis for the frontal cortex was performed as described above. Alternating sections of the frontal cortex were chosen for staining. After incubating with species-specific antibody, sections were washed with PBS and stained with fluorescent Nissl (NeuroTrace 435/455 Blue Fluorescent Nissl Stain, Invitrogen). Sections were incubated in fluorescent Nissl (1:100) for 20 min, washed for 10 min in 0.1% Triton X-100, washed with 1X PBS twice for 5 min each, and with a final wash step of 1X PBS for 2 hours. Sections were then mounted in ProLong Antifade kit without DAPI (Invitrogen). 5X images of both ipsilateral and contralateral hippocampus were obtained on a fluorescence microscope (Leica DFC345 FX).

5.3.3 Western blot analysis

Western blot analysis of both ipsilateral and contralateral frontal cortex and hippocampus was performed on sham and injured mice at 14, 30, 60, and 90 dpi. Mice were deeply anesthetized as described above, transcardially perfused with ice-cold PBS containing complete protease inhibitors (Thermo Fisher), and the ipsilateral and contralateral hippocampus and frontal cortex were rapidly dissected. Harvested tissue was then homogenized with the Bullet Blender (Next Advance) in radioimmunoprecipitation assay (RIPA) buffer (Sigma) with complete protease inhibitors (Thermo Fisher) and centrifuged at 10,000 RPM for 10 minutes at 4 °C. Protein concentrations were assayed using the Micro BCA Protein Assay Kit (Thermo Fisher). 20 µg and 10 µg of total protein were loaded for AQP4 and Kir4.1, respectively, and protein was resolved by SDS-PAGE with either 10% (for AQP4) or 12% polyacrylamide (for Kir4.1) and transferred to a 0.45 µm nitrocellulose membrane (Biorad). Membranes were then dried between two filter papers for 30 minutes, blocked in 5% milk in TBST for 1 hour and incubated in primary antibodies overnight in 4 °C for AQP4 (1:1000, Millipore AB3594), Kir4.1 (1:400, Alomone APC-035), and β-actin (1:10,000, Sigma A1978) which served as an internal control. Finally, membranes were incubated in species-specific secondary IR Dye for 1 hour and imaged using the Li-COR Odyssey Fc Western Imaging System.

5.3.4 Statistical analysis

5.3.4.1 Hippocampal immunohistochemistry

AQP4, Kir4.1, and GFAP immunoreactivity in ipsilateral and contralateral hippocampus was quantified. 1 – 3 sections for both ipsilateral and contralateral

hippocampi per animal at each time point were used for quantification. A total of 5 mice for each genotype (WT and AQP4 KO), treatment (sham and TBI), and time point (14, 30, 60, and 90) were used. Gray scale images were obtained using the Leica Application Suite X Lite software and regions of interest (ROI) was drawn in the grayscale DAPI channel using ImageJ. ROI boxes were drawn in the following hippocampal layers: stratum oriens, stratum pyramidale, stratum radiatum, stratum lacunosum moleculare, molecular layer, and upper blade of the dentate gyrus (Figure 5.1). The CA3 of the hippocampus was excluded from the analysis due to electrode track mark from the indwelling electrode positioned in the CA3. The intensity values were obtained using ImageJ and values were quantified using GraphPad Prism 8.

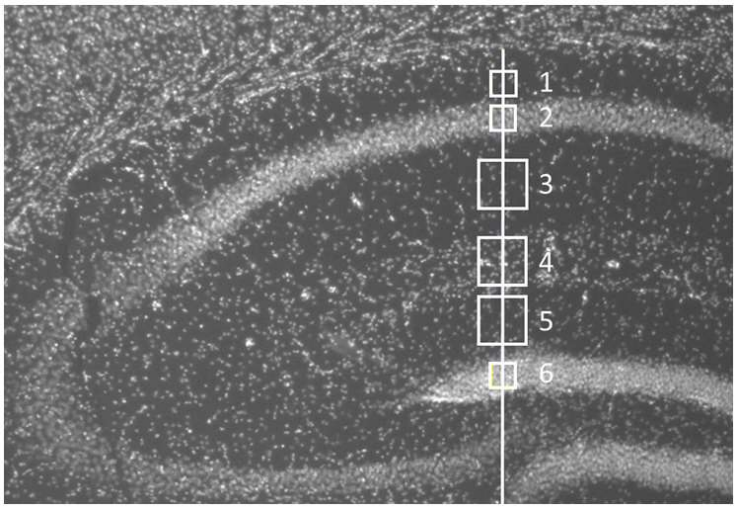

Figure 5.1 Schematic of IHC quantification. To ensure all ROI boxes were drawn in the same location for each section, a vertical line (red line) was drawn across the layers of the hippocampus with the rostral portion of lower blade of the dentate gyrus serving as the landmark. ROI boxes were then drawn centered with the line in the following layers of the hippocampus: (1) stratum oriens, (2) stratum pyramidale, (3) stratum radiatum, (4) stratum lacunosum moleculare, (5) molecular layer, (6) upper blade of dentate gyrus.

Comparisons between sham and TBI at each hippocampal layer was assessed with two-way ANOVA with Bonferroni *post hoc* analysis. All error bars are represented as mean ± standard error of the mean (SEM). Differences were considered statistically significant

when p value < 0.05. AQP4, Kir4.1, and GFAP immunoreactivity for ipsilateral and contralateral frontal cortex was only qualitatively analyzed to determine severity of injury over time.

5.3.4.2 Western blot analysis

Bands were visualized and quantified using the Li-COR Odyssey Fc Western Imaging System and protein levels were normalized to internal β-actin levels. For AQP4 and Kir4.1, the monomer bands ~30 kDa and ~42 kDA, respectively, are shown and quantified with GraphPad Prism 8. Comparisons between sham and TBI groups were analyzed with two-way ANOVA with Bonferroni *post hoc* analysis. All error bars are represented as mean ± standard error of the mean (SEM). Differences were considered statistically significant when p value < 0.05. N's for hippocampal Western blot analysis for all time points are the following: WT ipsilateral sham day 14 = 5, day 30 = 5, day 60 = 8, day 90 = 5; WT ipsilateral TBI day 14 = 5, day 30 = 7, day 60 = 11, day 90 = 7; WT contralateral sham day 14 = 5, day 30 = 5, day 60 = 8, day 90 = 5; WT contralateral TBI day 14 = 5, day 30 = 7, day 60 = 11, day 90 = 7; AQP4 KO ipsilateral sham days 14, 30, 60, and 90 = 5; AQP4 KO ipsilateral TBI day 14 = 6, days 30, 60, and 90 = 5; AQP4 KO contralateral sham day 14 = 6, day 30 = 5, day 60 = 5, day 90 = 7; AQP4 KO contralateral TBI days 14, 30, 60, and 90 = 5. N's for frontal cortex Western blot analysis for all time points are the following: WT ipsilateral sham day 14 = 5, day 30 = 5, day 60 = 8, day 90 = 6; WT ipsilateral TBI day 14 = 5, day 30 = 7, day 60 = 10, day 90 = 7; WT contralateral sham day 14 = 4, day 30 = 5, day 60 = 8, day 90 = 5, WT contralateral TBI day 14 = 5, day 30 = 7, day 60 = 11, day 90 = 7; AQP4 KO ipsilateral sham days 14 – 30 = 5, day 90 = 9; AQP4 KO ipsilateral TBI day 14 = 6, day 30 = 5, day

60 = 4, day 30 = 7; AQP4 KO contralateral sham day 14 = 4, day 30 = 4, day 60 = 5, day 90 = 8; AQP4 KO contralateral TBI days 14 – 60 = 5, day 90 = 6.

5.3.4.3 Western blot analysis of mice with and without PTE

Western blot analysis of AQP4 and Kir4.1 in the ipsilateral frontal cortex and hippocampus was analyzed in mice with and without PTE. Due to limited sample sizes, the total number of mice with and without PTE at all timepoints were determined (see Chapter 2) and analyzed with Student's t-test. Comparison between genotypes with and without PTE was analyzed using two-way ANOVA with Bonferroni *post hoc* analysis. All error bars are represented as mean ± standard error of the mean (SEM). Differences were considered statistically significant when p value < 0.05. N's for WT mice without PTE = 20 and with PTE = 4 and n's for AQP4 KO mice without PTE = 13 and with PTE = 3.

5.4 Results

5.4.1 Frontal cortex immunohistochemistry

An increase in AQP4 and Kir4.1 colocalized with reactive astrocytes can be seen in the lesion in both WT and AQP4 KO mice (Figure 5.2). The lesion was also evident at all time points after injury (data not shown).

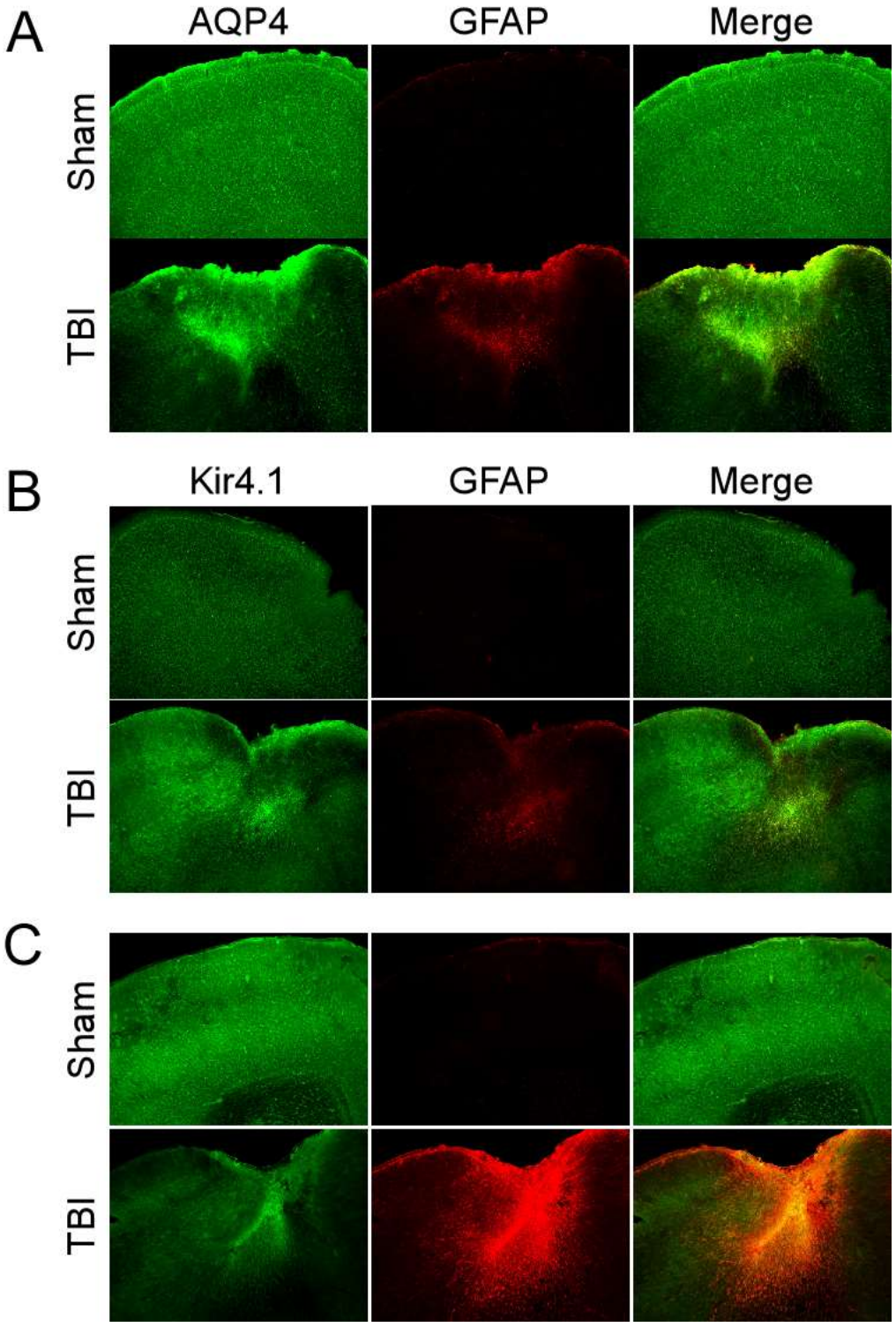
A
AQP4
GFAP
Merge
Sham
TBI
B
Kir4.1
GFAP
Merge
Sham
TBI
C
Sham
TBI

Figure 5.2 Increase in AQP4 and Kir4.1 after TBI. Representative images of the frontal cortex in WT **(A-B)** and AQP4 KO **(C)** sham and TBI mice. An increase in AQP4 and Kir4.1 are observed in the lesion that is colocalized with reactive astrocytes (increased GFAP immunoreactivity). The lesion was evident at all time points (data not shown). Images were taken at 5X.

5.4.2 Hippocampal immunohistochemistry

An increase in AQP4 immunoreactivity was observed in the ipsilateral and contralateral stratum lacunosum moleculare and contralateral stratum radiatum of WT sham mice at 14 day. No differences in Kir4.1 immunoreactivity was observed in WT mice between sham and TBI groups. An increase in GFAP immunoreactivity was observed in the ipsilateral and contralateral stratum radiatum and contralateral stratum lacunosum moleculare of WT sham mice at 14 day compared with injured mice (Figure 5.3). No significant differences in Kir4.1 and GFAP immunoreactivity were detected in AQP4 KO mice between sham and TBI groups (Figure 5.4).

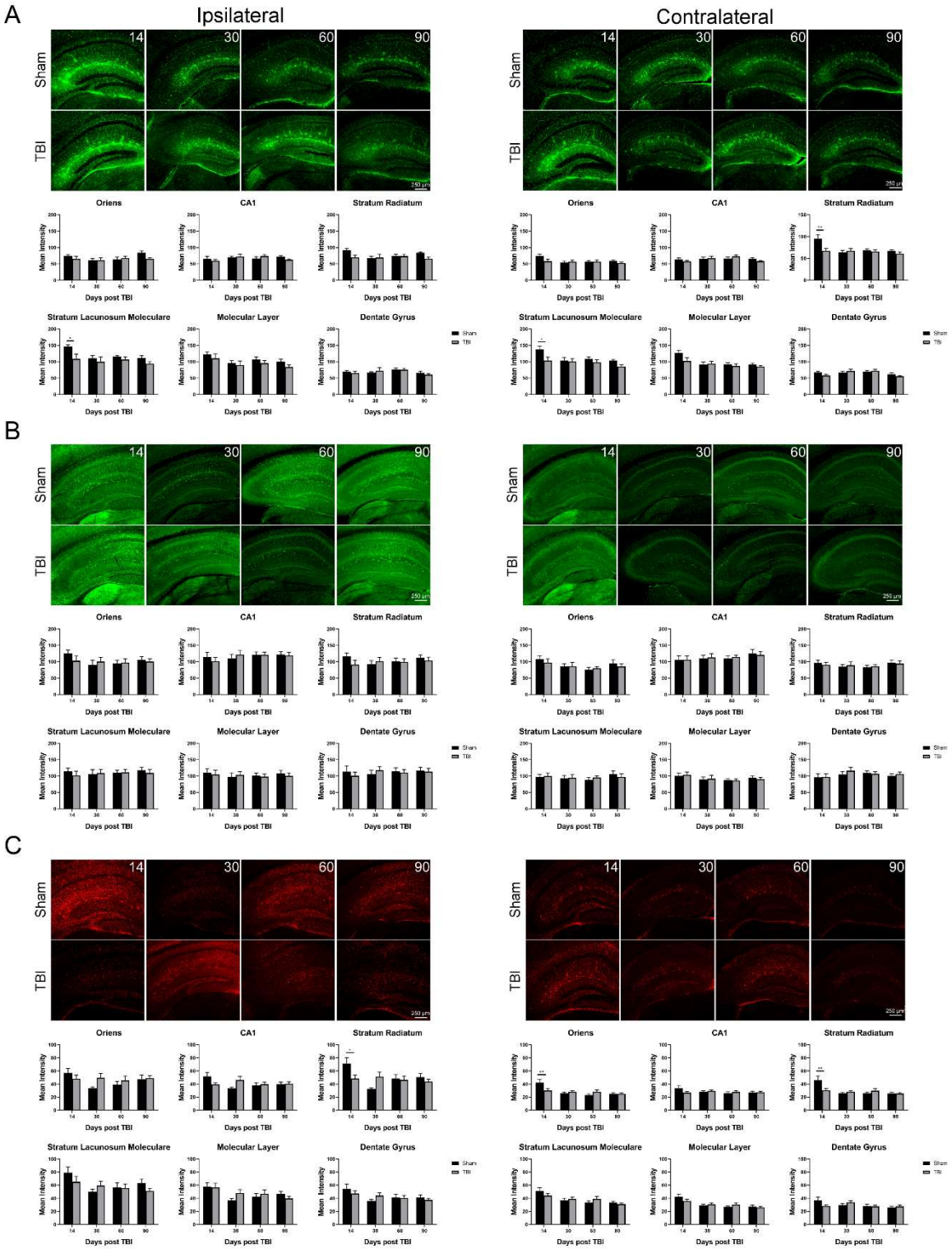
A
Ipsilateral
Contralateral
Sham
TBI
14
30
60
90
Oriens
CA1
Stratum Radiatum
Stratum Lacunosum Moleculare
Molecular Layer
Dentate Gyrus
Mean Intensity
Days post TBI
B
C

Figure 5.3 TBI in the frontal cortex does not alter hippocampal expression of AQP4 and Kir4.1. A. An increase in AQP4 was observed in the ipsilateral and contralateral stratum lacunosum moleculare and the contralateral stratum radiatum in 14 day sham mice. **B.** No differences in Kir4.1 were observed. **C.** GFAP immunoreactivity was increased in the contralateral oriens, ipsilateral and contralateral stratum radiatum, and contralateral stratum lacunosum moleculare in 14 day sham mice. For AQP4 analysis, two-way ANOVA detected a significant difference in treatment ($F(1,70) = 7.803$, $p = 0.0067$) in ipsilateral stratum lacunosum moleculare, and a significant difference in interaction ($F(3,71) = 3.565$, $p = 0.0183$), time ($F(3,71) = 4.769$, $p = 0.0044$), and treatment ($F(1,71) = 5.841$, $p = 0.0182$) in contralateral stratum radiatum. For GFAP analysis, two-way ANOVA revealed a significant difference in interaction ($F(3,147) = 4.310$, $p = 0.0060$) and time ($F(3,147) = 7.938$, $p < 0.001$) in contralateral oriens, a significant difference in interaction ($F(3,154) = 4.171$, $p = 0.0071$) and time ($F(3,154) = 3.280$, $p = 0.0226$ in ipsilateral stratum radiatum, a significant difference in interaction ($F(3,152) = 5.032$, $p = 0.0024$) and time ($F(3,152) = 8.481$, $p < 0.0001$ in contralateral stratum radiatum, and a significant difference in time ($F(3,153) = 7.650$, $p < 0.0001$) in contralateral stratum lacunosum moleculare. Bonferroni *post hoc* analysis was used for all. * $p < 0.05$, ** $p < 0.01$. Error bars are SEM.

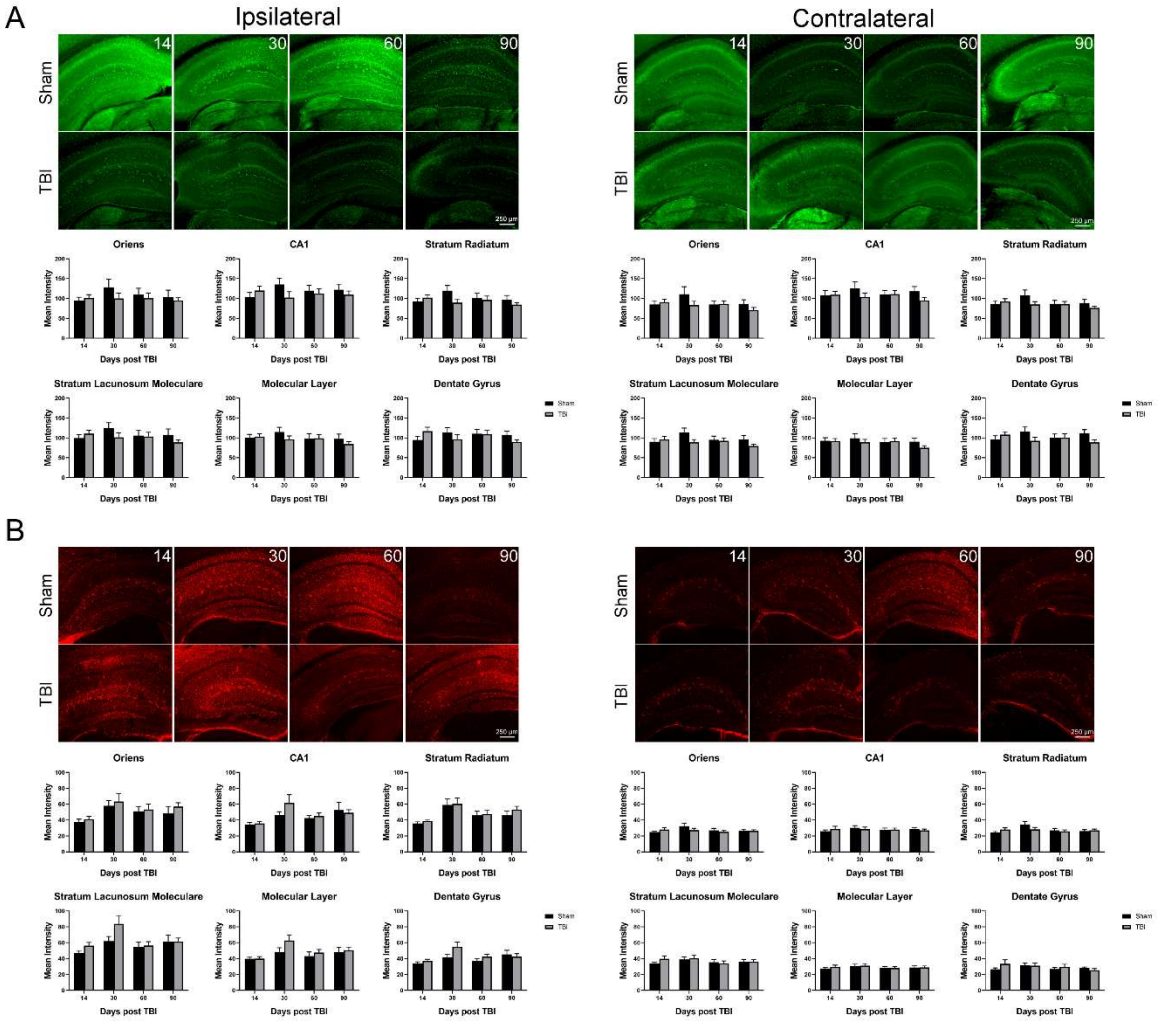

Figure 5.4 TBI in the frontal cortex does not induce alterations in hippocampal Kir4.1 in AQP4 KO mice. No significant differences in Kir4.1 **(A)** and GFAP **(B)** was detected in the ipsilateral and contralateral hippocampus of AQP4 KO mice after TBI.

5.4.3 Hippocampal Western blot

No significant differences in AQP4 and Kir4.1 levels were detected in ipsilateral and contralateral hippocampus of WT mice between sham and TBI groups (Figure 5.5A-B). No significant differences in Kir4.1 levels were detected in ipsilateral and contralateral hippocampus of AQP4 KO mice between sham and TBI groups (Figure 5.5C).

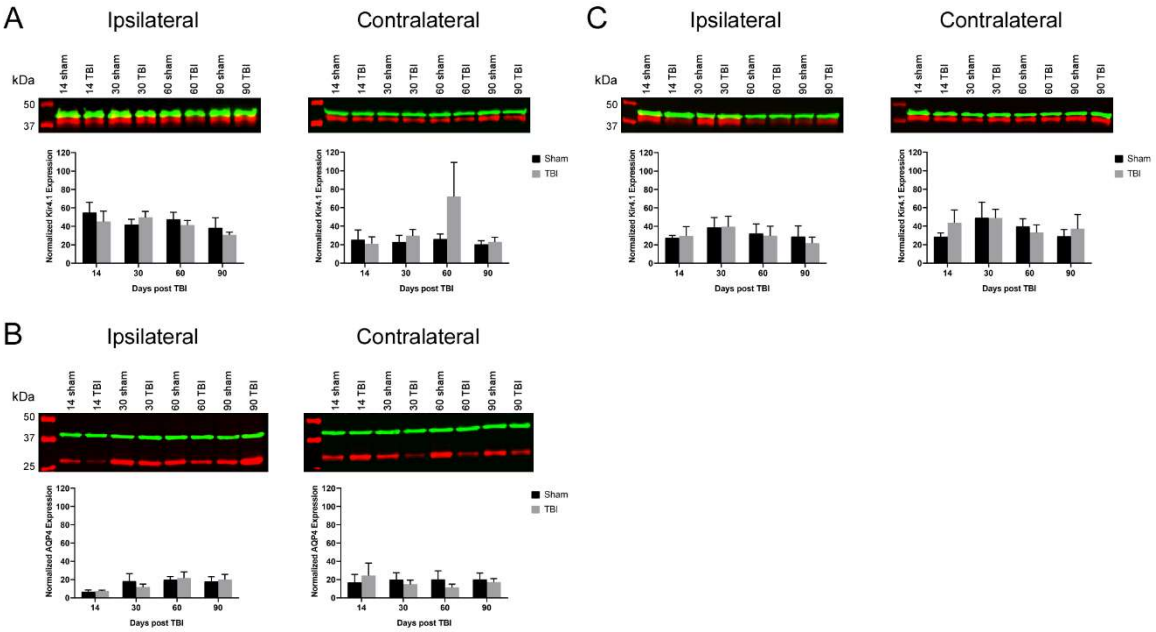

Figure 5.5 TBI does not change AQP4 and Kir4.1 protein levels in the hippocampus. Overall hippocampal AQP4 **(A)** and Kir4.1 **(B)** protein levels were not significantly different at all time points after TBI in the hippocampus of WT mice. Kir4.1 protein levels were also not statistically different in AQP4 KO mice **(C)**. The monomer of AQP4 (~32 kDa) and Kir4.1 (~42 kDa) is shown (red band). β-actin (~42 kDa, green band) served as internal control.

5.4.4 Frontal cortex Western blot

No significant differences in AQP4 and Kir4.1 levels were detected in ipsilateral and contralateral frontal cortex of WT mice between sham and TBI groups (Figure 5.6A-B). No significant differences in Kir4.1 levels were detected in ipsilateral and contralateral frontal cortex of AQP4 KO mice between sham and TBI groups (Figure 5.6C).

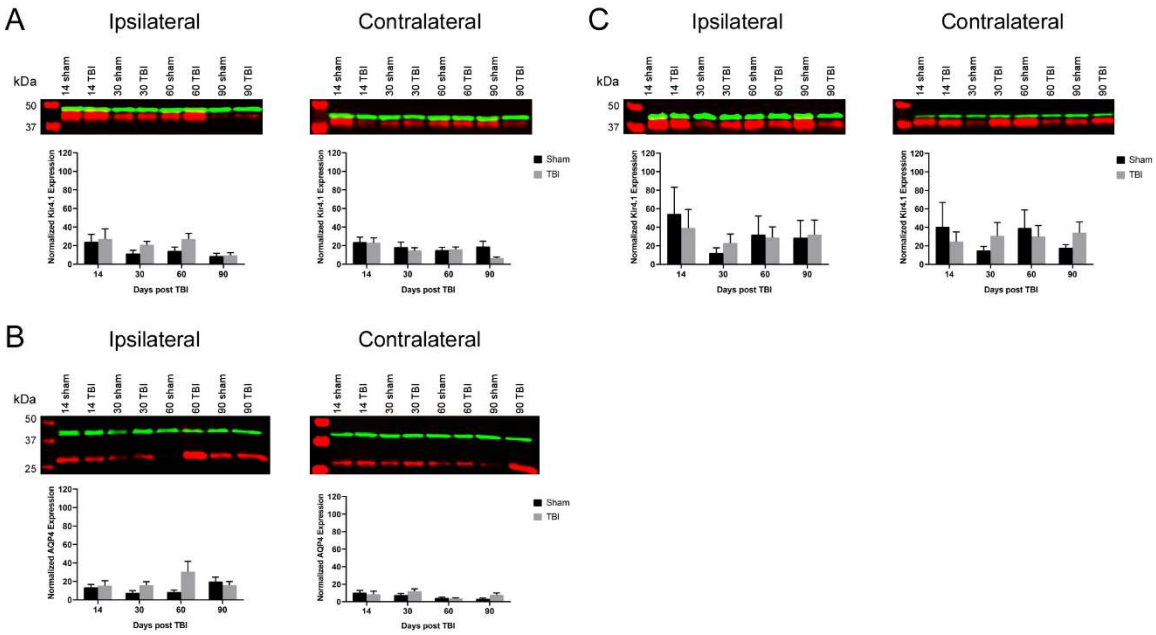

Figure 5.6 TBI does not change AQP4 and Kir4.1 protein levels in the frontal cortex. Overall hippocampal AQP4 **(A)** and Kir4.1 **(B)** protein levels were not significantly different at all time points after TBI in the frontal of WT mice. Kir4.1 protein levels were also not statistically different in AQP4 KO mice **(C)**. The monomer of AQP4 (~32 kDa) and Kir4.1 (~42 kDa) is shown (red band). β-actin (~42 kDa, green band) served as internal control.

5.4.5 Hippocampal and frontal cortex Western blot of mice with and without PTE

A significant increase in AQP4 expression was detected in both the ipsilateral frontal cortex and hippocampus of WT mice that developed PTE compared with mice that did not develop PTE (Figure 5.7). No significant differences in Kir4.1 expression were observed in both the frontal cortex and hippocampus of WT and AQP4 KO mice with and without PTE (Figure 5.8). Interestingly, a significant increase in Kir4.1 expression was detected in the hippocampus of WT mice that did not develop PTE compared with AQP4 KO mice that did not develop PTE (Figure 5.8B).

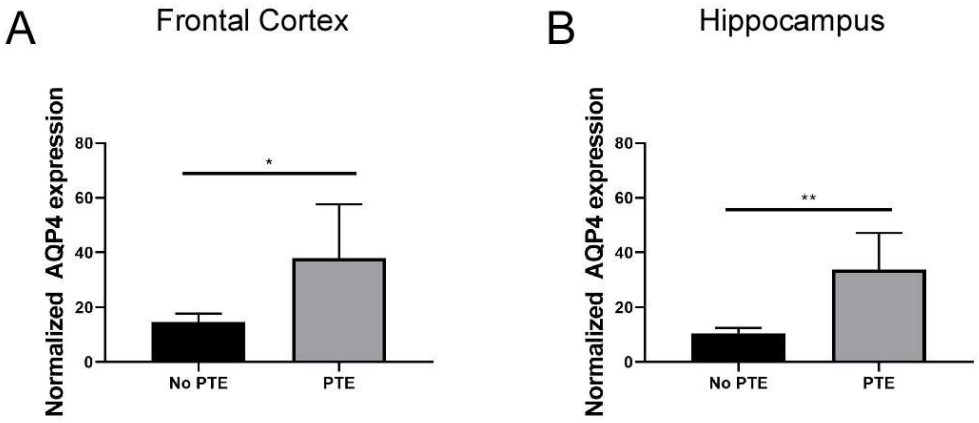

Figure 5.8 Upregulation of AQP4 in the frontal cortex and hippocampus of mice with PTE. A significant increase in AQP4 expression was detected in the frontal cortex **(A)** and hippocampus **(B)**. Data was analyzed with Student's t-test. N's for no PTE and PTE are 20 and 4, respectively. p = 0.0381 for frontal cortex, p = 0.0034 for hippocampus

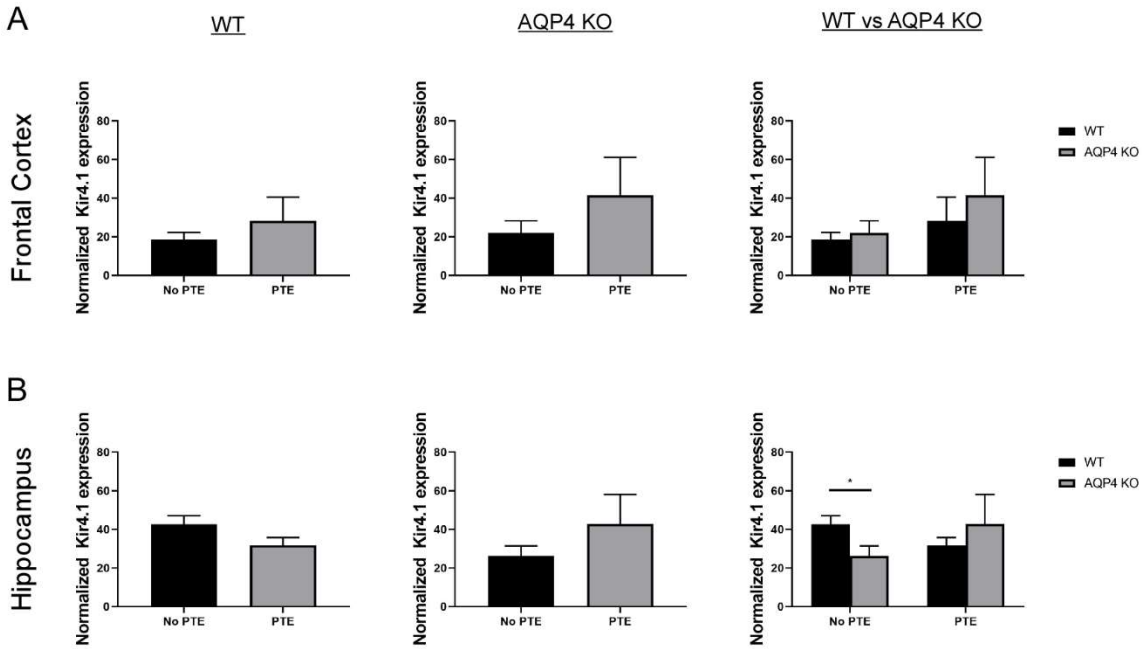

Figure 5.7 Kir4.1 expression in mice with and without PTE. No significant differences in Kir4.1 protein levels in the ipsilateral frontal cortex and hippocampus were detected in mice with and without PTE in both genotypes. However, an increase in Kir4.1 expression was detected in WT mice without PTE relative to AQP4 KO mice without PTE **(B, right)**. Student's t-test was used to compare Kir4.1 expression in mice with and without PTE. N's for WT mice without PTE are 18 and 20 for the frontal cortex and hippocampus, respectively. N's for WT mice with PTE are 3 and 4 for the frontal cortex and hippocampus, respectively. N for AQP4 KO mice without PTE is 13 for both frontal cortex and hippocampus. N's for AQP4 KO mice with PTE are 2 and 3 for frontal cortex and hippocampus, respectively. Comparison of Kir4.1 expression levels between genotypes was analyzed with two-way ANOVA with Bonferonni *post hoc* analysis (p = 0.0440).

5.5 Discussion

Maintenance for a healthy CNS requires tight regulation of water and ion homeostasis. Two critical astrocytic molecules involved in these processes are AQP4 and Kir4.1. Impaired water and ion homeostasis are defining characteristics in both TBI and epilepsy (D'Ambrosio, Maris et al. 1999; Guo, Sayeed et al. 2006; Binder, Nagelhus et al. 2012; Devinsky, Vezzani et al. 2013). After a head injury, delayed onset of cerebral edema may develop which can increase intracranial pressure and lead to deleterious consequences such as death (Maas, Stocchetti et al. 2008; Donkin and Vink 2010). Indeed, the initial impact can cause vascular damage which can break down the BBB, impair metabolic dysfunction, and alter ion concentrations (Werner and Engelhard 2007; Chodobski, Zink et al. 2011). In this study, I sought to determine whether a single TBI in the frontal cortex can lead to alterations in astrocytic proteins AQP4 and Kir4.1 to modulate neuronal hyperexcitability in the hippocampus. Additionally, changes in astrocyte reactivity were also examined to determine their role in the development of PTE.

During neuronal activity, potassium ions are released into the ECS increasing extracellular K^+ concentrations (Somjen 1979). Clearance of extracellular K^+ is critical in regulating neuronal excitability (Walz 2000) as even submillimolar increases in extracellular K^+ can dramatically increase epileptiform activity (Traynelis and Dingledine 1989). In fact, seizure-like activity were shown to be induced by 10 mM K^+ in sclerotic hippocampal slices from humans with intractable TLE and with even higher (12 mM) concentration of K^+ in non-sclerotic hippocampal slices (Gabriel, Njunting et al. 2004). Early studies demonstrated that astrocytes are the specific cell type involved in maintaining K^+ homeostasis (Hertz 1978; Orkand 1986) via the inwardly rectifying K^+

channel Kir4.1 (Djukic, Casper et al. 2007). Additionally, it is thought that water and K^+ fluxes are coupled due to morphological studies demonstrating colocalization of the two proteins (Nagelhus, Horio et al. 1999). Indeed, findings have shown that absence or mislocalization of AQP4 can lead to altered neurotransmitter release after K^+ stimulation (Ding, Sha et al. 2007) and decreased K^+ kinetics (Amiry-Moghaddam, Williamson et al. 2003; Binder, Yao et al. 2006). Thus, it is not surprising that alterations in K^+ and water regulation are seen in various CNS pathologies, in particular epilepsy (Benninger, Kadis et al. 1980; Heinemann, Konnerth et al. 1986; Hinterkeuser, Schröder et al. 2000; Lee, Eid et al. 2004; Eid, Lee et al. 2005; Binder, Yao et al. 2006; Lee, Hsu et al. 2012).

Due to their critical functions in regulating water and K^+ homeostasis in the brain, AQP4 and Kir4.1 were investigated in a model of PTE. Surprisingly, Western blot analysis revealed no significant differences in overall AQP4 and Kir4.1 protein levels after TBI in the hippocampus and frontal cortex of both WT and AQP4 KO mice. IHC analysis detected a significant increase in AQP4 immunoreactivity in the contralateral stratum radiatum and ipsilateral and contralateral stratum lacunosum moleculare in the 14-day sham group. Additionally, an increase in GFAP immunoreactivity was also detected in the contralateral stratum oriens, ipsilateral and contralateral stratum radiatum, and contralateral stratum lacunosum moleculare layers of the hippocampus in WT 14-day sham mice compared to injured mice. It may be possible that surgical procedures contributed to these changes since the electrode was only implanted 4 days after craniotomy and creation of the thinned skull cortical window; however, these changes were not consistent in throughout all layers of the hippocampi in both WT and AQP4 KO mice. Additionally, GFAP immunoreactivity was not observed in the 14-day

sham AQP4 KO mice, suggesting that surgical techniques may not be the sole contributor to these alterations.

Because PTE was only detected in a subset of mice, I sought to investigate whether differences in AQP4 and Kir4.1 exist between mice that developed PTE compared with mice that did not. Surprisingly, no differences in Kir4.1 expression levels were detected in the ipsilateral frontal cortex and hippocampus of either WT and AQP4 KO mice with and without PTE. When comparing Kir4.1 expression between genotypes, WT mice without PTE showed a significant increase in Kir4.1 levels in the hippocampus, and not in the frontal cortex, relative to AQP4 KO mice without PTE (Figure 5.8). This suggests that Kir4.1 may be upregulated in response to the injury to aid in the reuptake or buffering of extracellular K^+ released by active neurons.

Of greatest interest, AQP4 expression levels were significantly higher in both the frontal cortex and hippocampus of mice that developed PTE compared to mice that did not. These findings suggest that upregulation (or dysregulation) of AQP4 after TBI in both the injured cortex and the ipsilateral hippocampus correlates with the development of PTE. Indeed, AQP4 has been shown to be upregulated in the contused cortex after acute TBI that was correlated with increased brain swelling (Sun, Honey et al. 2003; Zhang, Chen et al. 2015). The increase in AQP4 suggests that the brain may be attempting to prevent vasogenic edema at the site of injury. Undoubtedly, the development of vasogenic edema can occur immediately after a TBI as a result of BBB breakdown (Unterberg, Stover et al. 2004). While levels of AQP4 have not been examined at chronic time points following injury, increased levels of AQP4 have been previously reported in chronic studies of epilepsy. In particular, increased AQP4 levels have been documented in postmortem human sclerotic hippocampal tissue with TLE

(Lee, Eid et al. 2004). The increased AQP4 was noted to reflect the mislocalization of AQP4 away from perivascular endfeet and has been proposed as the underlying mechanism of impaired K^+ clearance (Lee, Eid et al. 2004; Eid, Lee et al. 2005). Surprisingly, in this study, WT mice without PTE had a significant increase in Kir4.1 in the ipsilateral hippocampus that may be associated with redistribution of AQP4. This finding corroborates with previous human and experimental models of epilepsy. For example, using an intrahippocampal kainic acid (IHKA) model of epilepsy, an upregulation of Kir.41 was observed in reactive astrocytes in the stratum radiatum and stratum lacunosum moleculare layers of the hippocampus (Lee, Hsu et al. 2012). An increase in Kir4.1 away from astrocytic fine processes was also observed after TBI (Stewart, Eastman et al. 2010) and in postmortem human hippocampal sclerotic tissue with TLE (Heuser, Eid et al. 2012). Moreover, altered hippocampal Kir conductances have also been reported as early as 2 dpi after FPI (D'Ambrosio, Maris et al. 1999) as well as 1 month dpi in the neocortex but not the hippocampus (Stewart, Eastman et al. 2010) indicating impaired K^+ homeostasis in the hippocampus leading to increased excitability. These findings indicate that Kir4.1 is dysregulated at acute time points after injury and that compensatory mechanisms may aid in the recovery of Kir conductances at chronic time points, specifically in the hippocampus. In mice without PTE, WT mice displayed a trending increase in Kir4.1 expression levels in the ipsilateral hippocampus compared with AQP4 KO mice. Unfortunately, specific patterns of Kir4.1 regulation was not observed in a time course specific manner thus it is unknown whether the increase in expression was greater in the acute or chronic time points. Therefore, my studies, along with previously reported findings, suggests that AQP4 and Kir4.1 are distinctly regulated

and may be possibly mislocalized after a CNS insult ultimately contributing to the development of PTE.

Mounting evidence has pointed to reactive astrocytes as key players in the pathophysiology of epilepsy and TBI (Lee, Eid et al. 2004; Sofroniew 2005; Myer, Gurkoff et al. 2006; Laird, Vender et al. 2008; Sofroniew 2009; Lee, Hsu et al. 2012; Hubbard, Szu et al. 2016). Besides altered morphology after CNS insults, many astrocytic proteins are up- or down-regulated which can cause changes in cellular functions. For example, loss of Kir currents and abnormal accumulation of extracellular K^+ have been shown in reactive astrocytes in the hippocampus after FPI (D'Ambrosio, Maris et al. 1999) and significant downregulation of hippocampal AQP4 in reactive astrocytes were observed after IHKA (Lee, Hsu et al. 2012; Hubbard, Szu et al. 2016). Besides an increase in the 14-day sham group of WT mice, IHC analysis did not detect any significant differences in GFAP immunoreactivity between sham and TBI mice at each time point in the present study. This indicates that TBI in the frontal cortex did not significantly injure the distant hippocampus and that electrode implantation also did not disturb the hippocampus considerably. Interestingly, Western blot analysis identified alterations in Kir4.1 and AQP4 expression levels in the hippocampus which are commonly observed colocalized with reactive astrocytes. This implies that alterations in astrocytic proteins can occur without overt reactive astrocytosis. Therefore, future studies should investigate whether differences in GFAP exists between mice with and without PTE and if reactive astrocytes (or lack thereof) are associated with the observed changes in AQP4 and Kir4.1

The main findings in this study suggest possible dysregulation and/or mislocalization of AQP4 after TBI which may possibly modulate seizure activity in PTE.

Here, the loss or redistribution of AQP4 can lead to astrocyte endfeet swelling due to decreased efflux of water and K^+ from astrocyte endfeet into the blood vessels resulting in increased seizure susceptibility. Several lines of evidence have demonstrated that cellular swelling can directly lead to increased neuronal excitability (Rowntree 1926; Risher, Andrew et al. 2009; Lauderdale, Murphy et al. 2015) by decreasing the ECS and increasing ephaptic interactions (Wetherington, Serrano et al. 2008). Because AQP4 is found highly polarized to astrocyte endfeet (Verkman, Binder et al. 2006), loss of perivascular AQP4 can induce swelling of the astrocytes which is thought to contribute to increased seizure activity (Binder 2018). Indeed, astrocytic endfeet swelling has been observed in TBI (Østergaard, Engedal et al. 2014), which can promote further pathology, such as PTE. Altogether, these findings suggest that astrocytes and its key molecules, AQP4 and Kir4.1, are essential for the development of PTE and can serve as potential therapeutic targets.

5.6 References

Allen, N. J. and Barres, B. A. (2009). "Neuroscience: glia—more than just brain glue." Nature **457**(7230): 675.

Amiry-Moghaddam, M., Frydenlund, D., et al. (2004). "Anchoring of aquaporin-4 in brain: molecular mechanisms and implications for the physiology and pathophysiology of water transport." Neuroscience **129**(4): 997-1008.

Amiry-Moghaddam, M., Williamson, A., et al. (2003). "Delayed K+ clearance associated with aquaporin-4 mislocalization: phenotypic defects in brains of α-syntrophin-null mice." Proceedings of the National Academy of Sciences **100**(23): 13615-13620.

Badaut, J., Fukuda, A. M., et al. (2014). "Aquaporin and brain diseases." Biochimica et Biophysica Acta (BBA)-General Subjects **1840**(5): 1554-1565.

Benninger, C., Kadis, J., et al. (1980). "Extracellular calcium and potassium changes in hippocampal slices." Brain research **187**(1): 165-182.

Binder, D. K. (2018). "Astrocytes: Stars of the Sacred Disease." Epilepsy currents **18**(3): 172-179.

Binder, D. K., Nagelhus, E. A., et al. (2012). "Aquaporin-4 and epilepsy." Glia **60**(8): 1203-1214.

Binder, D. K., Papadopoulos, M. C., et al. (2004). "In vivo measurement of brain extracellular space diffusion by cortical surface photobleaching." Journal of Neuroscience **24**(37): 8049-8056.

Binder, D. K., Yao, X., et al. (2006). "Increased seizure duration and slowed potassium kinetics in mice lacking aquaporin-4 water channels." Glia **53**(6): 631-636.

Bush, T. G., Puvanachandra, N., et al. (1999). "Leukocyte infiltration, neuronal degeneration, and neurite outgrowth after ablation of scar-forming, reactive astrocytes in adult transgenic mice." Neuron **23**(2): 297-308.

Butt, A. M. and Kalsi, A. (2006). "Inwardly rectifying potassium channels (Kir) in central nervous system glia: a special role for Kir4. 1 in glial functions." Journal of cellular and molecular medicine **10**(1): 33-44.

Cheung, G., Sibille, J., et al. (2015). "Activity-dependent plasticity of astroglial potassium and glutamate clearance." Neural plasticity **2015**.

Chodobski, A., Zink, B. J., et al. (2011). "Blood–brain barrier pathophysiology in traumatic brain injury." Translational stroke research **2**(4): 492-516.

Connors, N. C. and Kofuji, P. (2006). "Potassium channel Kir4. 1 macromolecular complex in retinal glial cells." Glia **53**(2): 124-131.

D'Ambrosio, R., Fairbanks, J. P., et al. (2004). "Post-traumatic epilepsy following fluid percussion injury in the rat." Brain **127**(2): 304-314.

D'Ambrosio, R., Maris, D. O., et al. (1999). "Impaired K+ homeostasis and altered electrophysiological properties of post-traumatic hippocampal glia." Journal of Neuroscience **19**(18): 8152-8162.

Devinsky, O., Vezzani, A., et al. (2013). "Glia and epilepsy: excitability and inflammation." Trends in neurosciences **36**(3): 174-184.

Ding, J.-H., Sha, L.-L., et al. (2007). "Alterations of striatal neurotransmitter release in aquaporin-4 deficient mice: An in vivo microdialysis study." Neuroscience letters **422**(3): 175-180.

Djukic, B., Casper, K. B., et al. (2007). "Conditional knock-out of Kir4. 1 leads to glial membrane depolarization, inhibition of potassium and glutamate uptake, and

enhanced short-term synaptic potentiation." Journal of Neuroscience **27**(42): 11354-11365.

Donkin, J. J. and Vink, R. (2010). "Mechanisms of cerebral edema in traumatic brain injury: therapeutic developments." Current opinion in neurology **23**(3): 293-299.

Eid, T., Lee, T.-S. W., et al. (2005). "Loss of perivascular aquaporin 4 may underlie deficient water and K+ homeostasis in the human epileptogenic hippocampus." Proceedings of the National Academy of Sciences **102**(4): 1193-1198.

Faulkner, J. R., Herrmann, J. E., et al. (2004). "Reactive astrocytes protect tissue and preserve function after spinal cord injury." Journal of Neuroscience **24**(9): 2143-2155.

Fiacco, T. A., Agulhon, C., et al. (2009). "Sorting out astrocyte physiology from pharmacology." Annual review of pharmacology and toxicology **49**: 151-174.

Gabriel, S., Njunting, M., et al. (2004). "Stimulus and potassium-induced epileptiform activity in the human dentate gyrus from patients with and without hippocampal sclerosis." Journal of Neuroscience **24**(46): 10416-10430.

Guo, Q., Sayeed, I., et al. (2006). "Progesterone administration modulates AQP4 expression and edema after traumatic brain injury in male rats." Experimental neurology **198**(2): 469-478.

Heinemann, U., Konnerth, A., et al. (1986). "Extracellular calcium and potassium concentration changes in chronic epileptic brain tissue." Advances in neurology **44**: 641-661.

Hertz, L. (1978). "An intense potassium uptake into astrocytes, its further enhancement by high concentrations of potassium, and its possible involvement in potassium homeostasis at the cellular level." Brain Research **145**(1): 202-208.

Heuser, K., Eid, T., et al. (2012). "Loss of perivascular Kir4. 1 potassium channels in the sclerotic hippocampus of patients with mesial temporal lobe epilepsy." Journal of Neuropathology & Experimental Neurology **71**(9): 814-825.

Hibino, H., Inanobe, A., et al. (2010). "Inwardly rectifying potassium channels: their structure, function, and physiological roles." Physiological reviews **90**(1): 291-366.

Hinterkeuser, S., Schröder, W., et al. (2000). "Astrocytes in the hippocampus of patients with temporal lobe epilepsy display changes in potassium conductances." European Journal of Neuroscience **12**(6): 2087-2096.

Hubbard, J. A., Szu, J. I., et al. (2016). "Regulation of astrocyte glutamate transporter-1 (GLT1) and aquaporin-4 (AQP4) expression in a model of epilepsy." Experimental neurology **283**: 85-96.

Kofuji, P., Ceelen, P., et al. (2000). "Genetic inactivation of an inwardly rectifying potassium channel (Kir4. 1 subunit) in mice: phenotypic impact in retina." Journal of Neuroscience **20**(15): 5733-5740.

Kofuji, P. and Newman, E. (2004). "Potassium buffering in the central nervous system." Neuroscience **129**(4): 1043-1054.

Laird, M. D., Vender, J. R., et al. (2008). "Opposing roles for reactive astrocytes following traumatic brain injury." Neurosignals **16**(2-3): 154-164.

Larsson, Å., Wilhelmsson, U., et al. (2004). "Increased cell proliferation and neurogenesis in the hippocampal dentate gyrus of old GFAP−/− Vim−/− mice." Neurochemical research **29**(11): 2069-2073.

Lauderdale, K., Murphy, T., et al. (2015). "Osmotic edema rapidly increases neuronal excitability through activation of NMDA receptor-dependent slow inward currents in juvenile and adult hippocampus." ASN neuro **7**(5): 1759091415605115.

Lee, D. J., Hsu, M. S., et al. (2012). "Decreased expression of the glial water channel aquaporin-4 in the intrahippocampal kainic acid model of epileptogenesis." Experimental neurology **235**(1): 246-255.

Lee, T. S., Eid, T., et al. (2004). "Aquaporin-4 is increased in the sclerotic hippocampus in human temporal lobe epilepsy." Acta neuropathologica **108**(6): 493-502.

Li, J., Patil, R. V., et al. (2002). "Mildly abnormal retinal function in transgenic mice without Muller cell aquaporin-4 water channels." Investigative ophthalmology & visual science **43**(2): 573-579.

Li, J. and Verkman, A. (2001). "Impaired hearing in mice lacking aquaporin-4 water channels." Journal of Biological Chemistry **276**(33): 31233-31237.

Lu, D. C., Zador, Z., et al. (2011). "Aquaporin-4 reduces post-traumatic seizure susceptibility by promoting astrocytic glial scar formation in mice." Journal of neurotrauma(ja).

Ma, T., Yang, B., et al. (1997). "Generation and phenotype of a transgenic knockout mouse lacking the mercurial-insensitive water channel aquaporin-4." The Journal of Clinical Investigation **100**(5): 957-962.

Maas, A. I., Stocchetti, N., et al. (2008). "Moderate and severe traumatic brain injury in adults." The Lancet Neurology **7**(8): 728-741.

MacAulay, N. and Zeuthen, T. (2012). "Glial K+ clearance and cell swelling: key roles for cotransporters and pumps." Neurochemical research **37**(11): 2299-2309.

Manley, G. T., Binder, D., et al. (2004). "New insights into water transport and edema in the central nervous system from phenotype analysis of aquaporin-4 null mice." Neuroscience **129**(4): 981-989.

Marcus, D. C., Wu, T., et al. (2002). "KCNJ10 (Kir4. 1) potassium channel knockout abolishes endocochlear potential." American Journal of Physiology-Cell Physiology **282**(2): C403-C407.

Masaki, H., Wakayama, Y., et al. (2010). "Immunocytochemical studies of aquaporin 4, Kir4. 1, and α1-syntrophin in the astrocyte endfeet of mouse brain capillaries." Acta histochemica et cytochemica **43**(4): 99-105.

Matthias, K., Kirchhoff, F., et al. (2003). "Segregated expression of AMPA-type glutamate receptors and glutamate transporters defines distinct astrocyte populations in the mouse hippocampus." Journal of Neuroscience **23**(5): 1750-1758.

Menet, V., Prieto, M., et al. (2003). "Axonal plasticity and functional recovery after spinal cord injury in mice deficient in both glial fibrillary acidic protein and vimentin genes." Proceedings of the National Academy of Sciences **100**(15): 8999-9004.

Myer, D., Gurkoff, G., et al. (2006). "Essential protective roles of reactive astrocytes in traumatic brain injury." Brain **129**(10): 2761-2772.

Nagelhus, E., Mathiisen, T., et al. (2004). "Aquaporin-4 in the central nervous system: cellular and subcellular distribution and coexpression with KIR4. 1." Neuroscience **129**(4): 905-913.

Nagelhus, E. A., Horio, Y., et al. (1999). "Immunogold evidence suggests that coupling of K+ siphoning and water transport in rat retinal Müller cells is mediated by a

coenrichment of Kir4. 1 and AQP4 in specific membrane domains." Glia **26**(1): 47-54.

Nagelhus, E. A. and Ottersen, O. P. (2013). "Physiological roles of aquaporin-4 in brain." Physiological reviews **93**(4): 1543-1562.

Neusch, C., Rozengurt, N., et al. (2001). "Kir4. 1 potassium channel subunit is crucial for oligodendrocyte development and in vivo myelination." Journal of Neuroscience **21**(15): 5429-5438.

Oberheim, N. A., Tian, G.-F., et al. (2008). "Loss of astrocytic domain organization in the epileptic brain." Journal of Neuroscience **28**(13): 3264-3276.

Oberheim, N. A., Wang, X., et al. (2006). "Astrocytic complexity distinguishes the human brain." Trends Neurosci **29**(10): 547-553.

Olsen, M. L. and Sontheimer, H. (2008). "Functional implications for Kir4. 1 channels in glial biology: from K+ buffering to cell differentiation." Journal of neurochemistry **107**(3): 589-601.

Orkand, R. K. (1986). "Introductory remarks: Glial-interstitial fluid exchange." Annals of the New York Academy of Sciences **481**(1): 269-272.

Østergaard, L., Engedal, T. S., et al. (2014). "Capillary transit time heterogeneity and flow-metabolism coupling after traumatic brain injury." Journal of Cerebral Blood Flow & Metabolism **34**(10): 1585-1598.

Parpura, V., Basarsky, T. A., et al. (1994). "Glutamate-mediated astrocyte-neuron signalling." Nature **369**(6483): 744-747.

Pekny, M. and Nilsson, M. (2005). "Astrocyte activation and reactive gliosis." Glia **50**(4): 427-434.

Pekny, M. and Pekna, M. (2016). "Reactive gliosis in the pathogenesis of CNS diseases." Biochimica et Biophysica Acta (BBA)-Molecular Basis of Disease **1862**(3): 483-491.

Pekny, M., Wilhelmsson, U., et al. (2014). "The dual role of astrocyte activation and reactive gliosis." Neuroscience letters **565**: 30-38.

Reichenbach, A. and Wolburg, H. (2005). "Astrocytes and ependymal glia." Neuroglia **2**: 19-35.

Ren, Z., Iliff, J. J., et al. (2013). "'Hit & Run'model of closed-skull traumatic brain injury (TBI) reveals complex patterns of post-traumatic AQP4 dysregulation." Journal of Cerebral Blood Flow & Metabolism **33**(6): 834-845.

Risher, W. C., Andrew, R. D., et al. (2009). "Real-time passive volume responses of astrocytes to acute osmotic and ischemic stress in cortical slices and in vivo revealed by two-photon microscopy." Glia **57**(2): 207-221.

Rowntree, L. G. (1926). "The effects on mammals of the administration of excessive quantities of water." Journal of Pharmacology and Experimental Therapeutics **29**(1): 135-159.

Ruiz-Ederra, J., Zhang, H., et al. (2007). "Evidence against functional interaction between aquaporin-4 water channels and Kir4. 1 potassium channels in retinal Müller cells." Journal of Biological Chemistry **282**(30): 21866-21872.

Rutecki, P. A., Lebeda, F. J., et al. (1985). "Epileptiform activity induced by changes in extracellular potassium in hippocampus." Journal of Neurophysiology **54**(5): 1363-1374.

Saadoun, S., Papadopoulos, M. C., et al. (2005). "Involvement of aquaporin-4 in astroglial cell migration and glial scar formation." Journal of cell science **118**(24): 5691-5698.

Saadoun, S., Tait, M., et al. (2009). "AQP4 gene deletion in mice does not alter blood–brain barrier integrity or brain morphology." Neuroscience **161**(3): 764-772.

Seifert, G., Hüttmann, K., et al. (2009). "Analysis of astroglial K+ channel expression in the developing hippocampus reveals a predominant role of the Kir4. 1 subunit." Journal of Neuroscience **29**(23): 7474-7488.

Skucas, V. A., Mathews, I. B., et al. (2011). "Impairment of select forms of spatial memory and neurotrophin-dependent synaptic plasticity by deletion of glial aquaporin-4." Journal of Neuroscience **31**(17): 6392-6397.

Sofroniew, M. V. (2005). "Reactive astrocytes in neural repair and protection." The Neuroscientist **11**(5): 400-407.

Sofroniew, M. V. (2009). "Molecular dissection of reactive astrogliosis and glial scar formation." TRENDS in Neurosciences **32**(12): 638-647.

Sofroniew, M. V. and Vinters, H. V. (2010). "Astrocytes: biology and pathology." Acta neuropathologica **119**(1): 7-35.

Solenov, E., Watanabe, H., et al. (2004). "Sevenfold-reduced osmotic water permeability in primary astrocyte cultures from AQP-4-deficient mice, measured by a fluorescence quenching method." American Journal of Physiology-Cell Physiology **286**(2): C426-C432.

Somjen, G. G. (1979). "Extracellular potassium in the mammalian central nervous system." Annual review of physiology **41**(1): 159-177.

Steinhäuser, C., Seifert, G., et al. (2012). "Astrocyte dysfunction in temporal lobe epilepsy: K+ channels and gap junction coupling." Glia **60**(8): 1192-1202.

Stewart, T. H., Eastman, C. L., et al. (2010). "Chronic dysfunction of astrocytic inwardly rectifying K+ channels specific to the neocortical epileptic focus after fluid percussion injury in the rat." Journal of neurophysiology **104**(6): 3345-3360.

Sun, M.-C., Honey, C. R., et al. (2003). "Regulation of aquaporin-4 in a traumatic brain injury model in rats." Journal of neurosurgery **98**(3): 565-569.

Swartz, B. E., Houser, C. R., et al. (2006). "Hippocampal cell loss in posttraumatic human epilepsy." Epilepsia **47**(8): 1373-1382.

Szu, J. I. and Binder, D. K. (2016). "The role of astrocytic aquaporin-4 in synaptic plasticity and learning and memory." Frontiers in integrative neuroscience **10**.

Tait, M. J., Saadoun, S., et al. (2008). "Water movements in the brain: role of aquaporins." TRENDS in Neurosciences **31**(1): 37-43.

Traynelis, S. F. and Dingledine, R. (1988). "Potassium-induced spontaneous electrographic seizures in the rat hippocampal slice." Journal of Neurophysiology **59**(1): 259-276.

Traynelis, S. F. and Dingledine, R. (1989). "Role of extracellular space in hyperosmotic suppression of potassium-induced electrographic seizures." Journal of Neurophysiology **61**(5): 927-938.

Unterberg, A., Stover, J., et al. (2004). "Edema and brain trauma." Neuroscience **129**(4): 1019-1027.

Verkman, A. (2005). "More than just water channels: unexpected cellular roles of aquaporins." J Cell Sci **118**(15): 3225-3232.

Verkman, A., Binder, D. K., et al. (2006). "Three distinct roles of aquaporin-4 in brain function revealed by knockout mice." Biochimica et Biophysica Acta (BBA)-Biomembranes **1758**(8): 1085-1093.

Verkman, A. and Mitra, A. K. (2000). "Structure and function of aquaporin water channels." American Journal of Physiology-Renal Physiology **278**(1): F13-F28.

Voskuhl, R. R., Peterson, R. S., et al. (2009). "Reactive astrocytes form scar-like perivascular barriers to leukocytes during adaptive immune inflammation of the CNS." Journal of Neuroscience **29**(37): 11511-11522.

Walz, W. (2000). "Role of astrocytes in the clearance of excess extracellular potassium." Neurochemistry international **36**(4-5): 291-300.

Werner, C. and Engelhard, K. (2007). "Pathophysiology of traumatic brain injury." BJA: British Journal of Anaesthesia **99**(1): 4-9.

Wetherington, J., Serrano, G., et al. (2008). "Astrocytes in the epileptic brain." Neuron **58**(2): 168-178.

Wilhelmsson, U., Faiz, M., et al. (2012). "Astrocytes negatively regulate neurogenesis through the Jagged1-mediated Notch pathway." Stem Cells **30**(10): 2320-2329.

Zhang, C., Chen, J., et al. (2015). "Expression of aquaporin-4 and pathological characteristics of brain injury in a rat model of traumatic brain injury." Molecular medicine reports **12**(5): 7351-7357.

Zhang, H. and Verkman, A. (2008). "Aquaporin-4 independent Kir4. 1 K+ channel function in brain glial cells." Molecular and Cellular Neuroscience **37**(1): 1-10

Chapter 6: Conclusions and future directions

One of the biggest challenges in posttraumatic epilepsy (PTE) is identifying effective treatments that can prevent the development of epilepsy after traumatic brain injury (TBI). Due to our limited understanding of the mechanisms underlying PTE, biomarkers of PTE have yet to be identified. PTE is both widely acknowledged in the clinical and preclinical settings, however, advancement in our knowledge of PTE has been meager. For instance, the majority of existing animal models of PTE have primarily focused on inducing the injury over the parietotemporal cortex and examining changes in the cortex and the underlying hippocampus. In the present study, I used the controlled cortical impact (CCI) injury model to induce a single TBI in the right frontal lobe of CD1 wildtype (WT) and aquaporin-4 knockout (AQP4 KO) mice. Changes in the ipsilateral hippocampus were then investigated at 14, 30, 60, and 90 days post injury (dpi). Optical coherence tomography (OCT) imaging, chronic *in vivo* video-encephalographic (vEEG), immunohistochemistry, and Western blot analysis of AQP4 and Kir4.1 were also performed to identify any potential biomarkers of PTE.

The first step in any experimental study of PTE is to develop a working model where the animal experiences late spontaneous posttraumatic seizures. In “Chapter 2: Mouse model of PTE”, I described my model of PTE where I used the well-established CCI injury model of TBI. With my parameters, I was able to induce and detect late spontaneous seizures in the ipsilateral hippocampus in both WT and AQP4 KO mice with similarities to the human condition. Chronic vEEG detected posttraumatic electrographic seizures that were characterized by high frequency and amplitude (fast polyspikes) or 3 Hz spikes. These electrographic seizures were correlated with immobility and facial automatisms, behavior commonly seen in human PTE. Moreover,

my model is the first to produce the highest yield of PTE in mice after CCI (17% of total WT mice and 27% of total AQP4 KO mice). Currently, there are only three existing studies of PTE in mice with CCI with only one study utilizing vEEG recording. Studies by Hunt et al. observed 36 – 40% of spontaneous seizures in CD1 mice after CCI in the parietotemporal cortex (Hunt, Scheff et al. 2009; Hunt, Scheff et al. 2010). These seizures were passively monitored from 42 days – 10 weeks post injury and did not include any vEEG recordings. Therefore, the high percentages of mice with spontaneous seizures may not truly represent PTE especially since behavioral observations without vEEG correlation can lead to false identification of seizure activity. Additionally, the authors of these studies excluded any nonconvulsive seizures that are commonly seen in human PTE and which can only be diagnosed with EEG evaluation (Vespa, Nuwer et al. 1999; Vespa, Miller et al. 2007; Vespa, McArthur et al. 2010). Finally, the last study used CCI to induce a TBI with 0.5 mm depth in the parietotemporal region of both CD1 and C57BL/6S mice. vEEG recordings with cortical screw electrodes were employed and monitored up to 9 months post injury. Even with the lesion extending all layers of the cortex and apparent hippocampal damage, only 9% of CD1 mice and 3% of C57BL/6S mice had spontaneous seizures 6 months after injury. Surprisingly, none of these mice had spontaneous seizures by 9 months after injury even a with a pentylenetetrazole (PTZ) challenge during the 6 month follow-up (Bolkvadze and Pitkänen 2012). Therefore, my model represents a valuable tool in studying PTE as it is both clinically translational and produced the highest known yield of epilepsy after TBI.

Despite the clinical significance of PTE, when and where PTE (or late posttraumatic seizures) develops remains unknown. It is widely agreed that immediate

and early posttraumatic seizures arise from the perilesional cortex (around the impact site). After TBI, a host of cellular and molecular changes occur to increase neuronal hyperexcitability. For instance, release of excitatory amino acids, such as glutamate and aspartate, at high concentrations can result in excitotoxicity and cell death (Ray, Dixon et al. 2002), loss of ion homeostasis can lead to depolarization of neurons and glia (Siesjö 1993), and increased levels of cytokines such as TNFα can potentiate excitatory transmission and maintain neuronal excitability (Burda, Bernstein et al. 2016). Indeed, immediate and early cortical seizures have been detected in a rat model of severe fluid percussion injury (FPI), although these seizures were only detected on the contralateral side (Kharatishvili, Nissinen et al. 2006). Thus, the question of where the first seizure initiated in this particular study remains unknown. It is noteworthy, however, that these seizures propagated to the contralateral side early after injury. In another study using the rat model of FPI, chronic electrocorticography (ECoG) recordings 9 – 16 weeks post injury detected seizure onset at the site of injury that can secondarily generalize over time (D'Ambrosio, Fairbanks et al. 2004). These findings are intriguing as it suggests that even at chronic time points, seizures can still initiate at the impact site.

To determine the anatomy of PTE, studies utilizing multiple electrodes are needed. Several groups have attempted to record from multiple sites in the brain after experimental TBI. As previously mentioned, ECoG recordings with multiple epidural electrodes (5 – 7 electrodes with one at the center of the impact) detected epileptiform activity that initiated at the lesion or perilesional cortex which spread to the adjacent cortical regions after FPI (D'Ambrosio, Fairbanks et al. 2004). To identify other epileptic foci, subsequent studies from the same group paired hippocampal depth electrodes with ECoG. In this study, the authors found that the majority of the seizures that began 2 – 3

weeks after TBI were focal seizures initiating at the lesion or near the perilesional cortex and that seizures ~14 weeks after TBI were mostly hippocampal (D'Ambrosio, Fender et al. 2005). In a separate study, chronic spontaneous hippocampal seizures were also detected after FPI in rats. Using two cortical electrodes and a hippocampal depth electrode, tonic-clonic seizures were observed originating in the ipsilateral hippocampus that spread to the contralateral cortex 11 weeks after FPI. Moreover, subclinical seizures (electrographic seizures with no behavioral correlate) were also detected in the ipsilateral hippocampus that propagated to the contralateral cortex 8 weeks after FPI (Kharatishvili, Nissinen et al. 2006). These studies demonstrate the utility of using multiple electrodes in detecting various epileptic foci after TBI with PTE most prominent in the hippocampus at chronic time points.

While the previously mentioned studies have provided invaluable information regarding when and where seizures start, the findings are limited as only a few electrodes were utilized. The use of multielectrode arrays (MEA) is one approach to fully capture electrical changes in widespread brain areas after TBI. In a pilot study using my model of PTE, a 30-channel MEA was implanted on the surface of the mouse skull and resting EEG recordings were performed on WT naïve and injured mice at 30 dpi. Preliminary findings detected interictal spikes at the site of injury that propagated to the contralateral frontal cortex (Figure 6.1). This finding supports previous reports that

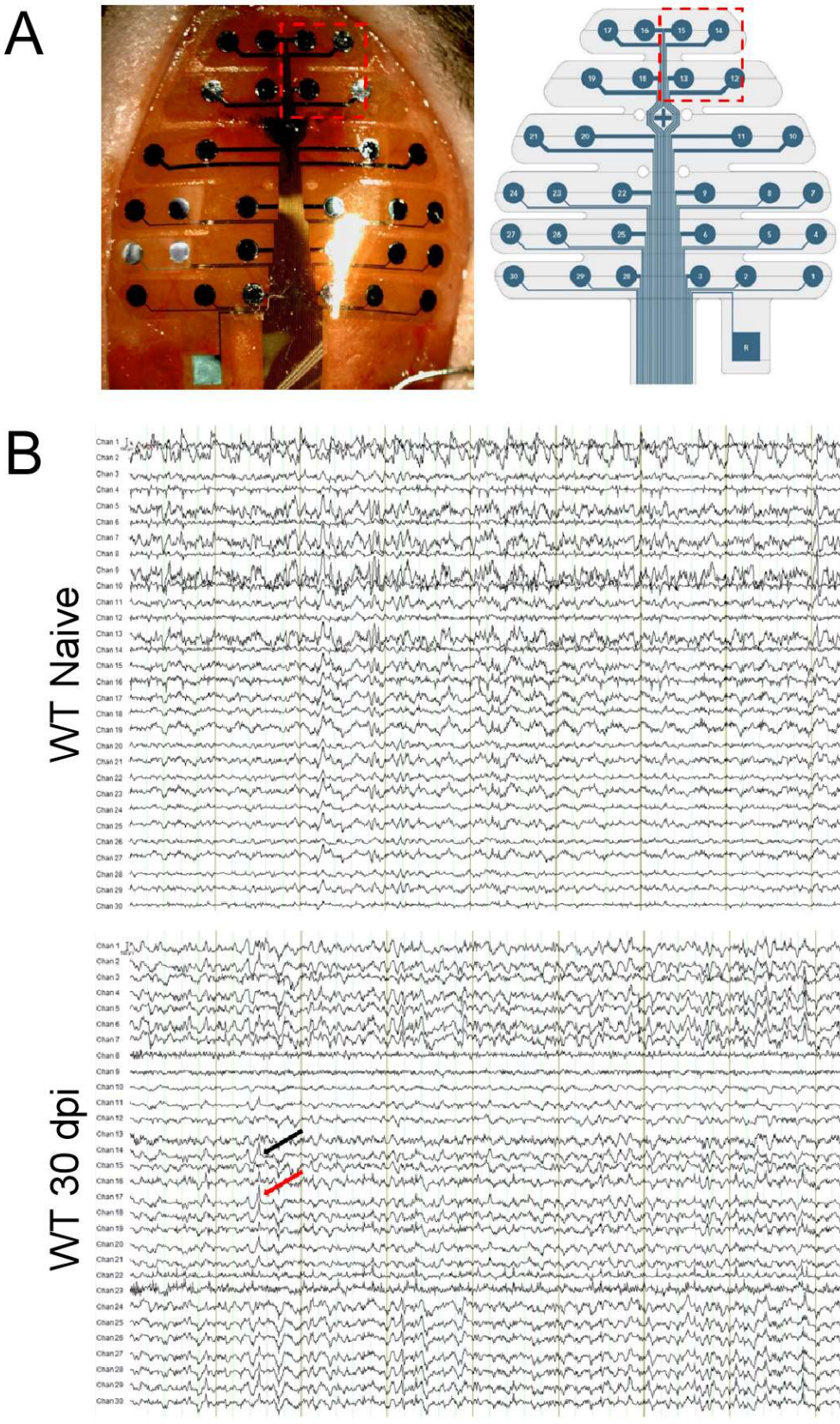
A
B
WT Naive
WT 30 dpi

Figure 6.1 MEA recordings after TBI. A. Implantation of a 30-channel MEA for chronic in vivo EEG recording (left) and map of the corresponding 30 channels (right). Dashed red square indicates area over CCI impact site. **B.** Preliminary MEA recordings in WT naïve and WT 30dpi mice. Interictal spikes were detected at the site of impact (black arrow, channel 14) that propagated to the contralateral frontal cortex (red arrow, channel 17).

studies with chronic MEA recordings beginning at earlier time points after TBI can allow determination of seizure onset and propagation throughout the entire cortex. Additionally, 32-channel depth electrode in the hippocampus could also be used concurrently with the 30-channel surface MEA allowing much greater insight into the evolution of seizure onset and spread patterns but also provide layer-specific anatomic and physiologic information regarding seizure generation and propagation in the hippocampus.

While mechanisms underlying immediate and early posttraumatic seizures are more defined, it remains unclear how late seizures are generated. The loss of blood-brain barrier (BBB) integrity after TBI has been shown to contribute to epilepsy. Indeed, previous studies have reported increased BBB permeability in PTE patients (Tomkins, Shelef et al. 2008). BBB-induced epileptogenesis is thought to be mediated by serum albumin extravasation into the extracellular space (ECS). In fact, experimental models showing BBB disruption and subsequent serum albumin extravasation can induce epileptiform discharges (Seiffert, Dreier et al. 2004). Furthermore, rats injected with albumin demonstrated increased spiking activity in the hippocampus 15 minutes after injection with spiking activity lasting up to 60 minutes. However, injection of kainic acid 24 hours after albumin injection resulted in prolonged epileptiform activity lasting up to 180 minutes after albumin injection. Even more notable was the significant decreased hippocampal seizure threshold 3 months after albumin injection even with no obvious albumin detected in the brain (Frigerio, Frasca et al. 2012). These findings suggest that

hippocampal hyperexcitability at chronic time points is activated by signaling pathways that is distinct from acute neuronal excitability induced by albumin alone. One possible mechanism that can contribute to increased hippocampal excitability at chronic time points may be due to the down-regulation of Kir4.1 mediated by uptake of albumin via astrocytic TGF-β receptor (Ivens, Kaufer et al. 2006). After BBB disruption by TBI, astrocytes become reactive and increase their TGF-β receptors which takes up extracellular albumin causing transcriptional downregulation of Kir4.1 ultimately impairing K^+ homeostasis resulting in long-term enhancement of neuronal excitability (Friedman, Kaufer et al. 2009; Heinemann, Kaufer et al. 2012).

Unfortunately, time course studies of Kir4.1 expression levels were not performed in this present study and alterations in Kir4.1 during the progression of PTE cannot be ascertained. Therefore, future studies should determine whether BBB permeability is compromised in the hippocampus and detect presence of albumin at the same time points. Bi-phasic opening of the BBB in the cortex and hippocampus has been previously reported in rats after CCI with increased BBB permeability between 4 – 6 hours and 3 days after TBI (Başkaya, Rao et al. 1997), however in this study, CCI was induced over the parietotemporal region where the hippocampus is highly vulnerable to injury. Thus, in my model, biphasic opening of the BBB, particularly in the hippocampus seems unlikely as it is distant from the frontal cortex (site of impact). Nevertheless, these studies would determine whether delayed BBB opening occurs in the hippocampus and whether albumin (and subsequent downregulation of Kir4.1) can induce seizure activity.

The colocalization of Kir4.1 and AQP4 suggests that regulation of AQP4 may follow that of Kir4.1. Here, Western blot and immunohistochemistry (IHC) analysis did

not detect any significant differences in AQP4 between sham *vs.* TBI at all time points except at 14 days where an increase in AQP4 immunoreactivity in sham mice was observed compared to injured mice. The increase in AQP4 immunoreactivity was observed in the ipsilateral and contralateral stratum lacunosum moleculare and the contralateral stratum radiatum of the hippocampus. The upregulation of AQP4 observed does not seem to be related to surgery (*i.e.*, preparation of thinned skull cortical window and electrode implant) since these changes were not observed in other layers of the ipsilateral hippocampus.

When comparing AQP4 expression levels between mice with and without PTE, a significant increase in AQP4 was detected in the ipsilateral frontal cortex and hippocampus in mice with PTE. This finding supports previous reports of increased AQP4 in human and animal models of TBI and epilepsy. The significant upregulation of AQP4 in PTE mice suggests deficits in water homeostasis caused by the possibility of mislocalized AQP4 from the perivalscular endfeet towards the neuropil. In this situation, rather than transporting water into the blood vessels, water is then extruded into the ECS, causing swelling of neurons and glial cells, constricting the ECS, and increasing neuronal hyperexcitability. To test this hypothesis, future studies can utilize electron microscopy to examine swollen astrocytic endfeet.

While dysregulation of AQP4 and Kir4.1 has been previously implicated, the mechanisms underlying such dysregulation should be considered in PTE. The adaptor protein α-syntrophin (α-syn) is thought to anchor AQP4 and Kir4.1 into the membrane and participates with the larger dystrophin-glycoprotein complex (DGC) (Amiry-Moghaddam, Otsuka et al. 2003; Amiry-Moghaddam, Williamson et al. 2003; Connors, Adams et al. 2004). Indeed, α-syn-null mice exhibited dramatic loss of perivascular

AQP4 and delayed extracellular K^+ clearance, although surprisingly, the decrease in perivascular Kir4.1 was not as pronounced. Moreover, these mice experienced greater seizure severity further suggesting that water and K^+ transport are coupled (Amiry-Moghaddam, Williamson et al. 2003). Therefore, in the present study, increased AQP4 expression in PTE mice may be due to loss of perivascular AQP4 expression and subsequent redistribution towards the neuropil. Additionally, Kir4.1 may also be modestly mislocalized which may contribute to PTE due to lack of proper K^+ uptake and clearance. However, changes in AQP4 and Kir4.1 expression may ultimately rely on alterations in α-syn, and thus, future studies investigating regulation of this adaptor protein and how it affects distribution of AQP4 and Kir4.1 may provide further insights into the development of PTE. Additionally, to confirm that AQP4 and Kir4.1 are in fact mislocalized, subcellular distribution of these proteins should be investigated. One approach would be to utilize super-resolution microscopy techniques such as photo-activated localization microscopy (PALM) or stochastic optical reconstruction microscopy (STORM) which allows localization of single molecules.

Spontaneous hippocampal seizures can also be attributed to mossy fiber sprouting (MFS) in which the axons of the dentate granule cells undergo long-term structural reorganization by forming new recurrent excitatory circuits (Scharfman, Sollas et al. 2003). Indeed, MFS has been observed in the hippocampus of epileptic patients (Sutula, Cascino et al. 1989; Babb, Kupfer et al. 1991; El Bahh, Lespinet et al. 1999; Schmeiser, Zentner et al. 2017) and the presence of MFS has also been previously documented in models of epilepsy and TBI. Dramatic MFS was observed in rats 27 weeks after induction of TBI using weight drop in which the rats also exhibited enhanced seizure susceptibility to PTZ 15 weeks after TBI (Golarai, Greenwood et al. 2001). After

FPI, MFS was more pronounced in rats with PTE compared with those that did not develop PTE (Kharatishvili, Nissinen et al. 2006). Hippocampal slices from severe MFS observed 42 – 71 days after CCI exhibited spontaneous hilar-evoked epileptiform activity, whereas such activity was not observed in slices from injured animals that did not display MFS (Hunt, Scheff et al. 2009). Rats with FPI also demonstrated increased MFS 1 week and 3 months after injury and hippocampal slices with MFS exhibited persistent decrease in seizure threshold (Santhakumar, Ratzliff et al. 2001). Together, these studies imply that mossy fiber reorganization may contribute to spontaneous seizures. However, it remains unknown whether MFS is a cause or consequence of these seizures. To extend on current findings and establish other potential histological biomarkers of PTE, MFS can be explored using Timm's sulphide silver staining protocol in which silver particles are generated within Zn^{2+} rich boutons of mossy fibers. Studies have shown that mossy fibers corelease Zn^{2+} with glutamate and can thus act as a neuromodulator (Coulter 2000; Vogt, Mellor et al. 2000). Interestingly, high concentrations of K^{+} have been shown to release endogenous Zn^{2+} from mossy fibers (Aniksztejn, Charton et al. 1987). Therefore, to further establish histological biomarkers with PTE, the degree of MFS can be determined in mice with and without PTE and correlated to Kir4.1 levels in both WT and AQP4 KO mice. In addition, these findings can also further answer how AQP4 modulates synaptic organization in the hippocampus for seizure generation.

A drawback of PTE biomarker development is the dearth of EEG analysis. In many animal models of PTE, vEEG analysis has been restricted to visual assessment of the raw data including counting the number of seizures, seizure duration, spikes, bursts, and determining the latency to the first seizure. While this information reveals increased

seizure susceptibility after TBI, differences in these outcomes have been reported across studies suggesting that such analyses may not be good indicators for PTE biomarker development. In fact, an attempt to predict PTE using EEG has been previously reported in an early study in which EEG records from 722 patients were analyzed. In this study, the authors found that EEG abnormalities were similar in patients with and without late epilepsy; for example, delayed EEG spikes did not predict the development of PTE (Jennett and Van De Sande 1975). Because EEG signals contain different signal frequencies (e.g., delta 1 – 4 Hz, theta 4 – 7 Hz, alpha 7 – 15 Hz, and beta 15 – 35 Hz) it is crucial to extract these signals and evaluate them in detail. In "Chapter 4: Hippocampal electrographic biomarkers of posttraumatic epilepsy", I aimed to define specific EEG biomarkers. First, power spectral density (PSD) analysis was performed on the 1-week vEEG recordings to determine if TBI induced any alterations in EEG signals. Overall, TBI caused an increase in hippocampal EEG power, particularly at the delta and theta bands and at earlier time points (14 and 30 dpi) which is thought to correlate with increased freezing behavior during spontaneous seizures and aging. Increased delta and theta waves in the cortex after TBI have been previously observed in humans and in experimental models of TBI (Courjon 1970; McIntosh, Vink et al. 1989; Kharatishvili, Nissinen et al. 2006; Tomkins, Shelef et al. 2008; Tomkins, Feintuch et al. 2011), although increased delta and theta powers were not statistically different from patients with and without PTE. Interestingly, the increased delta power from PTE patients were correlated with BBB permeability (Tomkins, Shelef et al. 2008; Tomkins, Feintuch et al. 2011). It is important to note that cortical and hippocampal EEG frequencies may have different implications, nevertheless, the increased slow waves in the hippocampus observed in the present study corroborate with the human studies

previously mentioned. Therefore, future studies could investigate whether increased delta and theta powers are correlated with increased BBB permeability in the hippocampus.

PSD analysis can also be applied to spontaneous seizures in mice with and without PTE. In a previous finding (CITE) decreased theta power was observed prior to seizure onset which increased during the seizure event, and decreased at seizure termination (D'Ambrosio, Fairbanks et al. 2004). Similar PSD analysis can also be applied to future studies, in particular in PTE *vs.* non-PTE seizures. Findings from this type of analysis can be able to identify whether changes in specific EEG power band is different during the preictal, ictal, and postical periods and can further serve as predictors of PTE.

Unfortunately, characterization of hippocampal EEG frequencies in the delta, alpha, and beta bands are scarce, thus interpretation of the PSD analysis remains a challenge. However, the hippocampal theta band has been well characterized and has been shown to be involved in voluntary movements, learning and memory, and REM sleep. In this study, AQP4 KO mice displayed an increase in power in the theta frequency at 14 dpi which may be correlated with learning and memory. Indeed, studies have shown that lack of AQP4 resulted in altered synaptic plasticity and memory deficits (Szu and Binder 2016). Future studies employing hippocampal EEG recordings during various behavioral assays would produce meaningful information regarding how EEG signal changes after TBI at various time points and what it means functionally and behaviorally.

To further identify alterations in EEG signals, Morlet wavelet analysis of seizures was performed. Remarkably, at each time point, EEG power was uniquely different in

WT mice, whereas AQP4 KO mice exhibited somewhat consistent pattern. Interestingly, a higher EEG power signal was detected ~ 5 seconds prior to seizure onset in WT mice 14 dpi. To determine the cause of this signal, all individual Morlet wavelets were analyzed in which a spike artifact was detected in a seizure at 14 dpi that caused the increase in EEG power observed before seizure initiation. Finally, Morlet wavelets from mice with PTE *vs.* mice without PTE were compared and a specific electrographic phenotype was distinguished. Surprisingly, both WT and AQP4 KO mice with PTE exhibited similar patterns in power compared with mice without PTE. Morlet wavelets from mice with PTE revealed lower EEG power across both time and frequency which can be associated with the increased delta and theta powers detected by PSD analysis. On the other hand, Morlet wavelets from mice without PTE had higher EEG power across both time and frequency. Thus, late spontaneous seizures specific to PTE can be determined using Morlet wavelet analysis and may potentially serve as an EEG biomarker of PTE.

Because only a single electrode was used in this study, additional complex EEG analysis was not carried out. Future studies with MEA can overcome this limitation and define other EEG phenotypes which can further facilitate biomarker development in PTE. As we know, the brain is composed of large-scale dynamic networks where communication between cells can occur across great distances. EEG phase (or synchronization) is thought represent the exact timing of communication and information processing between populations of cells. In PTE, seizures can propagate to various regions of the brain and can secondarily generalize, however how populations of cells are coupled and modulate seizure activity remains unknown. Therefore, functional outcome measures from MEA recordings can be determined by analyzing EEG phase

coupling including phase coherence, phase coupling between frequencies, and phase-locking. In brief, phase coherence measures oscillatory activity from two different recording sites and quantifies the similarities between the two sites. A high phase coherence suggests that the two regions are functionally connected (Sauseng and Klimesch 2008). Because networks of cells, either within close proximity of one another or further away, can oscillate at different frequencies, EEG coupling between frequencies or cross-frequency coupling can determine when frequencies from two different locations are synchronized (Sauseng and Klimesch 2008). This can, thus, identify the functional interaction between networks at a given time (Canolty and Knight 2010). Finally, phase-locking utilizes the presentation of an external stimulus and detects alterations in event-related potential (ERP) (Sauseng and Klimesch 2008). EEG phase-locking can thus identify if certain frequencies are more likely to be "phase-locked" to the stimulus and can also be used to establish any clinically relevant measures of human PTE.

One of the most valuable tools to identify biomarkers is the use of neuroimaging techniques. Magnetic resonance imaging (MRI) and extensions of MRI such as diffuse tensor imaging (DTI), computed tomography (CT), and positron emission tomography (PET) scans are commonly used to detect abnormalities in the brain after TBI and epilepsy and have been employed to identify potential predictors of PTE. Thus, I sought to use OCT, a minimally invasive imaging modality, to define potential imaging biomarkers of PTE (see "Chapter 3: Optical biomarkers of posttraumatic epilepsy"). To increase optical signal penetration, a thinned skull cortical window was created over the parietal bone for imaging. Due to extensive bleeding and unevenness of both the brain and the skull flap after TBI, OCT imaging over the injury site was avoided. Additionally,

OCT was performed over the parietotemporal area to identify any correlation between optical attenuation coefficient (μ) and hippocampal seizures. In the present study, changes in μ between sham *vs.* TBI were not statistically significant in both WT and AQP4 KO mice, suggesting that any pathological changes associated with μ were either present at earlier time points or at the site of injury. Indeed, cerebral edema after TBI has been shown to peak by 2 dpi and resolve by 7 dpi (Soares, Thomas et al. 1992; Bareyre, Wahl et al. 1997; Kiening, van Landeghem et al. 2002). The earliest OCT imaging was performed at 4 dpi and lack of alteration in μ was observed at this time. This further implies that early swelling of the brain does not diffuse to regions distant from the injury site and that edema was most likely localized to the lesion and peri-lesional cortex. However, changes in μ may not be present or minimal in AQP4 KO mice as AQP4 KO mice were shown to be protected from cytotoxic edema (Manley, Fujimura et al. 2000) and TBI (Yao, Uchida et al. 2015). This indicates that the absence of AQP4 may have neuroprotective effects after injury. Qualitatively, after TBI, AQP4 KO mice exhibited less bleeding and cerebral edema compared to its WT counterparts, although the lesion core and increased glial fibrillary acidic protein (GFAP) immunoreactivity was observed at the injury site up to 90 dpi. This observation was surprising because AQP4 KO mice had a higher incidence of PTE despite the clear resilience at the time of injury. Therefore, future studies with OCT may require earlier imaging time points or imaging near the injury site.

In conclusion, I have developed a clinically relevant model of PTE for identifying potential biomarkers of PTE. Most remarkable is the fact that my model was able to generate the highest yield of PTE after CCI in mice than previously reported in the literature. Furthermore, AQP4 KO mice had greater incidence of late spontaneous

seizures and PTE compared with WT mice. Late spontaneous seizures were also more evident at chronic time points (30 and 60 dpi) which decreased by 90 dpi. Surprisingly, AQP4 KO mice did not develop any spontaneous seizures at 90 dpi. Additionally, AQP4 KO mice exhibited increased late spontaneous seizure duration and intrahippocampal stimulation-induced seizure duration compared with WT mice. EEG phenotypes in mice with and without PTE were also identified. Specifically, WT and AQP4 KO mice with PTE displayed lower EEG power across time and frequency compared with mice that did not develop PTE. Interestingly, AQP4 expression was significantly increased in the ipsilateral frontal cortex and hippocampus of WT mice with PTE. In contrast, Kir4.1 expression was not significantly altered in mice with PTE. These findings suggest for the first time that altered regulation of AQP4 correlates with the development of PTE in the CCI model. Collectively, these findings serve as a foundation to develop other potential biomarkers of PTE and can aid in developing new therapeutic strategies to prevent epileptogenesis after TBI.

6.1 References

Amiry-Moghaddam, M., Otsuka, T., et al. (2003). "An α-syntrophin-dependent pool of AQP4 in astroglial end-feet confers bidirectional water flow between blood and brain." Proceedings of the National Academy of Sciences **100**(4): 2106-2111.

Amiry-Moghaddam, M., Williamson, A., et al. (2003). "Delayed K+ clearance associated with aquaporin-4 mislocalization: phenotypic defects in brains of α-syntrophin-null mice." Proceedings of the National Academy of Sciences **100**(23): 13615-13620.

Aniksztejn, L., Charton, G., et al. (1987). "Selective release of endogenous zinc from the hippocampal mossy fibers in situ." Brain research **404**(1-2): 58-64.

Babb, T. L., Kupfer, W., et al. (1991). "Synaptic reorganization by mossy fibers in human epileptic fascia dentata." Neuroscience **42**(2): 351-363.

Bareyre, F., Wahl, F., et al. (1997). "Time course of cerebral edema after traumatic brain injury in rats: effects of riluzole and mannitol." J Neurotrauma **14**(11): 839-849.

Başkaya, M. K., Rao, A. M., et al. (1997). "The biphasic opening of the blood–brain barrier in the cortex and hippocampus after traumatic brain injury in rats." Neuroscience letters **226**(1): 33-36.

Bolkvadze, T. and Pitkänen, A. (2012). "Development of post-traumatic epilepsy after controlled cortical impact and lateral fluid-percussion-induced brain injury in the mouse." J Neurotrauma **29**(5): 789-812.

Burda, J. E., Bernstein, A. M., et al. (2016). "Astrocyte roles in traumatic brain injury." Experimental neurology **275**: 305-315.

Canolty, R. T. and Knight, R. T. (2010). "The functional role of cross-frequency coupling." Trends in cognitive sciences **14**(11): 506-515.

Connors, N. C., Adams, M. E., et al. (2004). "The potassium channel Kir4. 1 associates with the dystrophin-glycoprotein complex via α-syntrophin in glia." Journal of Biological Chemistry **279**(27): 28387-28392.

Coulter, D. A. (2000). "Mossy Fiber Zinc and Temporal Lobe Epilepsy: Pathological Association with Altered “Epileptic” γ-Aminobutyric Acid A Receptors in Dentate Granule Cells." Epilepsia **41**: S96-S99.

Courjon, J. (1970). "A Longitudinal Electro-Clinical Study of 80 Cases of Post-Traumatic Epilepsy observed from the Time of the Original Trauma." Epilepsia **11**(1): 29-36.

D'Ambrosio, R., Fender, J. S., et al. (2005). "Progression from frontal–parietal to mesial–temporal epilepsy after fluid percussion injury in the rat." Brain **128**(1): 174-188.

D’Ambrosio, R., Fairbanks, J. P., et al. (2004). "Post-traumatic epilepsy following fluid percussion injury in the rat." Brain **127**(2): 304-314.

El Bahh, B., Lespinet, V., et al. (1999). "Correlations between granule cell dispersion, mossy fiber sprouting, and hippocampal cell loss in temporal lobe epilepsy." Epilepsia **40**(10): 1393-1401.

Friedman, A., Kaufer, D., et al. (2009). "Blood–brain barrier breakdown-inducing astrocytic transformation: novel targets for the prevention of epilepsy." Epilepsy research **85**(2-3): 142-149.

Frigerio, F., Frasca, A., et al. (2012). "Long-lasting pro-ictogenic effects induced in vivo by rat brain exposure to serum albumin in the absence of concomitant pathology." Epilepsia **53**(11): 1887-1897.

Golarai, G., Greenwood, A. C., et al. (2001). "Physiological and structural evidence for hippocampal involvement in persistent seizure susceptibility after traumatic brain injury." Journal of Neuroscience **21**(21): 8523-8537.

Heinemann, U., Kaufer, D., et al. (2012). "Blood-brain barrier dysfunction, TGFβ signaling, and astrocyte dysfunction in epilepsy." Glia **60**(8): 1251-1257.

Hunt, R. F., Scheff, S. W., et al. (2009). "Posttraumatic epilepsy after controlled cortical impact injury in mice." Exp Neurol **215**(2): 243-252.

Hunt, R. F., Scheff, S. W., et al. (2010). "Regionally localized recurrent excitation in the dentate gyrus of a cortical contusion model of posttraumatic epilepsy." J Neurophysiol **103**(3): 1490-1500.

Ivens, S., Kaufer, D., et al. (2006). "TGF-β receptor-mediated albumin uptake into astrocytes is involved in neocortical epileptogenesis." Brain **130**(2): 535-547.

Jennett, B. and Van De Sande, J. (1975). "EEG prediction of post-traumatic epilepsy." Epilepsia **16**(2): 251-256.

Kharatishvili, I., Nissinen, J., et al. (2006). "A model of posttraumatic epilepsy induced by lateral fluid-percussion brain injury in rats." Neuroscience **140**(2): 685-697.

Kiening, K. L., van Landeghem, F. K., et al. (2002). "Decreased hemispheric Aquaporin-4 is linked to evolving brain edema following controlled cortical impact injury in rats." Neuroscience letters **324**(2): 105-108.

Manley, G. T., Fujimura, M., et al. (2000). "Aquaporin-4 deletion in mice reduces brain edema after acute water intoxication and ischemic stroke." Nature medicine **6**(2): 159.

McIntosh, T. K., Vink, R., et al. (1989). "Traumatic brain injury in the rat: characterization of a lateral fluid-percussion model." Neuroscience **28**(1): 233-244.

Ray, S., Dixon, C., et al. (2002). "Molecular mechanisms in the pathogenesis of traumatic brain injury." Histology and histopathology **17**(4): 1137-1152.

Santhakumar, V., Ratzliff, A. D., et al. (2001). "Long-term hyperexcitability in the hippocampus after experimental head trauma." Ann Neurol **50**(6): 708-717.

Sauseng, P. and Klimesch, W. (2008). "What does phase information of oscillatory brain activity tell us about cognitive processes?" Neuroscience & Biobehavioral Reviews **32**(5): 1001-1013.

Scharfman, H. E., Sollas, A. L., et al. (2003). "Electrophysiological evidence of monosynaptic excitatory transmission between granule cells after seizure-induced mossy fiber sprouting." Journal of neurophysiology **90**(4): 2536-2547.

Schmeiser, B., Zentner, J., et al. (2017). "Extent of mossy fiber sprouting in patients with mesiotemporal lobe epilepsy correlates with neuronal cell loss and granule cell dispersion." Epilepsy research **129**: 51-58.

Seiffert, E., Dreier, J. P., et al. (2004). "Lasting blood-brain barrier disruption induces epileptic focus in the rat somatosensory cortex." Journal of Neuroscience **24**(36): 7829-7836.

Siesjö, B. K. (1993). "Basic mechanisms of traumatic brain damage." Annals of emergency medicine **22**(6): 959-969.

Soares, H. D., Thomas, M., et al. (1992). "Development of prolonged focal cerebral edema and regional cation changes following experimental brain injury in the rat." Journal of neurochemistry **58**(5): 1845-1852.

Sutula, T., Cascino, G., et al. (1989). "Mossy fiber synaptic reorganization in the epileptic human temporal lobe." Annals of Neurology: Official Journal of the American Neurological Association and the Child Neurology Society **26**(3): 321-330.

Szu, J. I. and Binder, D. K. (2016). "The role of astrocytic aquaporin-4 in synaptic plasticity and learning and memory." Frontiers in integrative neuroscience **10**.

Tomkins, O., Feintuch, A., et al. (2011). "Blood-brain barrier breakdown following traumatic brain injury: a possible role in posttraumatic epilepsy." Cardiovascular psychiatry and neurology **2011**.

Tomkins, O., Shelef, I., et al. (2008). "Blood–brain barrier disruption in post-traumatic epilepsy." Journal of Neurology, Neurosurgery & Psychiatry **79**(7): 774-777.

Vespa, P., McArthur, D., et al. (2010). "Nonconvulsive seizures after traumatic brain injury are associated with hippocampal atrophy." Neurology **75**(9): 792-798.

Vespa, P. M., Miller, C., et al. (2007). "Nonconvulsive electrographic seizures after traumatic brain injury result in a delayed, prolonged increase in intracranial pressure and metabolic crisis." Critical care medicine **35**(12): 2830.

Vespa, P. M., Nuwer, M. R., et al. (1999). "Increased incidence and impact of nonconvulsive and convulsive seizures after traumatic brain injury as detected by continuous electroencephalographic monitoring." Journal of neurosurgery **91**(5): 750-760.

Vogt, K., Mellor, J., et al. (2000). "The actions of synaptically released zinc at hippocampal mossy fiber synapses." Neuron **26**(1): 187-196.

Yao, X., Uchida, K., et al. (2015). "Mildly reduced brain swelling and improved neurological outcome in aquaporin-4 knockout mice following controlled cortical impact brain injury." J Neurotrauma **32**(19): 1458-1464.